AD

TECHNICAL REPORT
ECOM-00240-1, VOL. I

LIGHT TRANSPORT IN THE ATMOSPHERE

Volume I: Monte Carlo Studies

ANNUAL REPORT
1 August 1965 to 31 August 1966

By

M. B. WELLS, D. G. COLLINS,
and K. CUNNINGHAM

SEPTEMBER 1966

ECOM

UNITED STATES ARMY ELECTRONICS COMMAND • FORT MONMOUTH, N.J.

CONTRACT DA28-043 AMC-00240(E)

RADIATION RESEARCH ASSOCIATES, INC.
Fort Worth, Texas

TECHNICAL REPORT ECOM-00240-1, VOL. I
RRA-T63-1

SEPTEMBER 1966

LIGHT TRANSPORT IN THE ATMOSPHERE

Volume I: Monte Carlo Studies

Annual Report

1 August 1965 to 31 August 1966

Contract No. DA 28-043 AMC-00240(E)

Prepared by

M. B. Wells, D. G. Collins and K. Cunningham

RADIATION RESEARCH ASSOCIATES, INC.
Fort Worth, Texas

for
U. S. Army Electronics Command, Fort Monmouth, New Jersey

ABSTRACT

This is the first of three volumes. Volumes II and III contain other aspects of the study: description of the LITE codes and the two computer programs that were prepared for use in computing cross sections for light scattering by spherical aerosol particles with a complex index of refraction.

The Monte Carlo codes LITE-I and LITE-II were used to compute light transmission data for point and plane sources. The results of these calculations showed that there is no correlation between the scattered transmission data for point isotropic and plane parallel sources.

The LITE codes were used to analyze experimental data on light transport in the atmosphere. Reasonably good agreement was obtained for those cases where data were available to adequately describe the atmosphere at the time of the experiments.

Calculations were performed to determine the angular dependence of the number albedo from thick cumulus clouds for 0.45μ light incident at various angles to the cloud. The polar angular distributions of the reflected photons were found to be cosine distributions and the total number albedo was fitted by the expression

$$\alpha(\theta_o) = 0.639 - 0.154\cos\theta_o$$

where θ_o is the angle of incidence.

Studies were performed to determine the sensitivity of the LITE-I calculated scattered intensities for a point isotropic monochromatic source to changes in the source and receiver altitudes, aerosol number

density, aerosol phase function, altitude variation of the aerosol scattering coefficient and the altitude of the bottom of a cloud layer above the source point. It was found for the source-receiver geometry considered in these studies that the LITE calculations were more sensitive to changes in the number density of the aerosol particles than to changes in the shape of the aerosol phase function.

PREFACE

During the period 1 August 1965 to 31 August 1966 Monte Carlo studies were performed to determine light transport in the atmosphere under various environmental conditions. These studies consisted of 1) correlation analysis of light transport from a point isotropic source and a plane parallel source to determine the comparability of solar light transmission data and transmission properties for thermal radiation nuclear weapons, 2) development of machine codes for calculation of phase functions and scattering and absorption coefficients for spherical-homogeneous aerosol particles with a complex index of refraction, 3) an analysis of experimental field data on light transmission, 4) parametric studies to determine the specific influence of ground and cloud albedo, cloud height and aerosol number density and particle-size distribution on the transport of light in the atmosphere, 5) modifications to the LITE codes to increase their application to a wider range of atmospheric transport problems and 6) the development of a machine program for use in converting the scattered intensities computed by the LITE codes for a given ground albedo to data giving scattered intensities and scattered fluxes for other ground albedos. The results of these studies are presented in this report, which is divided into three volumes. The first volume describes the results of items 1, 3 and 4 outlined above. The second volume describes the machine programs developed for use in calculation of aerosol cross sections. The third volume contains utilization instructions for the modified versions of the LITE codes and for the code developed to convert the LITE results to data giving scattered intensities and fluxes for other ground albedos.

FOREWORD

The authors wish to express their appreciation to Henrietta Hendrickson and Hemma Francis of Oak Ridge National Laboratory who aided in the check out and running of test problems of the FORTRAN-IV version of the LITE codes. They also wish to acknowledge the assistance of Leon Leskowitz of the U. S. Army Electronics Laboratory in translating the FORTRAN-IV version of the LITE code to ALGOL language and in scheduling the LITE problems run on the B-5500 computer. Technical monitors of the work described in this report were I. Cantor of the Atmospheric Sciences Laboratory, USAECOM, Fort Monmouth, New Jersey and R. W. Fenn of the Air Force Cambridge Research Laboratories, Bedford, Massachusetts.

TABLE OF CONTENTS

LIST OF FIGURES

LIST OF TABLES

I. INTRODUCTION

The present report is Volume I of a three-volume annual report prepared under Contract No. DA 28-043 AMC-00240(E). The studies described in this volume were performed for the purpose of continuing to check the accuracy of the Monte Carlo codes, LITE-I and LITE-II, and to investigate the importance of the various parameters that affect the transport of light in the atmosphere. The LITE codes that were used in these studies are described in Volume III of this report and in Reference 1.

The first study undertaken during the reporting period was directed toward determining if a correlation exists between atmospheric transmission data for point and plane sources. The results of that study are given in Chapter II.

Although there is currently available in the literature a large body of measured data on light transport in the atmosphere, most of that data is not suitable for use in checking out the results of theoretical calculations. The main difficulty with the available measured data is the almost complete lack of information on the aerosol number density and size distribution and their variation with altitude. In many cases transmission measurements were taken for only one source altitude and as a result, it is almost impossible to infer the variation of the extinction cross section with altitude unless one can describe the atmosphere by a model, such as that suggested by Elterman (Reference 2).

In spite of the many uncertainties in the atmospheric conditions for a given set of measurements, several sets of measured data were selected for analysis. Chapter III presents the results of Monte Carlo calculations

performed for analysis of measured data from several experiments. Section 3.1 describes an analysis of transmission data reported by Cantor and Petriw (Reference 3) for point isotropic sources, Section 3.2 describes an analysis of some of the measured receiver response data from a searchlight experiment reported by Elterman (Reference 4), Section 3.3 discusses an analysis of some measured sunlight transmission data from an Air Force Cambridge Research Laboratory high altitude balloon flight and Section 3.4 shows a comparison between two different calculations of the dependence of light transmitted and reflected from an aerosol atmosphere on the shape of the aerosol phase function.

The need for information on the angular distribution of cloud albedos for use in the LITE-I code resulted in a study to determine the angular distribution of the number albedo for various angles of incidence of 0.45 micron light to a 1 km thick cumulus cloud. The results of the cloud albedo studies are presented in Chapter IV.

Since the LITE-I code is to be used to study the atmospheric transport of the thermal radiation emitted by a nuclear weapon, it is of considerable importance to have a knowledge of how variations in such parameters as the source altitude, receiver altitude, cloud height, aerosol number density, aerosol size distribution and altitude variation of the aerosol number density affect the transmission properties of the atmosphere. Chapter IV describes the results of Monte Carlo calculations that were performed for the purpose of studying the influence of the above mentioned parameters on the atmospheric transmission of light emitted by point isotropic sources.

II. CORRELATION STUDIES FOR POINT AND PLANE SOURCES

The availability of a large body of measured data (Reference 5) on the transmission of sunlight through the atmosphere leads one to inquire if this data could be used to compute the atmospheric transmission of the thermal radiation produced by a nuclear detonation in the atmosphere.

The scattered light intensity at a receiver depends on the source-receiver geometry, the variation of the scattering and absorption cross sections with altitude, and the source wave length. The direct radiation at the receiver depends only on the number of mean-free-paths between the source and receiver. The direct intensity transmitted through an atmosphere of ρ mean-free-paths in normal thickness for a broad beam monodirectional source of one photon per unit area incident to the top of the atmosphere at angle θ_o is given by

$$I_D(\theta_o) = I_o\, e^{-\rho \sec\theta_o} ,$$

where the incident intensity $I_o = \sec\theta_o$ (photons cm^{-2}). For a point isotropic source placed at the top of the atmosphere, the direct intensity at a receiver located at the bottom of the atmosphere and at a slant distance R from the source is given by

$$I_D(R = h\sec\theta_o) = \frac{e^{-\rho \sec\theta_o}}{4\pi h^2 \sec^2\theta_o}$$

where h is the normal thickness of the atmosphere and θ_o is the angle between a normal to the ground through the source and the source-receiver line. It is seen that

$$I_D(\theta_o)\cos\theta_o = 4\pi h^2 \sec^2\theta_o \cdot I_D(R = h\sec\theta_o) \ . \qquad (1)$$

The requirement that the point source be placed at the top of the atmosphere can be removed when calculating the direct intensity provided that the slant mean-free-path distance ρ' between the source and receiver be the same as that given by $\rho' = \rho\sec\theta_o$ where θ_o is the angle of incidence for the plane source. If the point source is located at altitude h_2 and the receiver at h_1 and the angle between a normal to the ground through the receiver and the source receiver line is α, then the mean-free-path distance between the source and receiver is given by

$$\rho' = \sec\alpha \int_{h_1}^{h_2} \Sigma(h)dh$$

where $\Sigma(h)$ is the extinction cross section at altitude h. The slant distance R is given by

$$R = (h_2 - h_1)\sec\alpha \ . \qquad (2)$$

Therefore, when the mean-free-path distance between the point source and receiver is the same as that along a slant path through the atmosphere for a plane source, we can estimate the direct intensity for the point source by use of the relation

$$I_D(R,\rho') = \frac{\cos\theta_o}{4\pi R^2} I_D(\theta_o,\rho') \qquad (3)$$

where $I_D(\theta,\rho')$ is the direct intensity at a depth of ρ' mean-free-paths into the atmosphere for a broad beam monodirectional source of one photon unit area incident at angle θ_o to the top of the atmosphere.

If the atmosphere was a pure absorbing medium so that no scattering occurs, then measured transmission data for sunlight incident on the top of the atmosphere could be used to predict the transmission for point sources. The mean-free-path distance from altitude h to the top of the atmosphere could be obtained from measurements of sunlight intensities at various altitudes.

The earth's atmosphere is not a pure absorbing medium, and scattering is an important process by which light is transported through the atmosphere. It would be instructive to investigate the validity of Equation 1 when the direct intensities are replaced by the scattered intensities. In addition to aerosol and Rayleigh scattering, another important scattering process is the reflection of both the direct-beam and the air-scattered light by the ground surface and clouds.

The scattered light intensity transmitted through the bottom of the atmosphere for a plane isotropic source emitting 0.5 photons cm^{-2} into the atmosphere may be computed from a knowledge of $I_S(\theta_o)$, the scattered intensity transmitted through the bottom of the atmosphere for a plane parallel source, and $I_S(R = h\sec\theta_o)$, the scattered intensity transmitted through the bottom of the atmosphere at a slant distance R from a point isotropic source located at the top of the atmosphere.

The transmitted intensity for a plane isotropic source is given by the equation

$$I_S = 2\pi \int_0^{\pi/2} \frac{I_S(\theta_o)}{4\pi} \sin\theta_o d\theta_o = \frac{1}{2} \int_0^{\pi/2} I_S(\theta_o)\sin\theta_o d\theta_o ,$$

where $\frac{1}{4\pi}$ is the source strength per steradian in direction θ_o and $I_S(\theta_o)$ is the scattered intensity transmitted through the bottom of the atmosphere per photon cm^{-2} incident at direction θ_o to the top of the atmosphere.

The scattered intensity transmitted through the bottom of the atmosphere for a plane isotropic source emitting 0.5 photons cm^{-2} into the atmosphere is also given by integrating the transmitted scattered intensity for a point isotropic source located at the top of the atmosphere over the area of the bottom of the atmosphere. If h is the thickness of the atmosphere, R the slant range between the source and receiver, and θ_o is the angle between R and a normal to the atmosphere through the source, then

$$I_S = 2\pi \int_0^{\pi/2} I_S(R = h\sec\theta_o) R^2 \tan\theta_o d\theta_o = \frac{1}{2} \int 4\pi R^2 I_S(R = h\sec\theta_o) \tan\theta_o d\theta_o$$

To show that the above integrals are equal, LITE-I calculations were run to determine $I_S(R)$ for a point isotropic source located at the top of a 0.5 mean-free-path thick Rayleigh atmosphere and for receivers placed parallel to the ground at ground level. Data for $I_S(\theta_o)$ were obtained from integration of the differential scattered intensity data reported by Coulson et al. (Reference 6). The results of the integrations are shown below for cases where the ground albedo was 0.0 and 0.8.

Scattered Intensity Transmitted Through a 0.5 Mean-free-path Thick Rayleigh Atmosphere for a Plane Isotropic Source

(photons cm^{-2}/0.5 source photons cm^{-2})

Ground Albedo	Transmitted Intensity	
	From Coulson Data	From LITE-I Calculations
0.0	0.332	0.351
0.8	0.561	0.568

It is seen that integrations over the plane and point source data give identical results within the accuracy of the graphical integration method used. The fact that the two integrals are equal, that is,

$$\frac{1}{2}\int_0^{\pi/2} I_S(\theta_o)\sin\theta_o d\theta_o = \frac{1}{2}\int_0^{\pi/2} 4\pi R^2(\theta_o) I(R = h\sec\theta_o)\tan\theta_o d\theta_o ,$$

and the fact that the direct intensities from the two sources are correlated, leads one to inquire if the scattered intensities from the two sources are also correlated.

If the two integrals were equal for all values of the upper limit of the interval of integration less than $\pi/2$, then differentiation of both integrals would give

$$I_S(\theta_o)\sin\theta_o = 4\pi R^2(\theta_o) I_S(R = h\sec\theta_o)\tan\theta_o ,$$

and a correlation would be obtained for point and plane source data. The fact that these integrals are equal only for the special case where the upper limit of the integration interval is $\pi/2$ is shown in Figure 1. It is seen from the two curves shown in Figure 1 that

$$\int_0^{\theta} I_S(\theta_o) d(\cos\theta_o) \neq \int_0^{\theta} 4\pi R^2(\theta_o)\sec\theta_o I_S(R = h\sec\theta_o) d(\cos\theta_o)$$

for values of $\theta<\pi/2$. It is also seen in Figure 1 that $4\pi R^2\sec\theta_o I(R=h\sec\theta_o)$ and $I_S(\theta_o)$ are equal only at two values of $\cos\theta_o$. Therefore, it can be stated that no real correlation exists between the scattered intensities for plane parallel and point isotropic sources.

A series of LITE-I and LITE-II problems were run for 0.45 and 0.65 micron plane parallel and point isotropic sources in an Elterman model

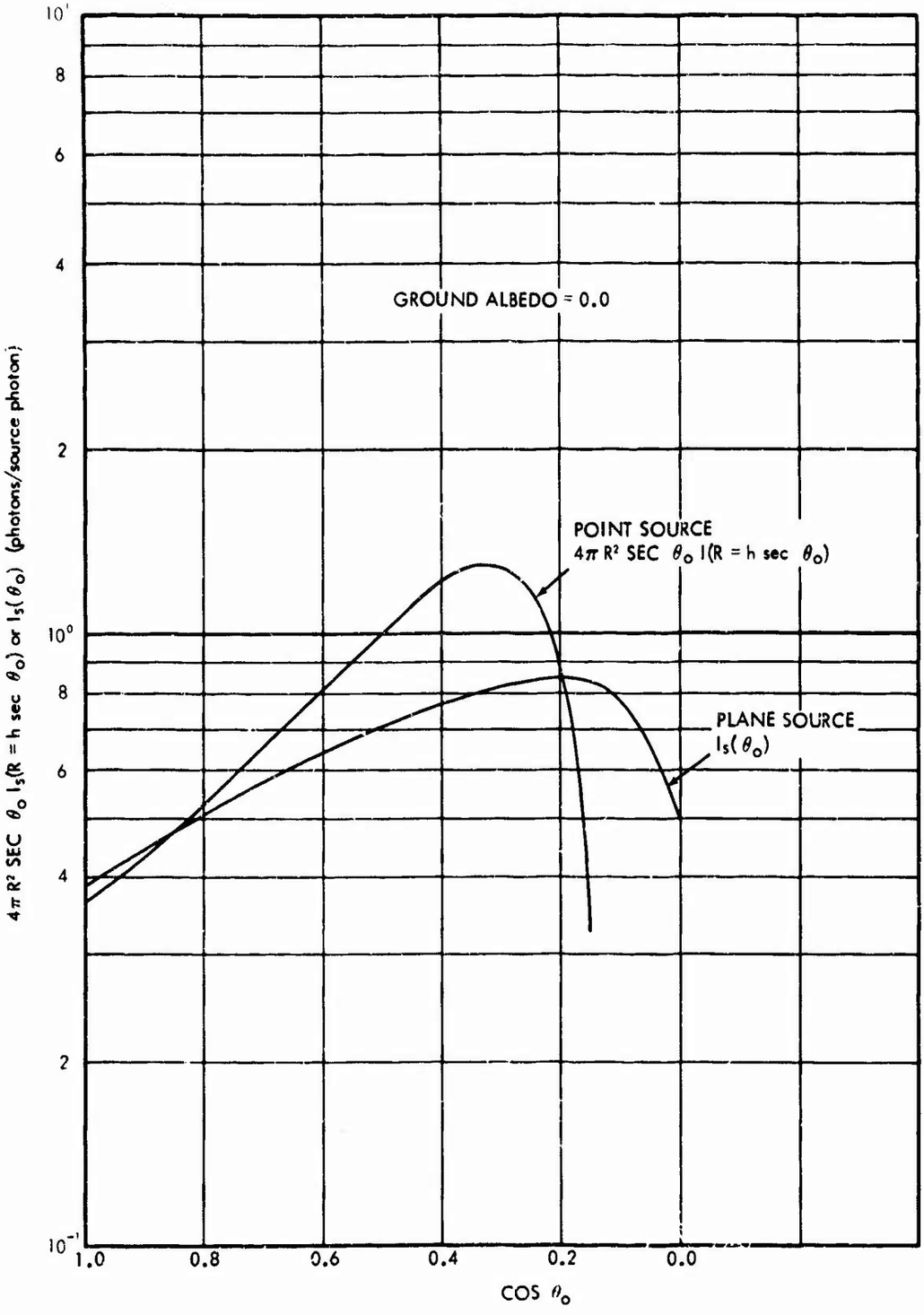

Fig. 1. Variation of $4\pi R^2$ Sec θ_o $I_s(R = h \sec \theta_o)$ and $I_s(\theta_o)$ with θ_o: 0.5 Mean-Free-Path Thick Rayleigh Atmosphere

atmosphere (Reference 2). The scattered transmission data for each source were plotted as a function of the angle θ_o and the results obtained showed that there was no correlation between $I_S(\theta_o)$ and $I_S(R = h\sec\theta_o)$ for both source wave lengths studied.

As a result of the analysis described above, it must be concluded that significant errors would be introduced by using measured sunlight transmission data to approximate the atmospheric transmission of the thermal radiation produced by nuclear weapon detonations in the atmosphere.

III. COMPARISON OF CALCULATED AND MEASURED TRANSMISSION DATA

A measure of the accuracy of any machine procedure for calculating the scattering of light by the atmosphere is its ability to predict measurements. As a part of the continuing effort to validate the LITE codes, several sets of experimental data were selected for analysis. Discussions of the LITE calculations and their comparison with experimental data are given in the following sections.

One of the difficulties that arise when performing an analysis of measured data is the almost complete lack of information concerning the atmospheric parameters that describe the atmosphere at the time the measurements were taken. In an attempt to overcome this difficulty, comparisons were also made with the results of calculations produced by other machine codes.

3.1 Analysis of Measured Data for Point Sources

Calculations were run using the LITE-I code to predict the scattering of yellow light (λ = 0.55 microns) in air over a snow-covered terrain for comparison with measurements (Reference 3) taken at Camp Haven, Wisconsin, on 30 and 31 March 1965. The source was located in the tail of an airplane flying at an altitude of 2650 ft and the receiver was located at an altitude of 20 ft.

The measured direct beam was used to obtain an estimate of the extinction coefficient for each day. The aerosol and extinction coefficients as given by Elterman's model were modified in order to duplicate the measured extinction coefficients for each day.

The measured data for 30 March gave a value of 0.15 $mile^{-1}$ for the extinction coefficient. The measured extinction coefficient for 31 March was 0.11 $mile^{-1}$. The atmosphere was clear on the night of 30 March and the surface albedo was estimated to be about 50 percent. There was an overcast at 3000 ft altitude on the night of 31 March and the surface albedo was estimated to be about 25°. The phase function for light scattering at ground level was measured on both evenings. The calculations for 31 March assumed that the overcast was a cloud of at least 1 km in thickness with the bottom of the cloud at a height of 3000 ft. Calculated fluxes for both evenings were obtained for a flat plate receiver which was assumed to be normal to the source-receiver axis.

The calculated and measured flux data for 30 March are compared in Figure 2. The measured data giving the total transmittance (receiver response times slant distance squared) were arbitrarily normalized to give a value of 1.0 at a slant range of R = 2.25 miles. Therefore, the calculated total transmittance data for a ground albedo of 0.5 were normalized to the measured data at R = 2.25 miles. The estimated albedo for the ground on the day the measurements were taken was 0.5. Although there are large fluctuations in the measured data, it is seen that the falloff of the total transmittance with slant distance as given by the calculated data is in good agreement with the measured data. The large fluctuations in the measured data make it impossible to estimate the value of the ground albedo from a comparison of the measured and calculated data.

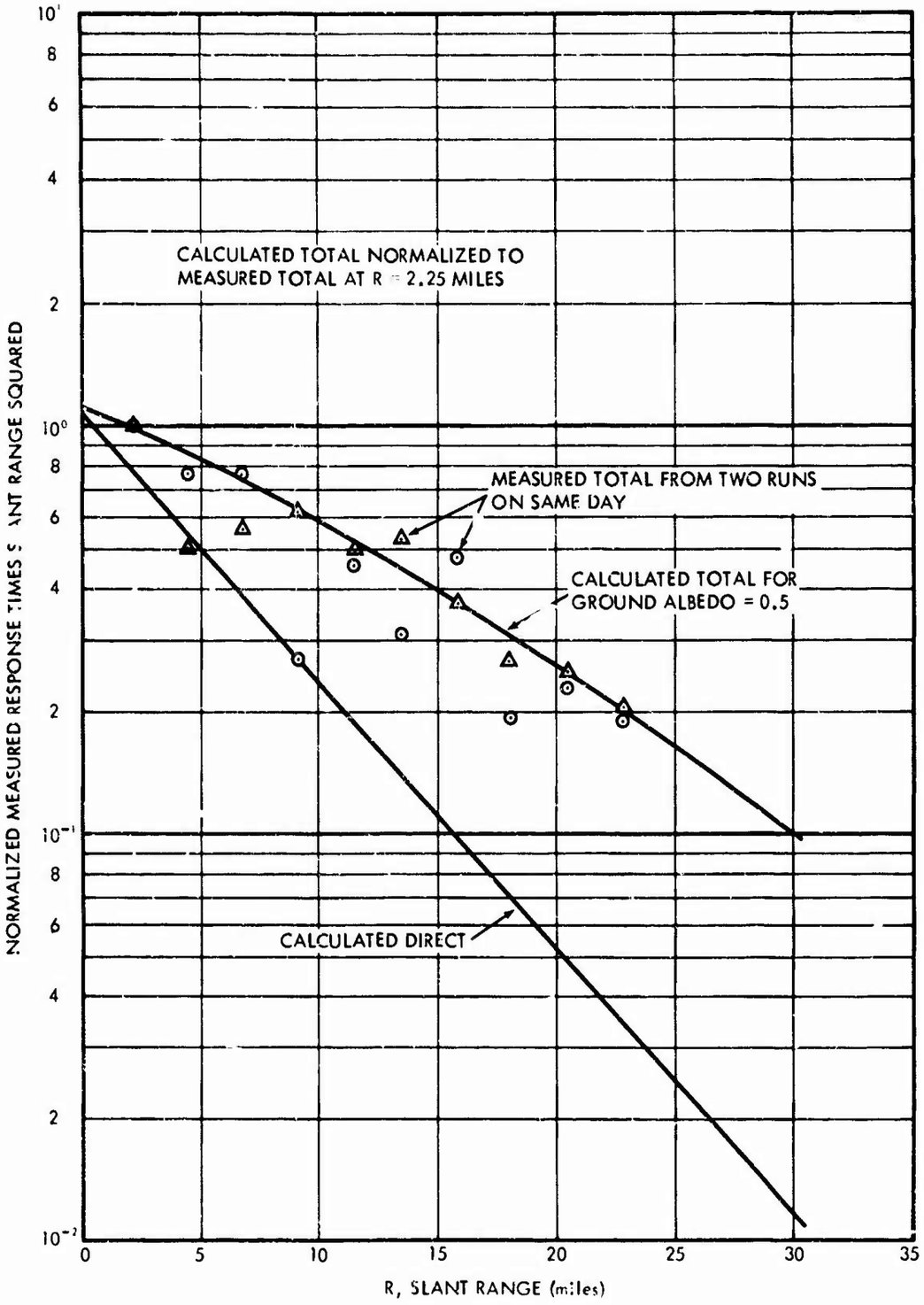

Fig. 2. Comparison of Calculated and Measured Receiver Response for Atmospheric Transmission of Yellow Light in a Wisconsin Area: 30 March 1965

Figure 3 presents a comparison of the calculated and measured total transmittance data for yellow-light scattering on March 31, 1965. The calculated and measured data giving the total transmittance were normalized to a value of 1 at R = 2.25 miles. It is noted that there is a wider spread between the calculated total and direct transmittance curves in Figure 3 for March 31 than that shown in Figure 2 for March 30. This difference results from the presence of the cloud located at a height of 3000 ft for the case shown in Figure 3. The comparison between the measured and calculated values of the total transmittance vs R indicates that the calculated data for a ground albedo of 0.25 are about 15 percent low for slant ranges between 4 and 15 miles.

3.2 Analysis of Searchlight Scattering Data

Elterman (Reference 4) has carried out scattering measurements from a searchlight beam to determine the aerosol properties of the atmosphere. He was able to derive the variation of the aerosol scattering coefficient with altitude from the measured receiver response data taking into consideration the contribution of single order aerosol and molecular scattering to the measured response. The measured response data obtained by Elterman for 8 May 1964 and the aerosol cross section variation with altitude that he obtained from that data have been analyzed by use of LITE-I.

The searchlight scene geometry as used in the LITE-I calculations is shown in Figure 4. The searchlight beam in the light scattering calculations was defined in terms of a θ, ϕ coordinate system so that it subtended the same solid angle as that used in the searchlight experiment.

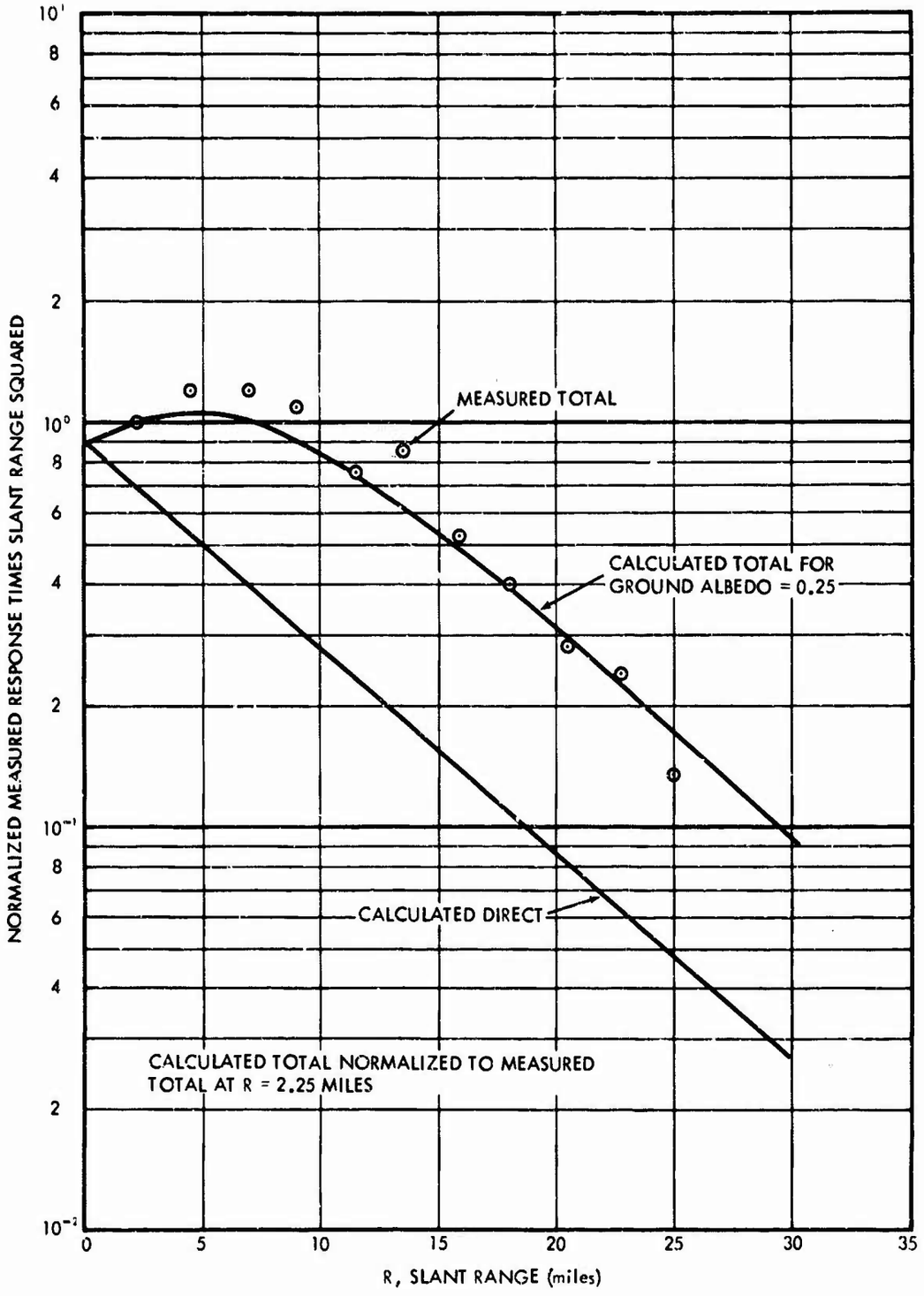

Fig. 3. Comparison of Colculated and Measured Receiver Response for Atmospheric Transmission of Yellow Light in a Wisconsin Area: 31 March 1965

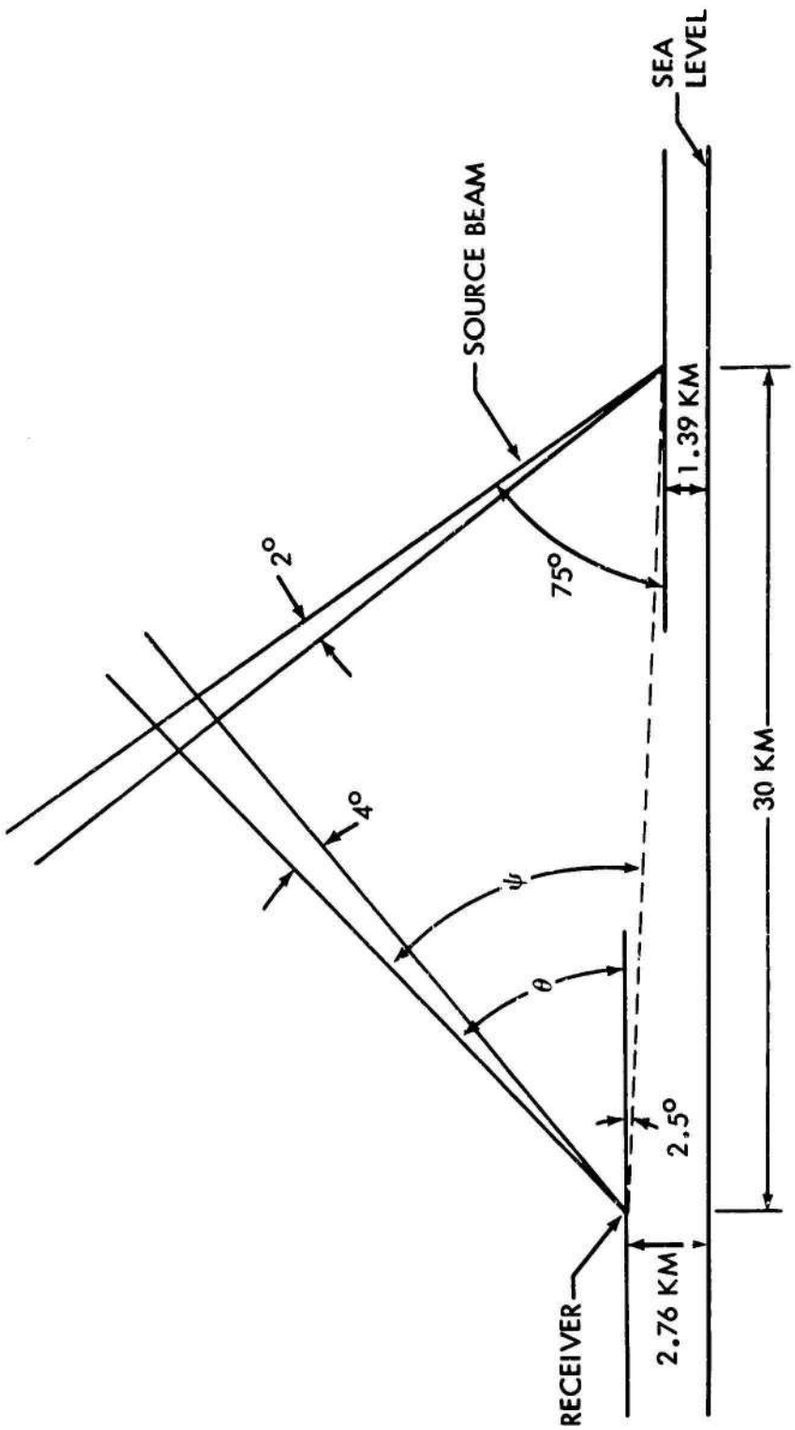

Fig. 4. Searchlight Scene Geometry

The scattered intensities at the receiver were recorded for those photons reaching the receiver through solid angles defined by 4° intervals in the receiver polar angle about the source-receiver line and 5.8° intervals of the azimuthal angle Φ (see Figure 5). Although it was not possible with the ψ, Φ coordinate system to define a receiver solid angle that did not vary with the receiver angle of elevation, the solid angle formed by the receiver polar and azimuthal angular intervals used in the calculations always included the searchlight beam. Therefore, the receiver solid angle for large receiver angles of elevation actually viewed a scattering volume that was slightly larger than the volume that would have been formed by the intersection of the searchlight beam and a constant receiver solid angle similar to that used in the experiment.

Figure 6 shows the altitude variation of the various cross sections for 0.55 micron wave length light as used in the LITE-I calculations. The extinction coefficient was taken to be the sum of the aerosol scattering, Rayleigh scattering, and ozone absorption coefficients. The Rayleigh scattering and ozone absorption coefficients shown in Figure 6 were taken from a tabulation reported by Elterman (Reference 2) for a "clear standard atmosphere." One of the aerosol scattering coefficient curves shown in Figure 6 were taken from Reference 2 and the other was that obtained by Elterman from an analysis of the searchlight data for 8 May 1964.

In his analysis of the measured data Elterman used an aerosol phase function that had been obtained from measurements reported by Reeger

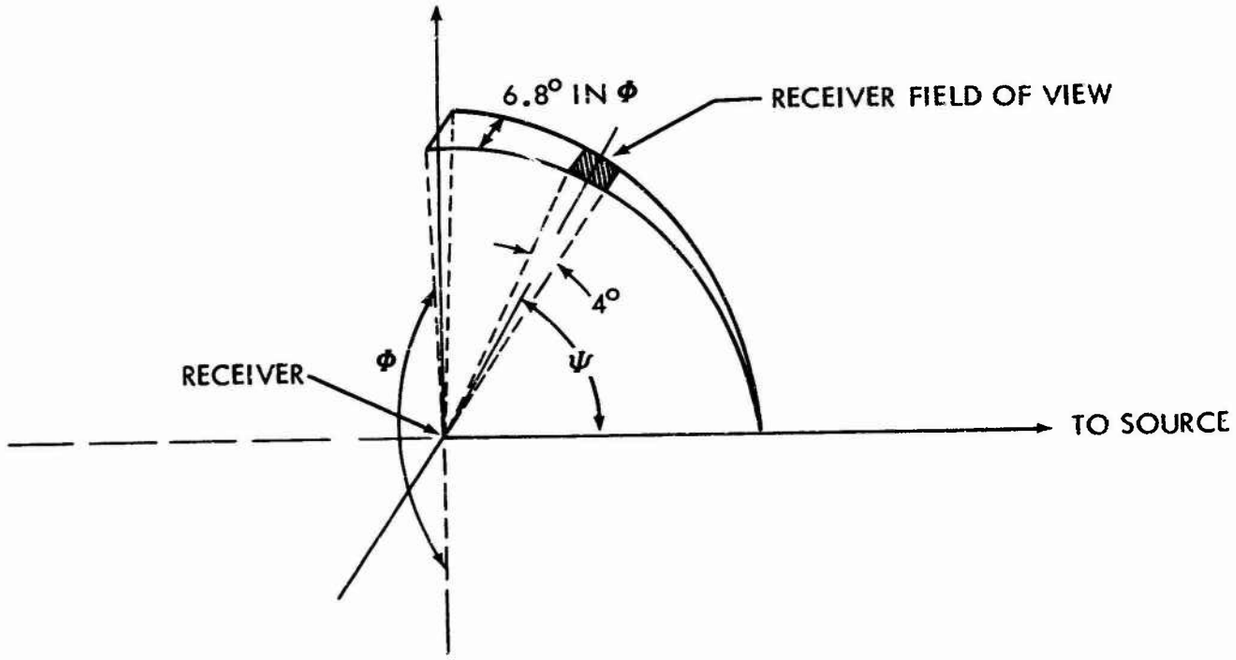

Fig. 5. Receiver Geometry

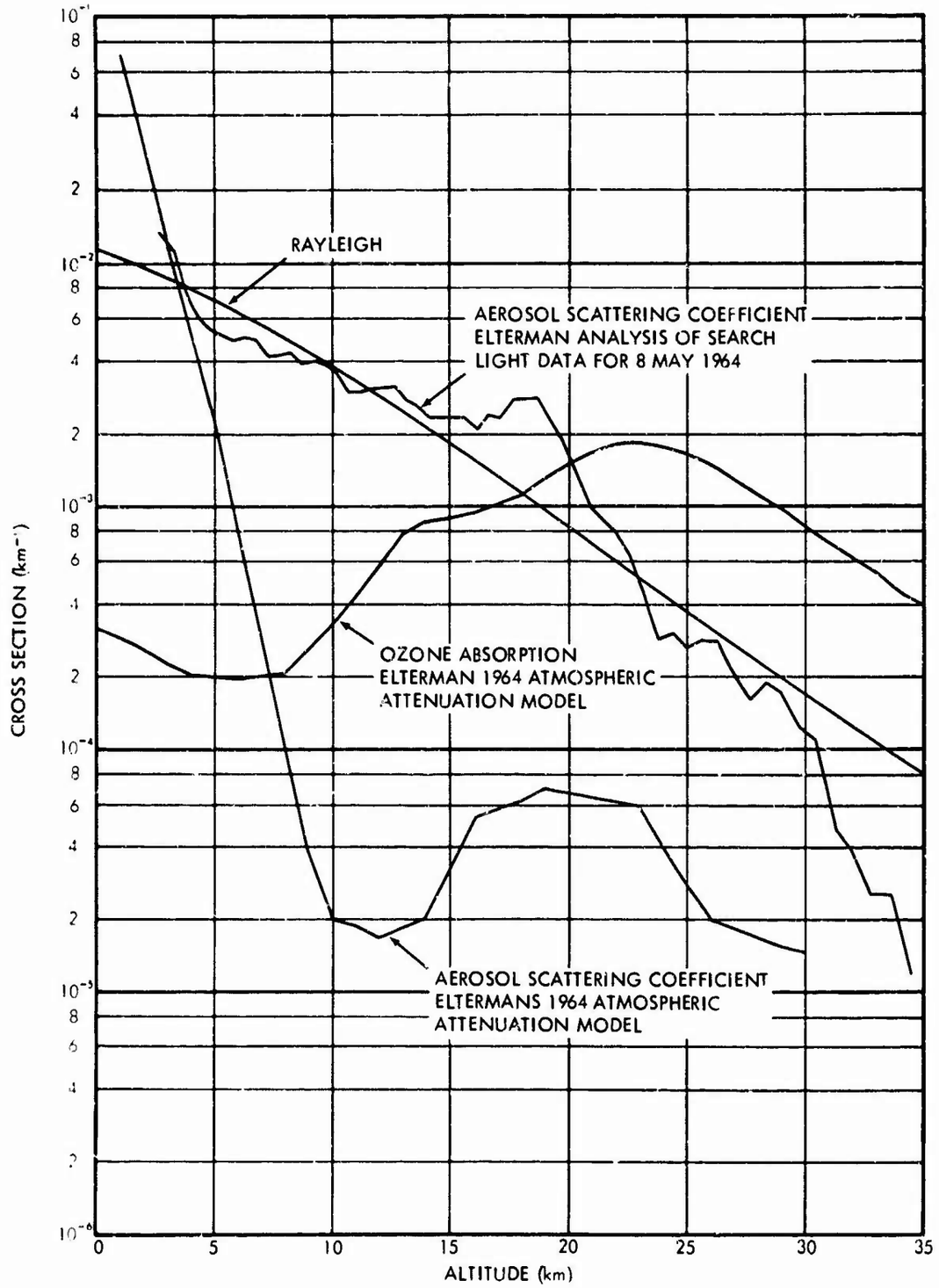

Fig. 6. Altitude Variation of the Rayleigh and Aerosol Scattering Coefficients and the Ozone Absorption Coefficient

and Siedentopf (Reference 7). A portion of the normalized Reeger and Siedentopf aerosol phase function for scattering angles between 75 and 145 degrees is presented in Figure 7. Also shown is the normalized phase function for Rayleigh scattering in the same scattering angle range. The phase functions shown in Figure 7 have been normalized so that the integral of the phase function over solid angle is unity.

Calculations were run on LITE-I to determine the single scattered intensity as a function of the receiver angle of elevation that resulted from Rayleigh scattering only and from both Rayleigh and aerosol scattering where the aerosol scattering coefficient variation with altitude was that obtained by Elterman from the measured searchlight data. The atmosphere used in the LITE-I calculations did not contain any ozone since Elterman's earlier analysis was based only on a Rayleigh plus aerosol scattering atmosphere. The results of the Monte Carlo calculations are presented in Figure 8 where they can be compared with the shape of the measured receiver response data as a function of the receiver angle of elevation. There is reasonably good agreement between the measured and calculated data when the calculated data was normalized to the measured data at $\theta = 54°$. The largest differences occur at receiver angles of elevation less than 14 degrees.

To study the effect of neglecting the attenuation of the scattered radiation by ozone absorption in Elterman's calculation of the aerosol coefficient, another problem was run in which the extinction coefficient was assumed to be made up of the sum of the Rayleigh and aerosol scattering and ozone absorption coefficients. The aerosol scattering coefficients

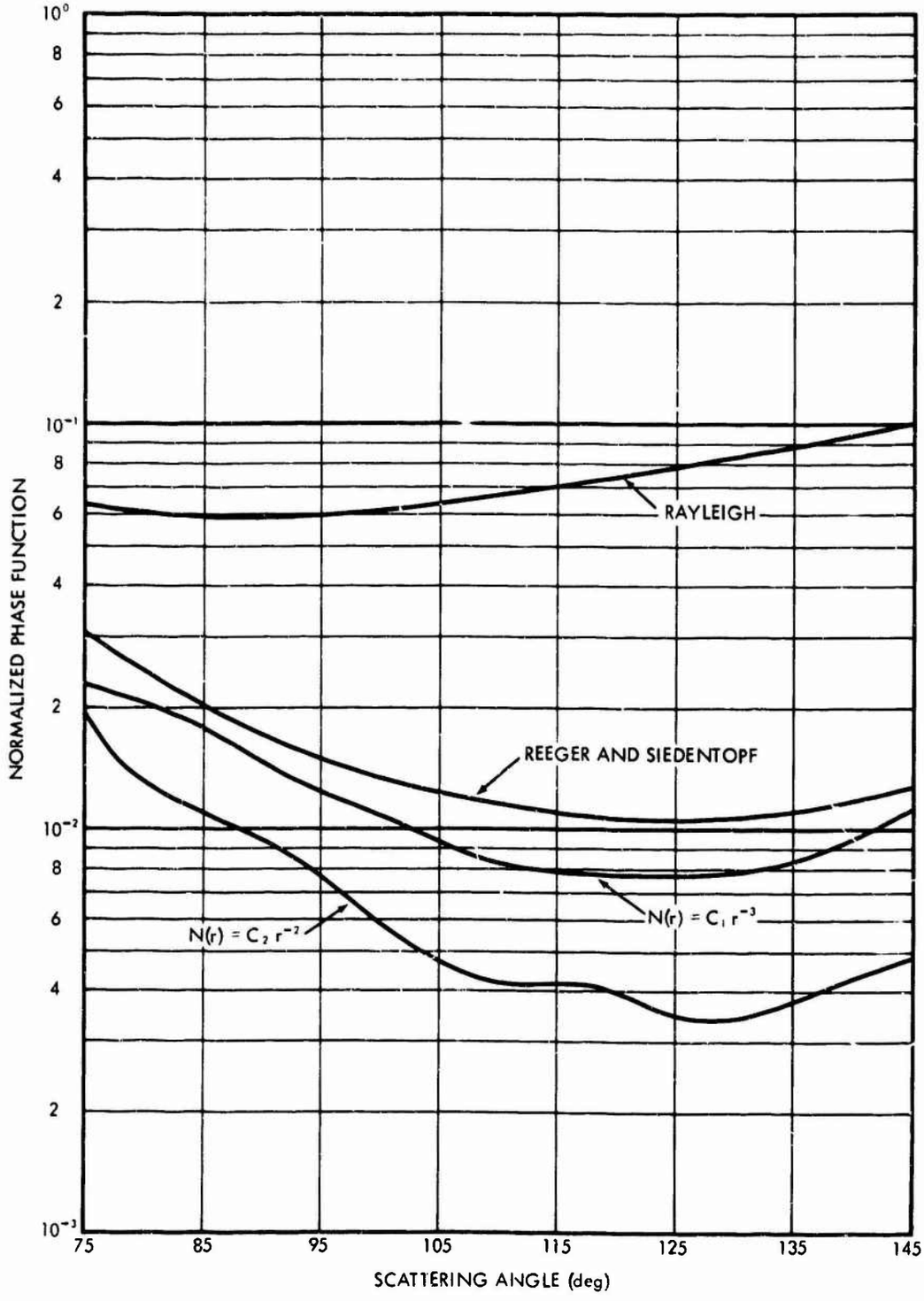

Fig. 7. Phase Functions for Rayleigh Scattering and Aerosal Scattering

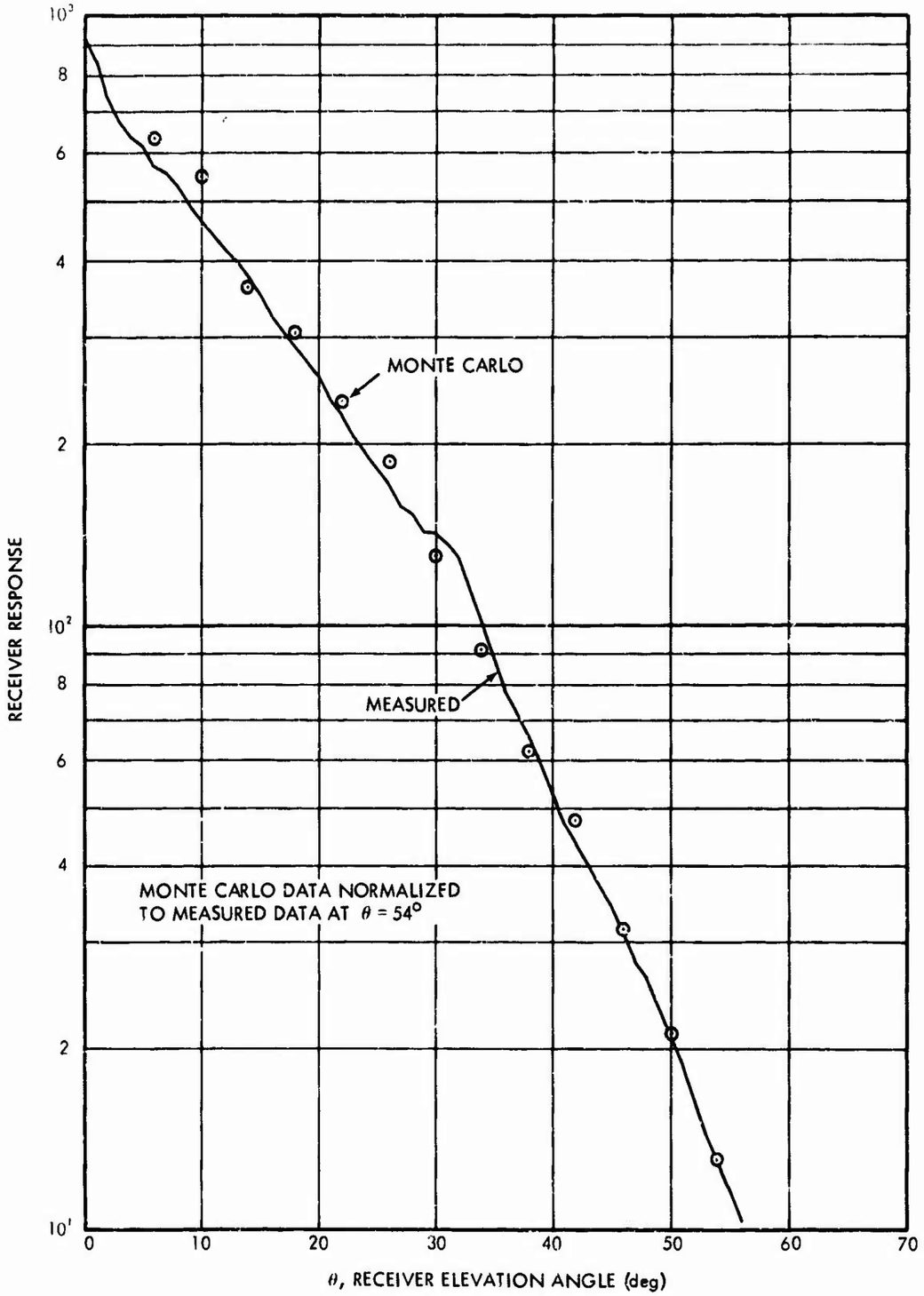

Fig. 8. Comparison of Single Scattering Calculations with Measured Data: No Ozone Absorption

used in the calculations were those obtained from the measured searchlight response data.

The calculated results for this case are presented in Figure 9 where they are compared with the shape of the measured receiver response. The calculated single scattered intensity summed over Rayleigh and aerosol scattering were normalized in Figure 9 to the measured response data for a receiver angle of elevation of 54°. It is seen that the total single scattered intensity (Rayleigh plus aerosol) falls off a slight bit faster with the angle of elevation than does the measured response data, indicating that there are probably some multiple scattering effects. The differences between the total (Rayleigh plus aerosol) single scattered intensity and the single Rayleigh scattered intensity become smaller with increasing angle of elevation, which indicate that the total single-scattered intensity results mainly from Rayleigh scattering at angles of elevation greater than about 40 degrees.

The LITE-I problem described above was rerun to obtain the total scattered intensity at the receiver for orders of scattering up to 20. Figure 10 shows, as a function of the receiver angle of elevation, a comparison of the computed total scattered intensity with the shape of the measured response data, where the total calculated data have been normalized to the measured response data at $\theta = 54$ degrees. It is seen that the multiple scattered intensity variation with receiver angle of elevation reproduces very well the shape of the measured response data. It is also seen from comparison of the total single scattered intensity curve in Figure 9 with the multiple scattered intensity curve in Figure 10

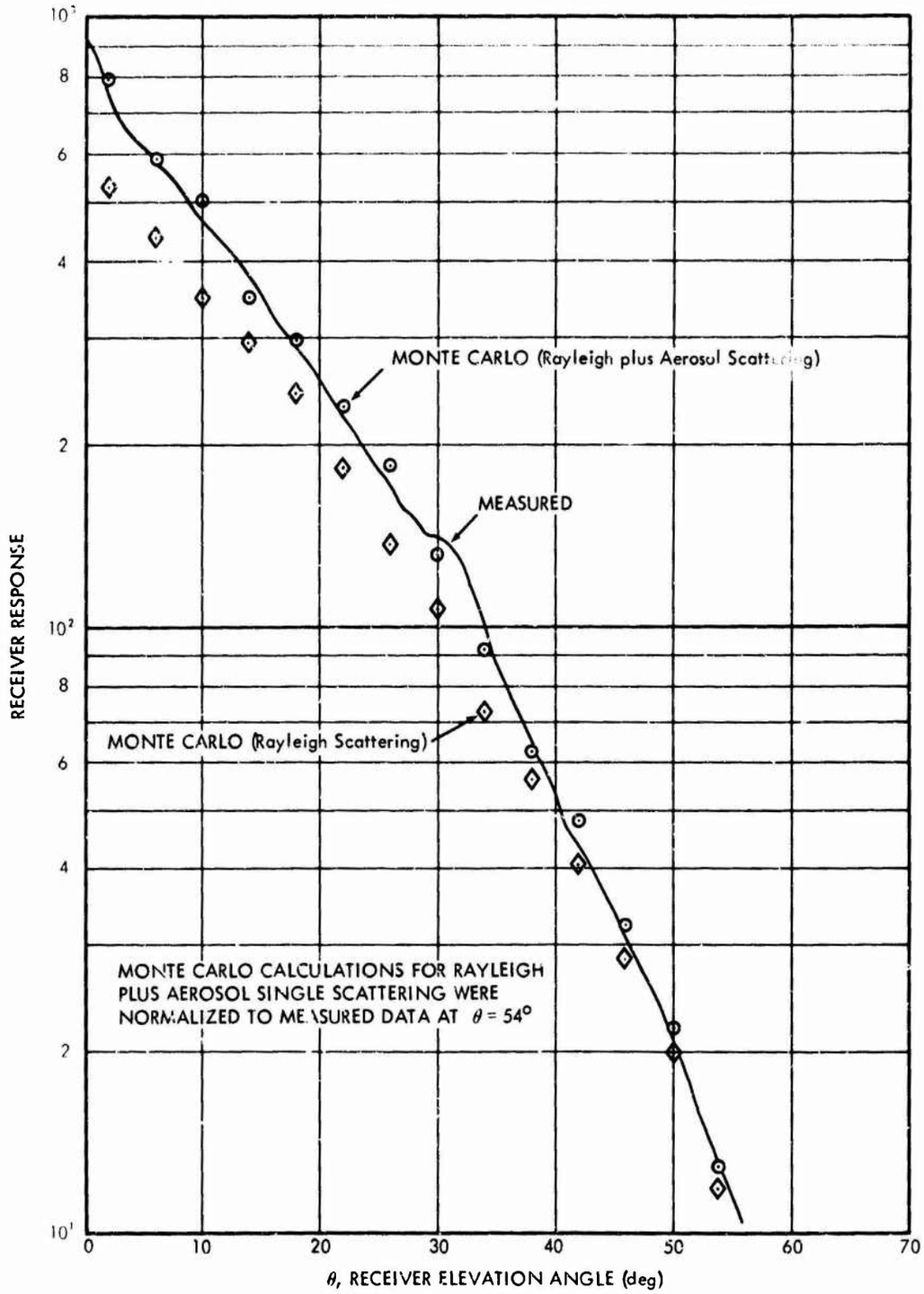

Fig. 9. Comparison of Single Scattering Calculations with Measured Data: Ozone Absorption Included

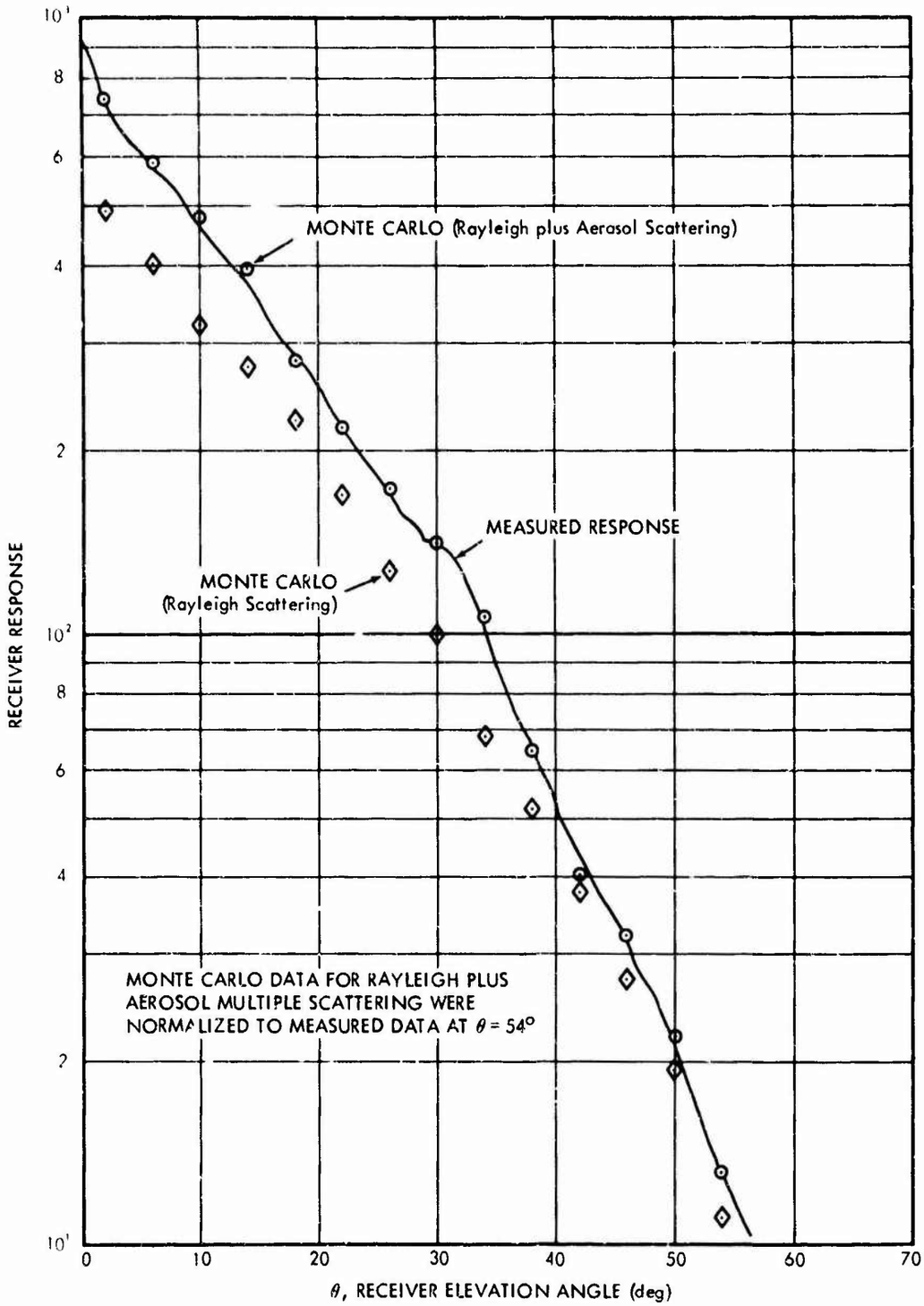

Fig. 10. Comparison of Multiple Scattering Calculations with Measured Data: Ozone Absorption Included

that the increase in the scattered intensity for a given receiver angle resulting from orders of scattering greater than one is small. The importance of orders of scattering greater than one increases with the receiver angle of elevation. At an angle of elevation of 54 degrees orders of scattering greater than one contribute about 12 percent to the calculated total intensity whereas at a receiver angle of 2°, orders of scattering greater than one contribute only about two percent of the total scattered intensity.

From a comparison of the calculated and measured response data shown in both Figures 9 and 10, it appears that the ozone absorption and multiple scattering effects, which were not considered by Elterman in his analysis of the measured data, cancel out each other. The good agreement between the calculated and measured data as seen in Figure 10 indicates that the aerosol scattering coefficient variation with altitude is accurately given by Elterman's analysis of the measured response data from the searchlight experiment.

The altitude variation of the aerosol scattering coefficient obtained by Elterman from the searchlight experiment is, as shown in Figure 6, considerably different from that given by his "clear standard atmosphere" model. To investigate the effect that the altitude variation of the aerosol scattering coefficient has on the calculated receiver response, a LITE-I problem was run to determine the variation of the single scattered intensities with receiver angle of elevation for an atmosphere described by Elterman's model for a "clear standard atmosphere". The Reeger and Siedentopf phase function was used to describe

the angular distribution for aerosol scattering. The results of the LITE-I single scattering problem for the "clear standard atmosphere" are compared in Figure 11 with the results obtained for an atmosphere where the aerosol scattering coefficient was taken to be that given by an analysis of the measured response data from the searchlight experiment. The single scattered intensities from the calculations for the two different aerosol atmospheres do not differ significantly except in the region between receiver angles of elevation of two to ten degrees. For receiver angles of elevation above ten degrees the "clear standard atmosphere" has a smaller aerosol cross section than does the atmosphere at the time of the searchlight experiment. This results in higher single Rayleigh scattered intensities due to the decreased attenuation along the path from the source-to-scattering volume-to-receiver.

The results of the LITE-I calculations for analysis of the searchlight experiment indicate that the LITE-I code is capable of predicting with reasonable accuracy the measured receiver response data.

3.3 Analysis of Measured Sunlight Transmission Data

The LITE-II code was used to analyze the results of a high altitude balloon flight carried out by the Air Force Cambridge Research Laboratory (Reference 8) which measured various brightness parameters at 100,000 altitude. The experimental data gave for the 100,000 foot level the illuminance (i.e., the incident radiation for a photopic spectral sensitivity) on a vertical surface as a function of the solar zenith angle. Data were taken for cases where the normal to the vertical surface was facing the sun ($\phi = 0°$) or facing opposite to the sun direction.

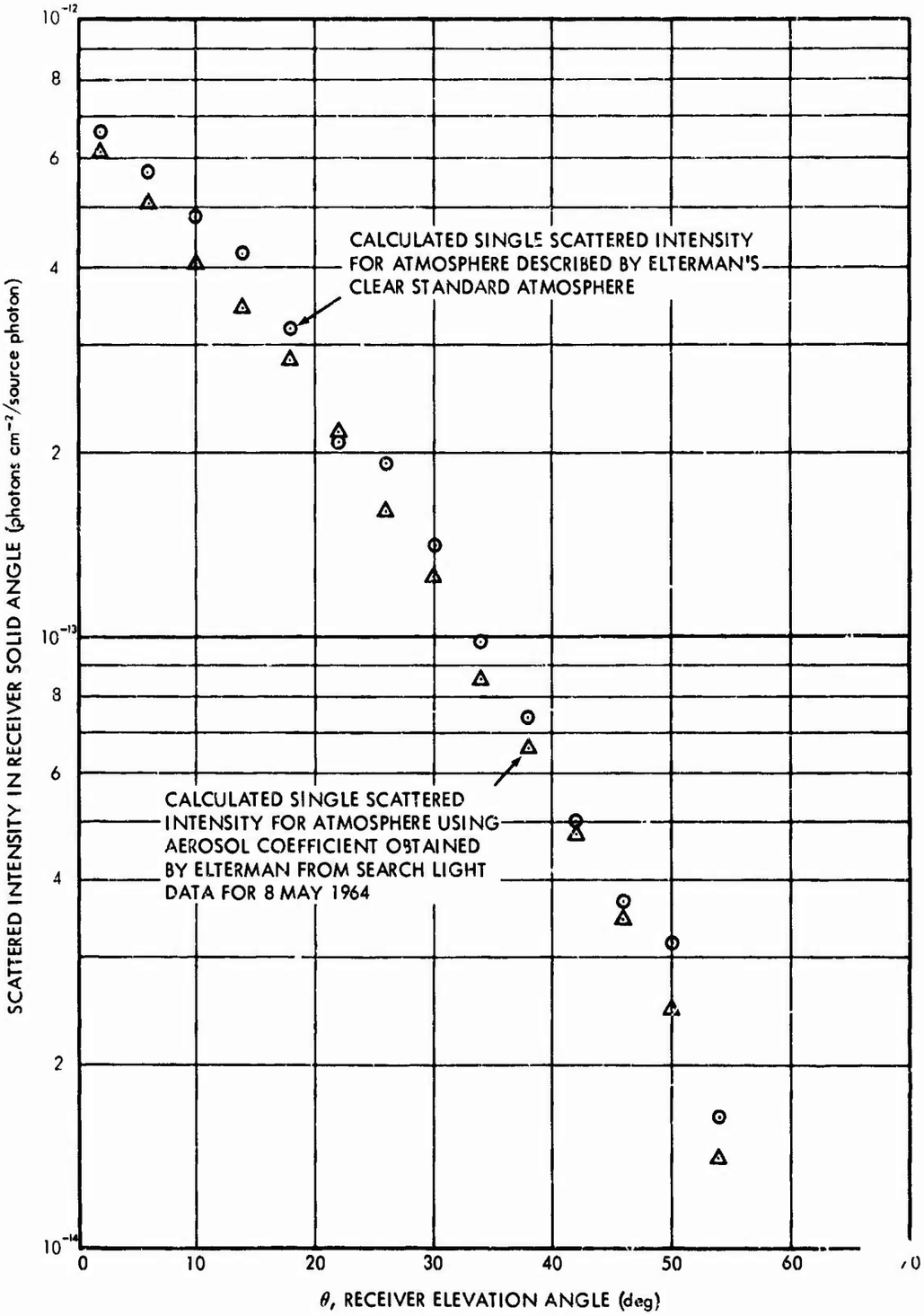

Fig. 11. Comparison of Single Scattering Calculations for Two Different Altitude Distributions of the Aerosol Coefficient

The calculations were made for 0.5 micron wave length plane parallel sources since that wave length corresponds approximately to the peak of the photopic curve. The atmosphere was described by the Elterman model for a "clear standard atmosphere". The phase function for aerosol scattering was described by Fraser's (Reference 9) Model C aerosol size distribution. The ground surface reflectivity was estimated to be about ten percent, but during the balloon flight, there was a change in cloud cover which could have changed the reflectivity to about 50 percent.

The LITE-II output gave the polar and azimuthal angular distributions of the scattered intensities at an altitude of 30 km. By use of the Albedo Conversion Code (Reference 10), the LITE-II output was converted from intensities to fluxes across vertical flat plate receivers oriented so that they were either facing the sun or facing opposite to the sun direction. The scattered flux data for each receiver azimuthal direction and sun zenith angle were multiplied by the secant of the solar zenith angle to give fluxes for a source strength of one photon cm^{-2} passing through a surface normal to the sun direction. The results so obtained for ground albedos of 0.0, 0.5 and 1.0 are presented in Table I. The direct flux incident on the vertical receiver per photon per cm^2 of area normal to the zenith direction is given by the equation

$$N_D(\theta_o) = \tan\theta_1 \, e^{-\rho \sec\theta_o} ,$$

where ρ is the normal mean-free-path distance from an altitude of 30 km to the top of the atmosphere. For 0.5 micron wave length light $\rho = 0.004$.

Table I. Number Current Passing Through a Vertical Surface at an Altitude of 30 km: λ = 0.5 microns

(photons cm^{-2}/source photon cm^{-2} for source area normal to zenith direction)

Zenith Angle θ_o (deg)	Direct Flux $\phi = 0°$	Albedo	Scattered Flux $\phi = 0°$	Scattered Flux $\phi = 180°$
30	0.5774	0.0	9.13-2	1.01-2
		0.5	2.75-1	2.96-1
		1.0	4.99-1	5.27-1
40	0.8391	0.0	1.30-1	1.25-1
		0.5	3.34-1	3.42-1
		1.0	5.83-1	6.05-1
50	1.192	0.0	1.98-1	1.92-1
		0.5	4.38-1	4.29-1
		1.0	7.28-1	7.19-1
60	1.732	0.0	3.31-1	2.78-1
		0.5	6.26-1	5.79-1
		1.0	9.85-1	9.44-1

Therefore, very little error would be introduced by taking $N_D(\theta_o) = \tan\theta_o$. From the data given in Table I it is seen that although the scattered flux incident on the receiver is highly dependent on the ground albedo, the scattered flux passing through either side of the flat plate receiver is approximately a constant for a given source zenith angle and ground albedo.

A comparison of the calculated data for a ground albedo of 0.0 with the measurements is shown in Figure 12. The calculated total fluxes have been normalized to the measured data for $\phi = 0°$ at a zenith angle of 30° The calculated data indicates that the effective ground albedo for the measurement was close to zero. The measured flux for $\phi = 180°$ was overpredicted by a factor of 1.4 at $\theta_o = 30°$ and a factor of 2 at $\theta_o = 60°$. The overprediction of the scattered flux for $\phi = 180°$ is believed to be due to the fact that although the peak in the solar spectrum is at about 0.5 microns, nearly 76.5 percent of the incident energy has wave lengths above 0.5 microns. Since the scattering cross section decreases with increasing wave length, it is expected that the scattered flux would also decrease with increasing wave length provided the ground albedo was negligible. The wave length which divides the solar spectrum into two intervals containing one half of the incident energy is 0.72 microns. A review of Coulson, Dave and Sekera's (Reference 6) calculations of the number of photons reflected from a Rayleigh atmosphere showed that for a ground albedo of 0.0, the number reflected is dependent on the mean-free-path thickness of the atmosphere and the angle of incidence. An assumption that the extinction cross section is made up entirely of Rayleigh scattering for wave lengths of 0.5 and 0.72 microns would

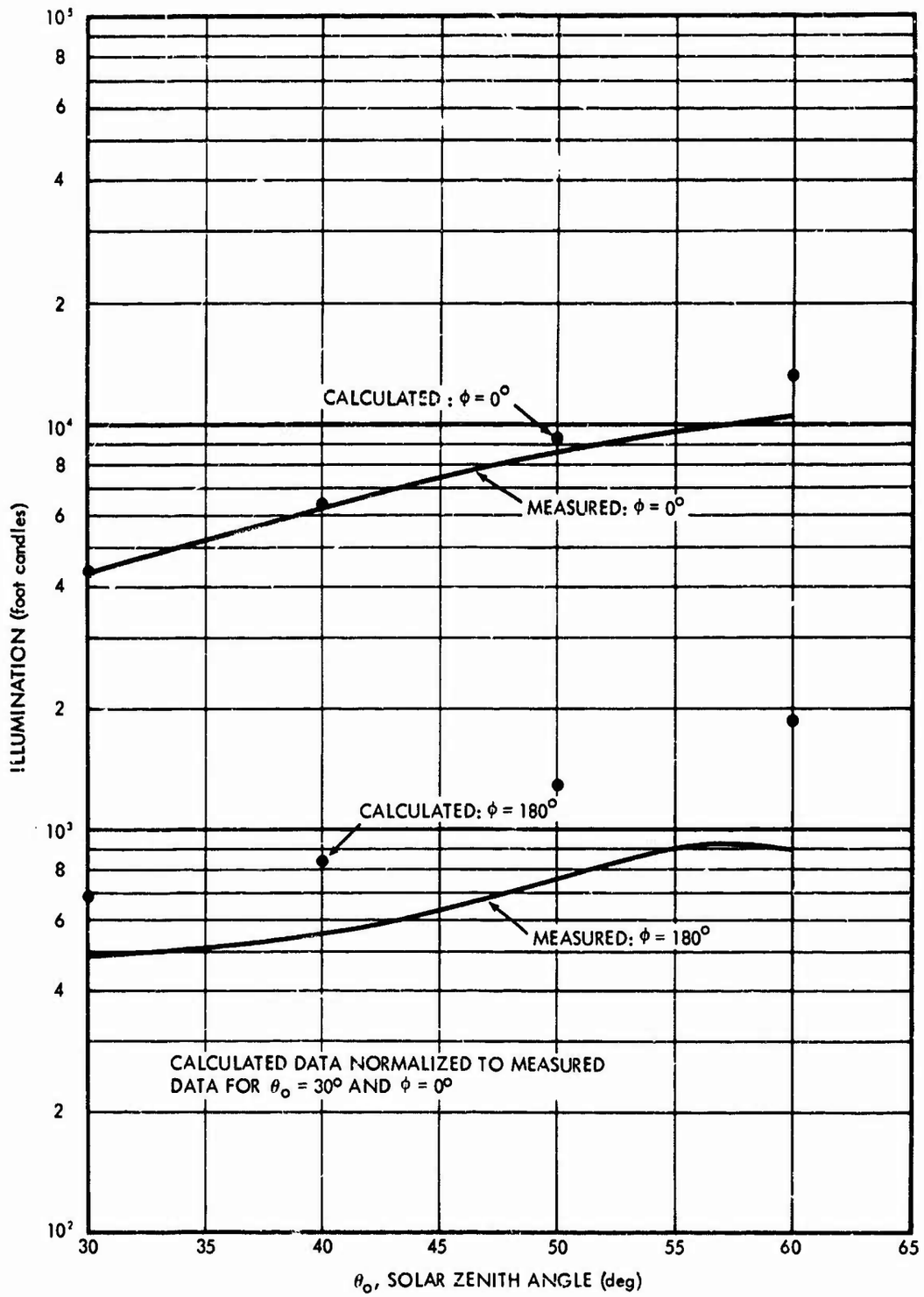

Fig. 12. Comparison of Calculated and Measured Illumination as seen by a Vertical Surface at an Altitude of 30 Km

result in about 1.5 times as many photons being reflected with a wave length of 0.5 microns as will be reflected with a wave length of 0.72 microns. A significant portion of the solar energy incident on top of the atmosphere with wave lengths above 0.7 microns will be absorbed by the water vapor and carbon dioxide in the atmosphere. Therefore, it is reasonable to expect that the scattered fluxes computed for 0.5 micron wave length light would be higher than those measured during the balloon experiment.

The percent transmission of light through the bottom of the atmosphere as a function of the source angle of elevation was obtained from the Monte Carlo calculations described above for 0.5 micron wave length light and from Monte Carlo calculations for 0.45 and 0.65 micron wave length light. The atmosphere for the 0.45 and 0.65 micron wave length sources was assumed to be that given by Elterman and the aerosol phase function was taken from Mie calculations for a size distribution proportional to r^{-4}. The results for a ground albedo of 0.0 are plotted in Figure 13 as a function of the source elevation angle. It is seen that the percent transmission increases with the source wave length and with the source elevation angle. The average percent transmission of sunlight for various solar angles of elevation was obtained from an analysis of measurements reported by 18 different weather stations (Reference 5). The results are compared in Figure 13 with the calculated data for 0.45, 0.50 and 0.65μ wave length light. The measured sunlight transmission data were taken from data compiled in Reference 5 for 0 to 30 percent cloud cover. There was no information available on the value of the ground albedo for each reporting station. It is difficult to draw any definite

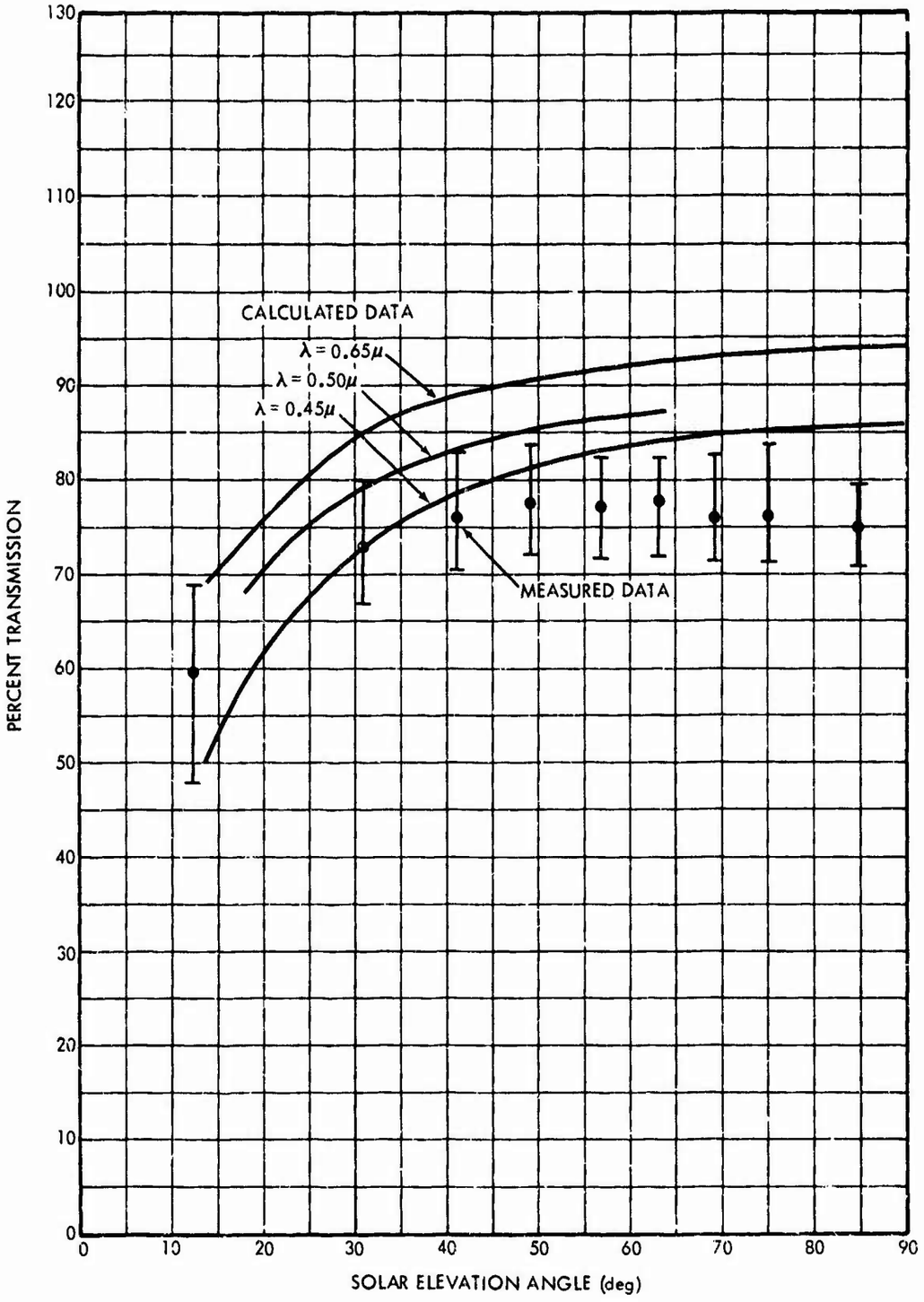

Fig. 13. Transmissivity as a Functian of Solar Elevation Angle: Ground Aibedo 0.0

conclusions about the agreement between the measured and calculated transmission data considering that the atmospheric conditions varied daily at each of the weather stations. It should be pointed out that the transmission for wave lengths above 0.7 microns should be less than that computed for a wave length of 0.65 microns since absorption by water vapor and CO_2 becomes important for wave lengths above 0.7 microns.

3.4 Comparison of LITE-II Calculations with Irvine's Calculations

Irvine (Reference 11) has conducted a study to determine the effect of varying the shape of the Mie scattering phase function on the angular intensities transmitted and reflected from both 0.5 and 1 mean-free-path length thick slab atmospheres. The phase functions used in Irvine's calculations were described by the expression

$$\phi(\cos\alpha) = b\phi_{HG}(g_1, \cos\alpha) + (1-b)\phi_{HG}(g_2, \cos\alpha)$$

where $\phi_{HG}(g, \cos\alpha) = \dfrac{1-g^2}{(1+g^2-2g\cos\alpha)^{3/2}}$.

We denote as case D the results obtained using values of 0.9724, 0.824 and -0.55 for b_1, g_1 and g_2, respectively in the equation for $\phi(\cos\alpha)$. The results obtained when $b_1 = 0.95$, $g_1 = 0.9$ and $g_2 = 0.75$ are denoted as case H. The phase function for case H is peaked more highly forward than is the phase function for case E. Figure 14 shows the cumulative distribution functions for cases E and H.

Two LITE-II problems were run for a plane source of light incident normal to an atmosphere one mean-free-path in thickness. In the first problem the phase function for case E was used, and in the second

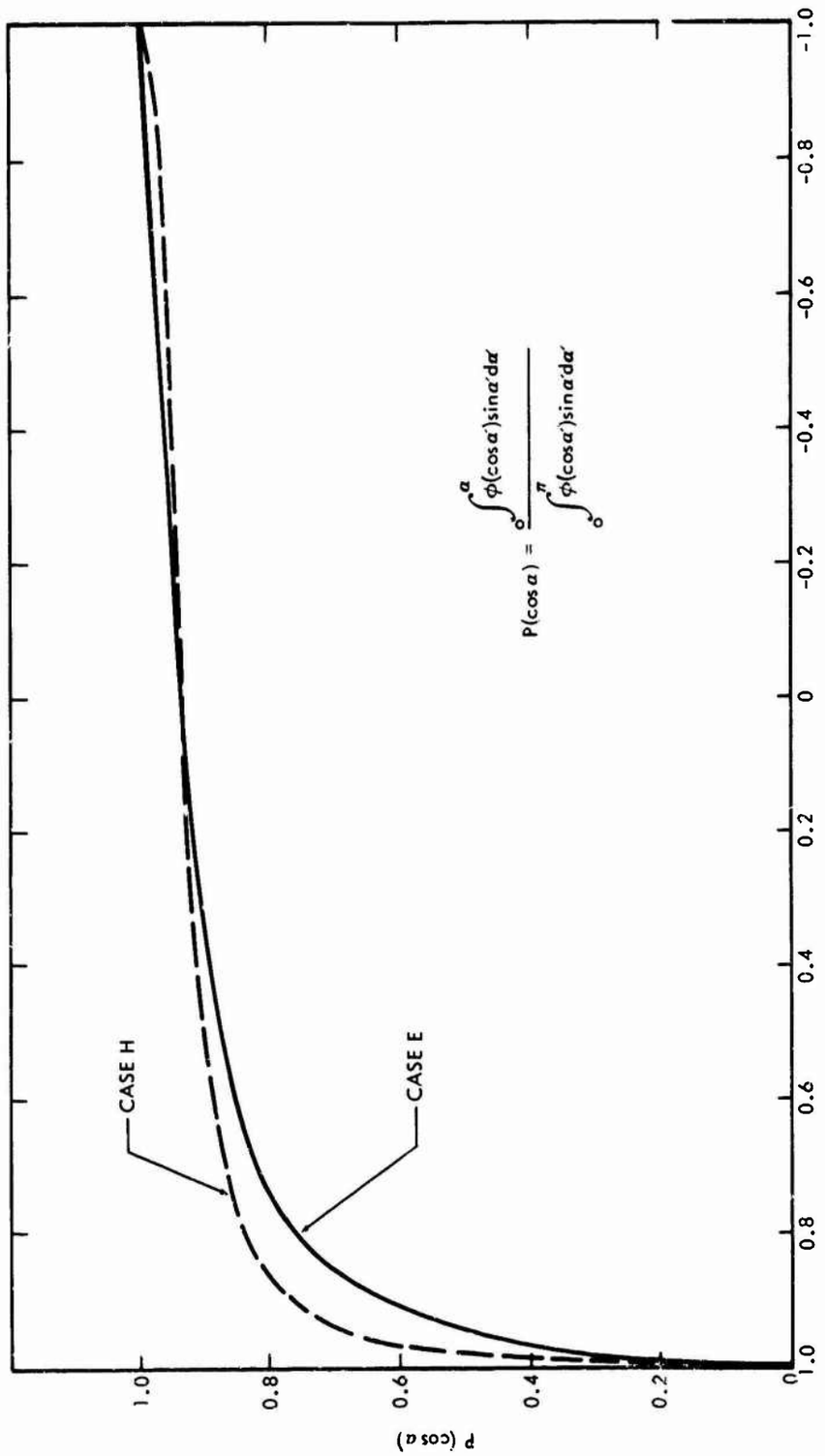

Fig.14. Cumulative Phase Functions for Cases E and H

problem, the phase function for case H was used. The results of the calculations for case E are compared in Figure 15. The LITE-II results and Irvine's results for case H are compared in Figure 16. The transmitted angular intensities obtained from the LITE-II results are in good agreement with Irvine's calculations. The differences between the results obtained from the LITE-II calculations and Irvine's calculations for the reflected intensities are probably due to poor statistics, since less than seven percent of the particles undergoing first collisions in the atmosphere scattered through an agnle greater than 90°. It is felt that better agreement in the reflected distribution would have been obtained if a larger number of histories had been used than the 4000 histories which were used in each of the LITE-II calculations.

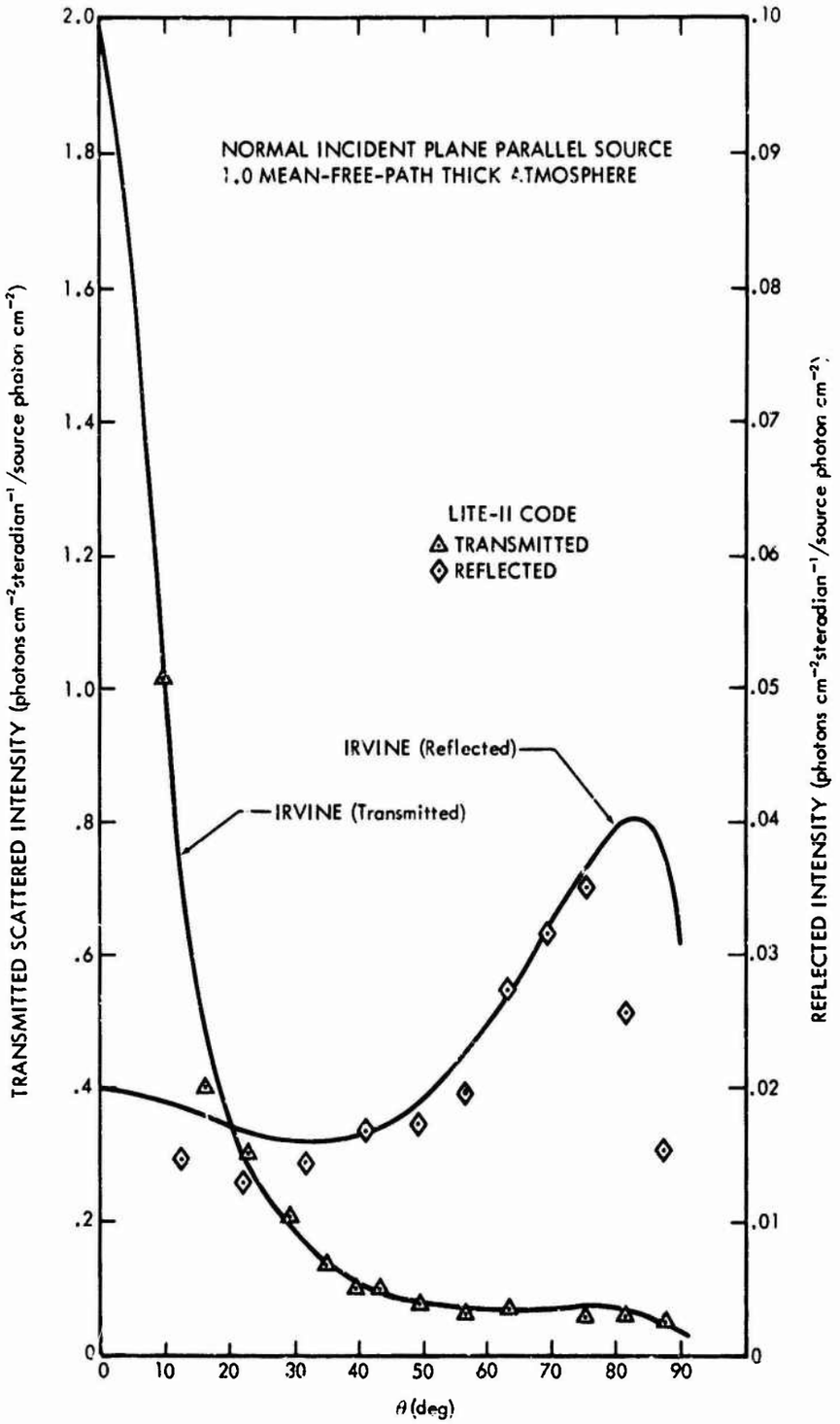

Fig.15. Diffuse Transmission and Reflection for Case E

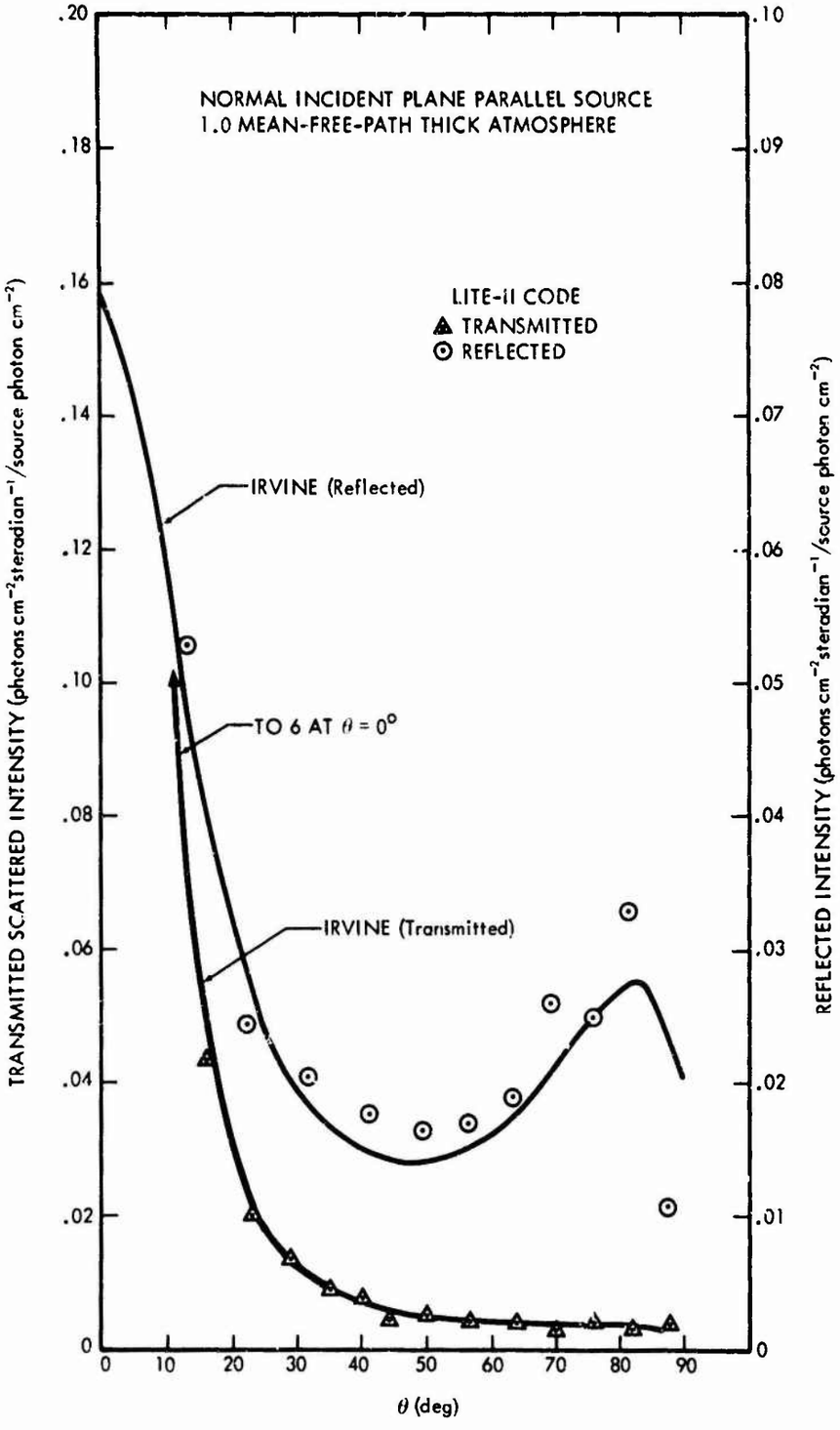

Fig. 16. Diffuse Transmission and Reflection for Case H

IV. CLOUD ALBEDO STUDIES

Monte Carlo calculations were run using the LITE-II code to determine the number albedo for 0.45 micron light incident to the top of a 1 km thick cloud at angles of incidence of 0, 30, 60 and 75 degrees. The phase function for 0.45 micron light scattering by the aerosol particles contained in the cloud was taken from the data reported in Reference 13 for an aerosol size distribution that had been suggested by Deirmendjian as typical of that found in cumulus clouds. The Monte Carlo results were obtained from sample sizes of 2000 histories per source angle with a maximum of 100 collisions per history. The Monte Carlo calculated scattered intensities in a given polar angle interval summed over all azimuthal angles of reflection were multiplied by

$$\frac{[\cos\theta_{i-1} + \cos\theta_i]}{4\pi(\cos\theta_{i-1} - \cos\theta_i)}$$

where θ_{i-1} and θ_i are the lower and upper bounds of the polar angle interval to give the number of photons reflected per steradian in direction θ per unit flux incident on the cloud.

Figures 17 through 20 present the calculated number albedo as a function of the polar angle of reflection for each angle of incidence considered. The smooth curves shown in Figures 17 through 20 are cosine distributions normalized so that the integral

$$2\pi N(\theta_o, \theta = 0°) \int_0^{\pi/2} \cos\theta \sin\theta d\theta ,$$

is equal to the Monte Carlo calculated value of the total number albedo, where $N(\theta_o, \theta = 0°)$ is the intercept at $\theta = 0°$ for the cosine

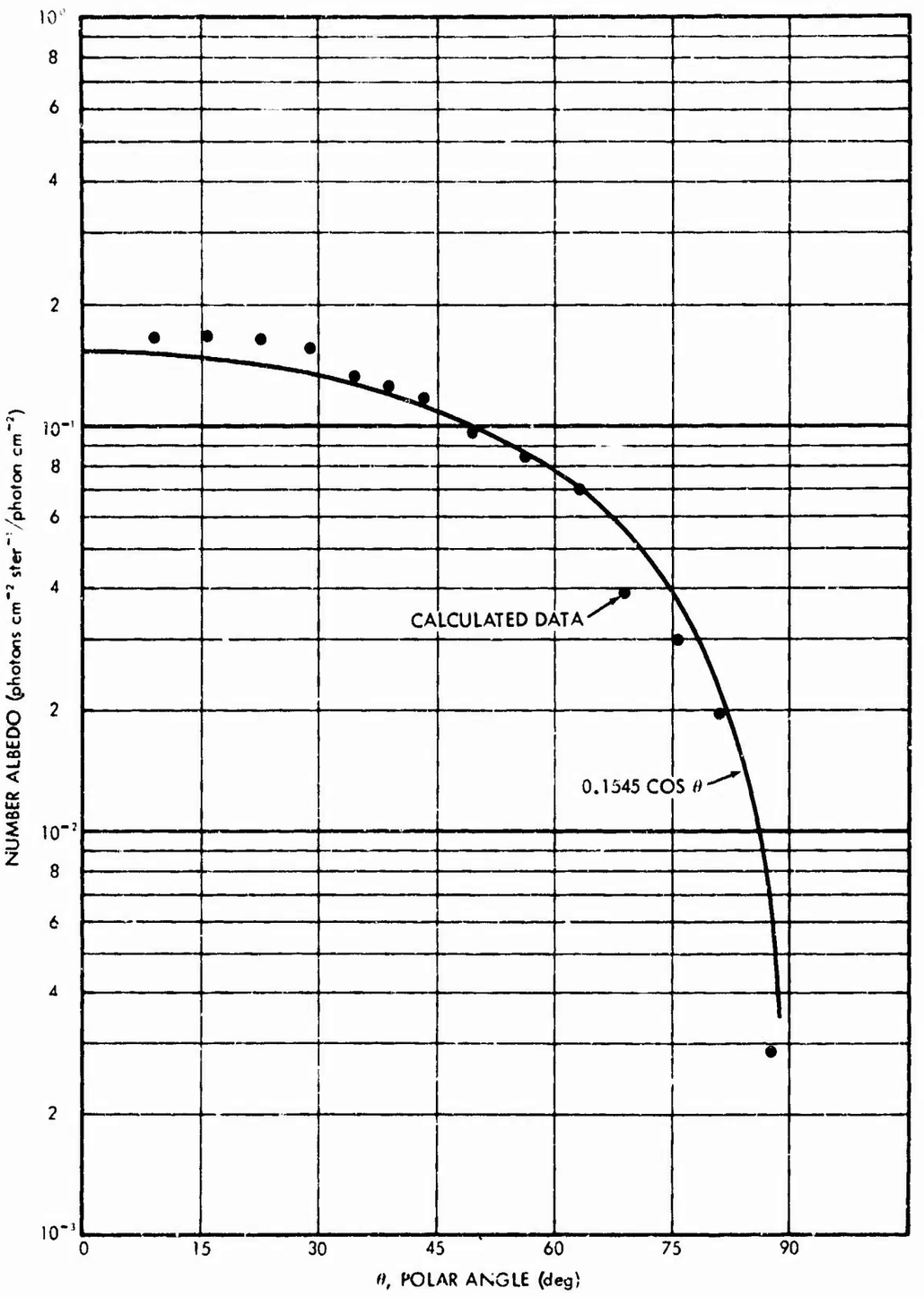

Fig. 17. Polar Angle Distribution of the Number Albedo for 0.45μ Light Incident on a 1 Km Thick Cumulus Cloud: θ_0 0°

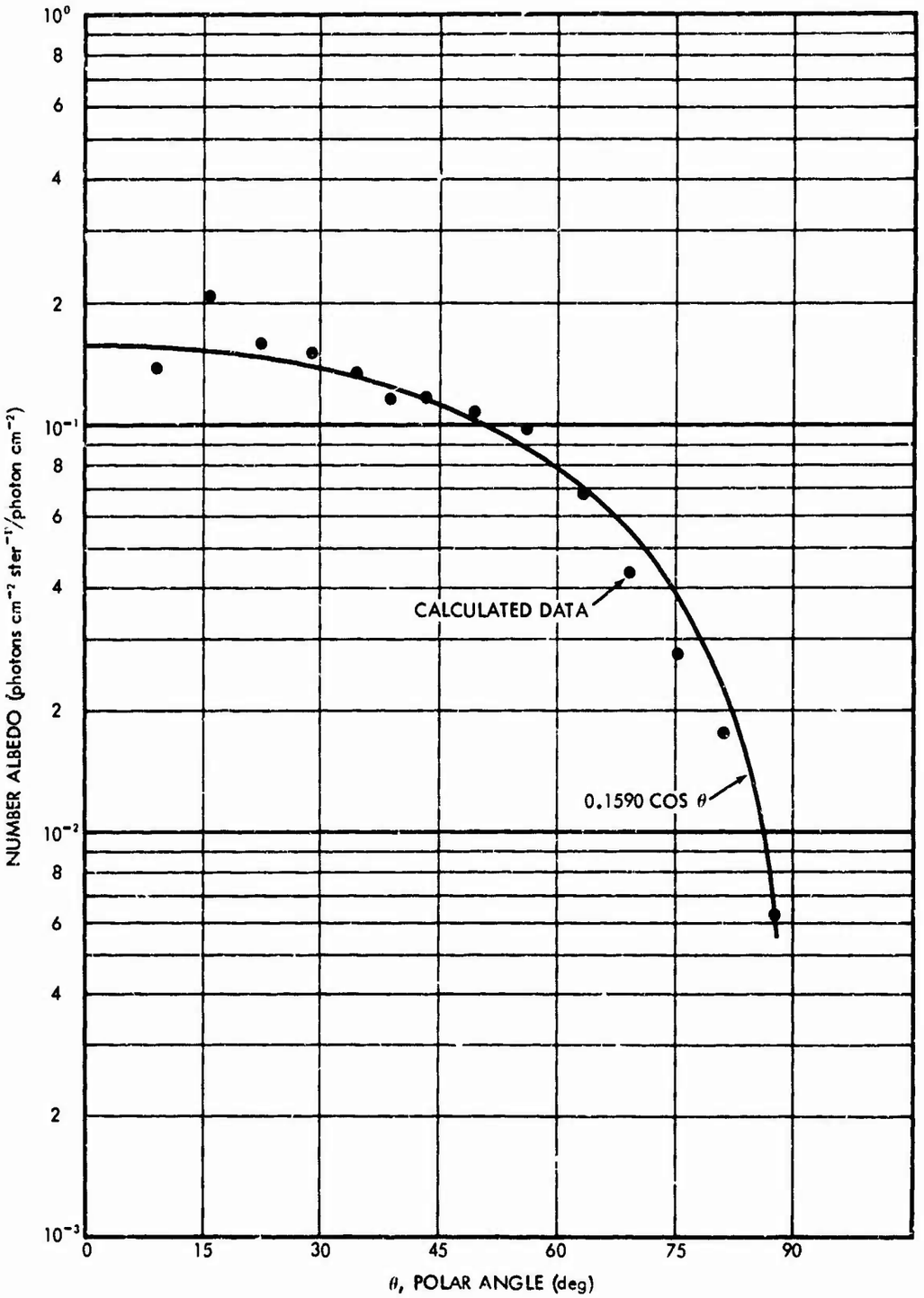

Fig. 18. Polar Angle Distribution of the Number Albedo for 0.45μ Light Incident on a 1 Km Thick Cumulus Cloud: $\theta_o = 30^o$

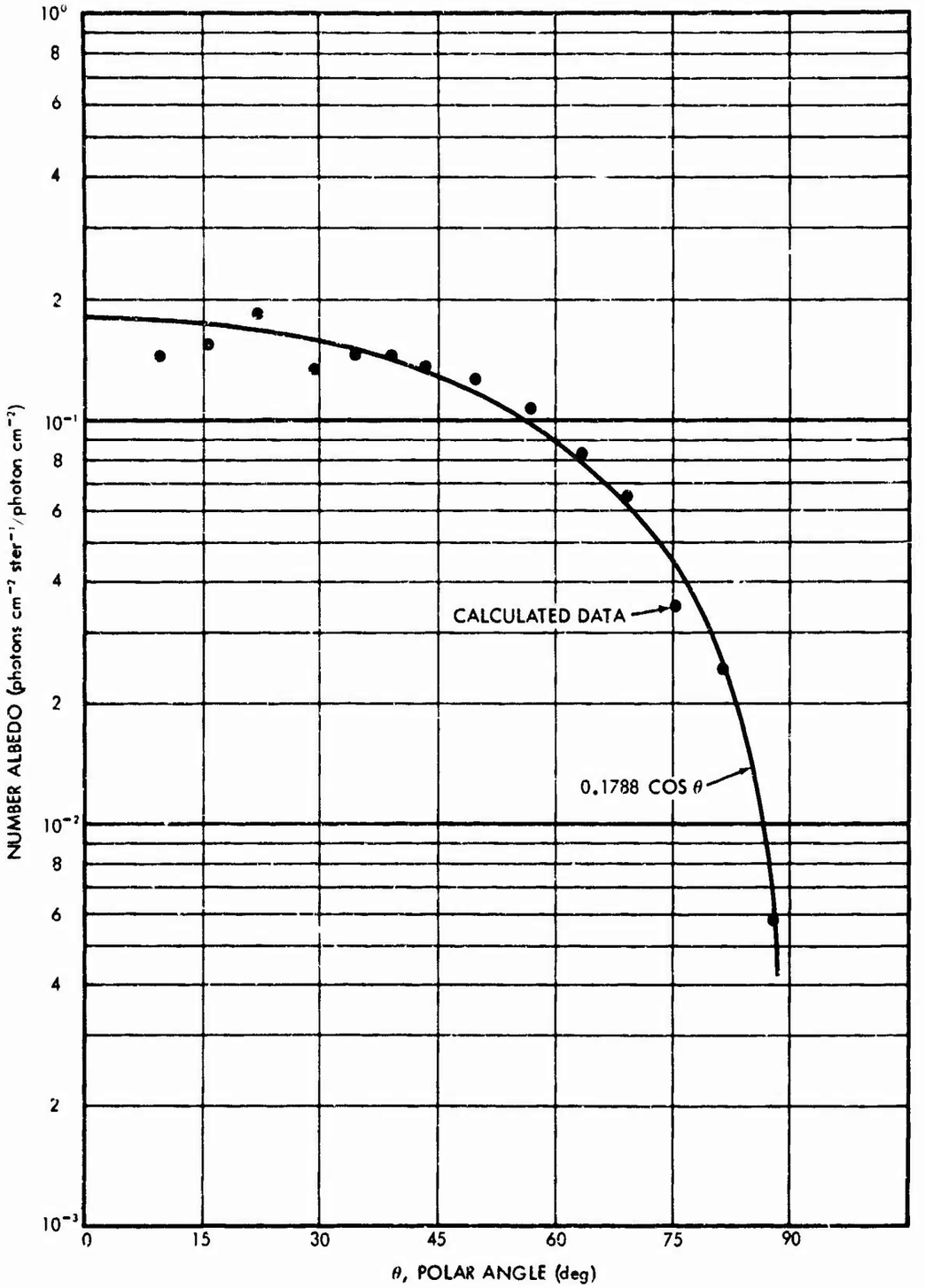

Fig. 19. Polar Angular Distribution of the Number Albedo for 0.45μ Light Incident on a 1 Km Thick Cumulus Cloud: $\theta_o = 60^o$

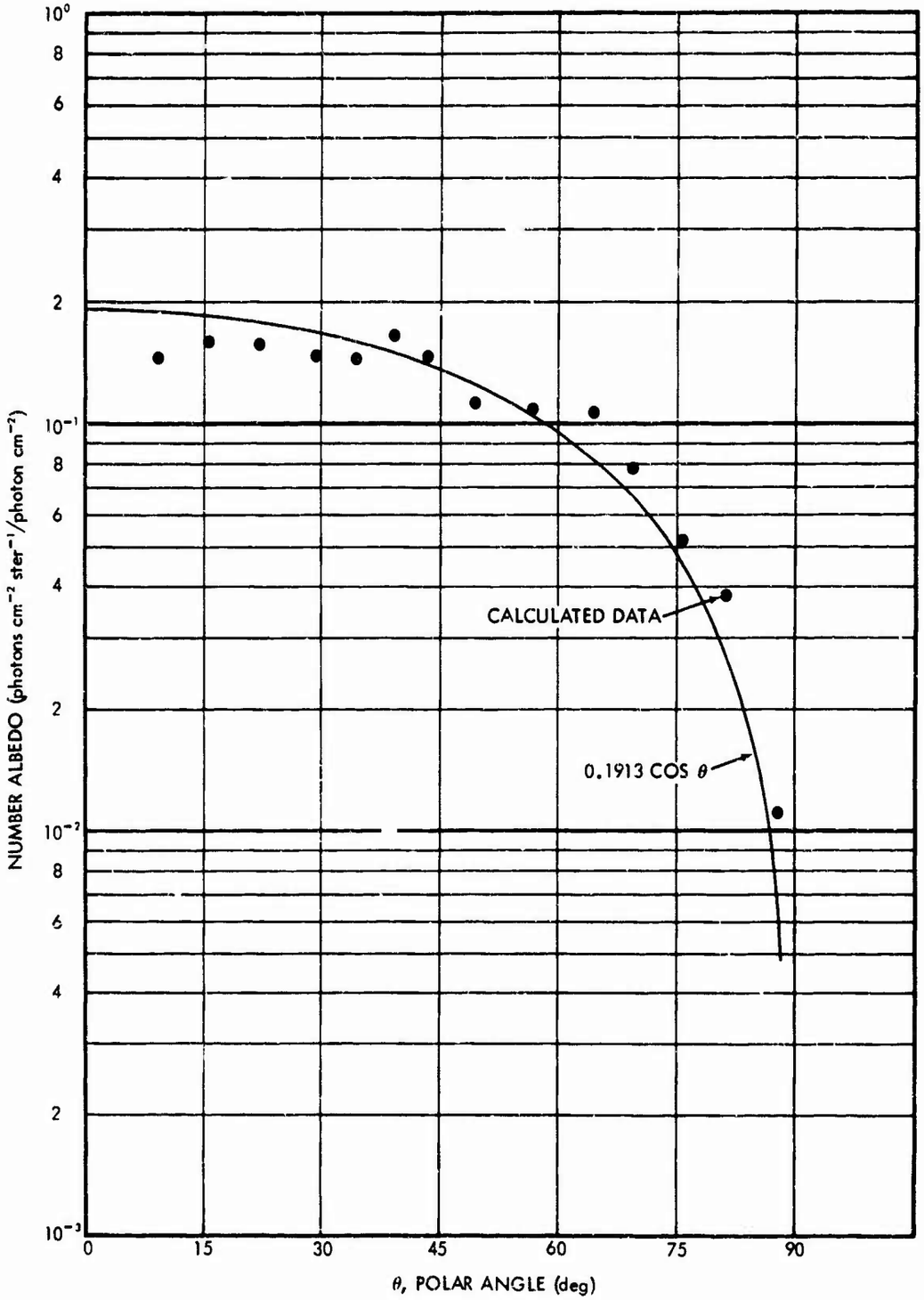

Fig. 20. Polar Angular Distribution of the Number Albedo for 0.45μ Light Incident on a 1 Km Thick Cumulus Cloud: $\theta_c = 75^\circ$

distribution. It is seen that the angular distributions as obtained from the Monte Carlo calculations are closely approximated by cosine distributions.

The total number albedo as a function of the angle of incidence was found to be closely approximated by the expression

$$\alpha(\theta_o) = 0.639 - 0.154\cos\theta_o$$

where θ_o is the angle of incidence. The results of Monte Carlo calculations reported by R. E. Maerker (Reference 12) for the thermal neutron number albedo of concrete gave the same functional dependence on the angle of incidence.

The differential number albedo for angles of incidence other than $\theta_o = 0°$ was found to be dependent on the azimuthal angle of reflection. Figure 21 illustrates this dependence for $\theta_o = 75°$. The data shown in Figure 21 give the dependence of differential number albedo on the polar angle of reflection in the plane of incidence.

The dependence of the intensity reflected from a cloud on the order of collision is shown in Figure 22. The rate at which the sum of the reflected intensity increases with collision number is seen to be dependent on the angle of incidence for collision numbers less than 30. For collision numbers greater than 30, the curves have the same shape, indicating that the contribution to the sum of the reflected intensities by a given order of collision is independent of the angle of incidence. One can infer from these data that the fraction of the total reflected intensity that has arisen from orders of scattering greater than 30 is

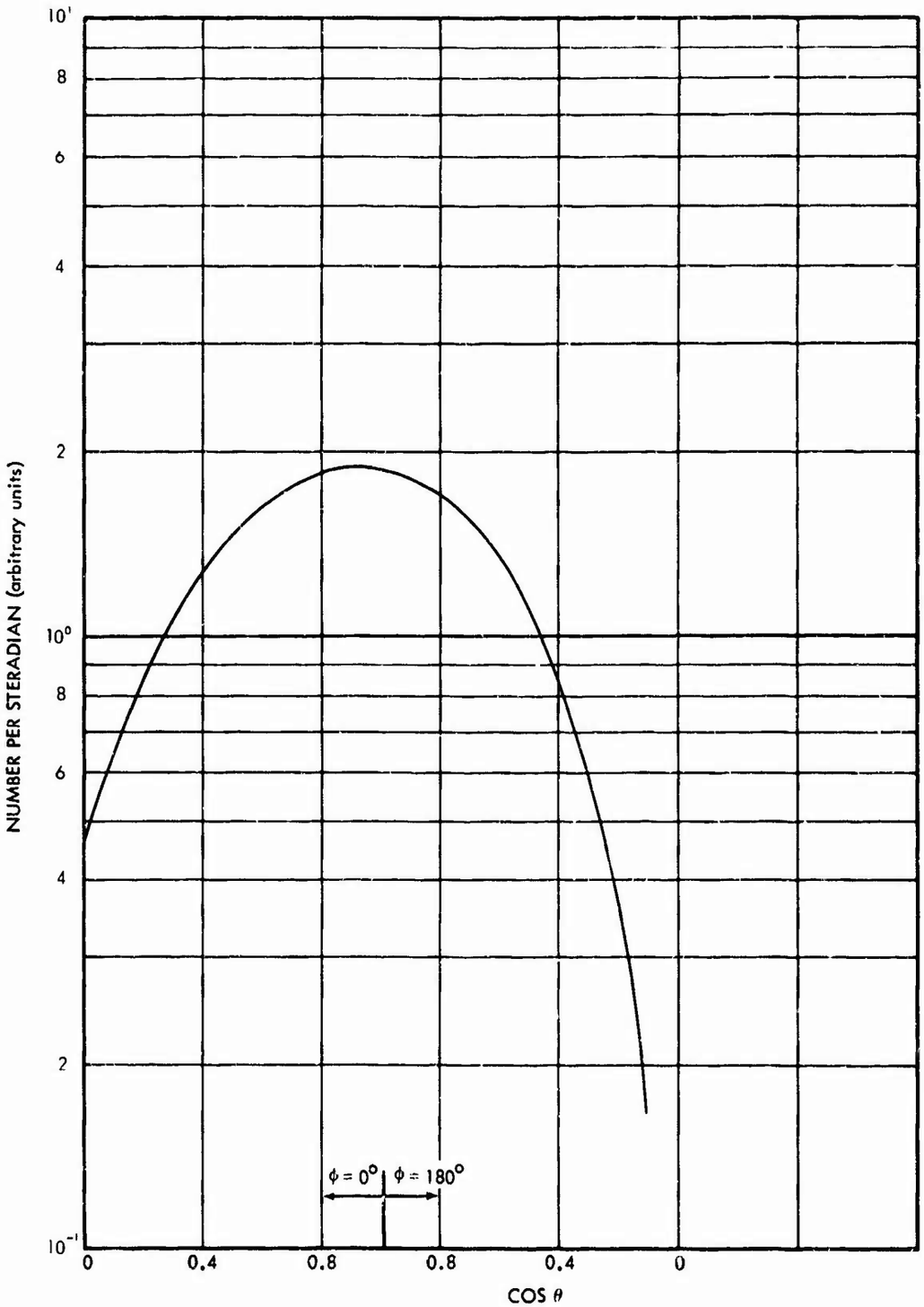

Fig. 21. Polar Angular Distribution of the Differential Number Albedo in the Plane of Incidence: $\theta_o = 75^o$

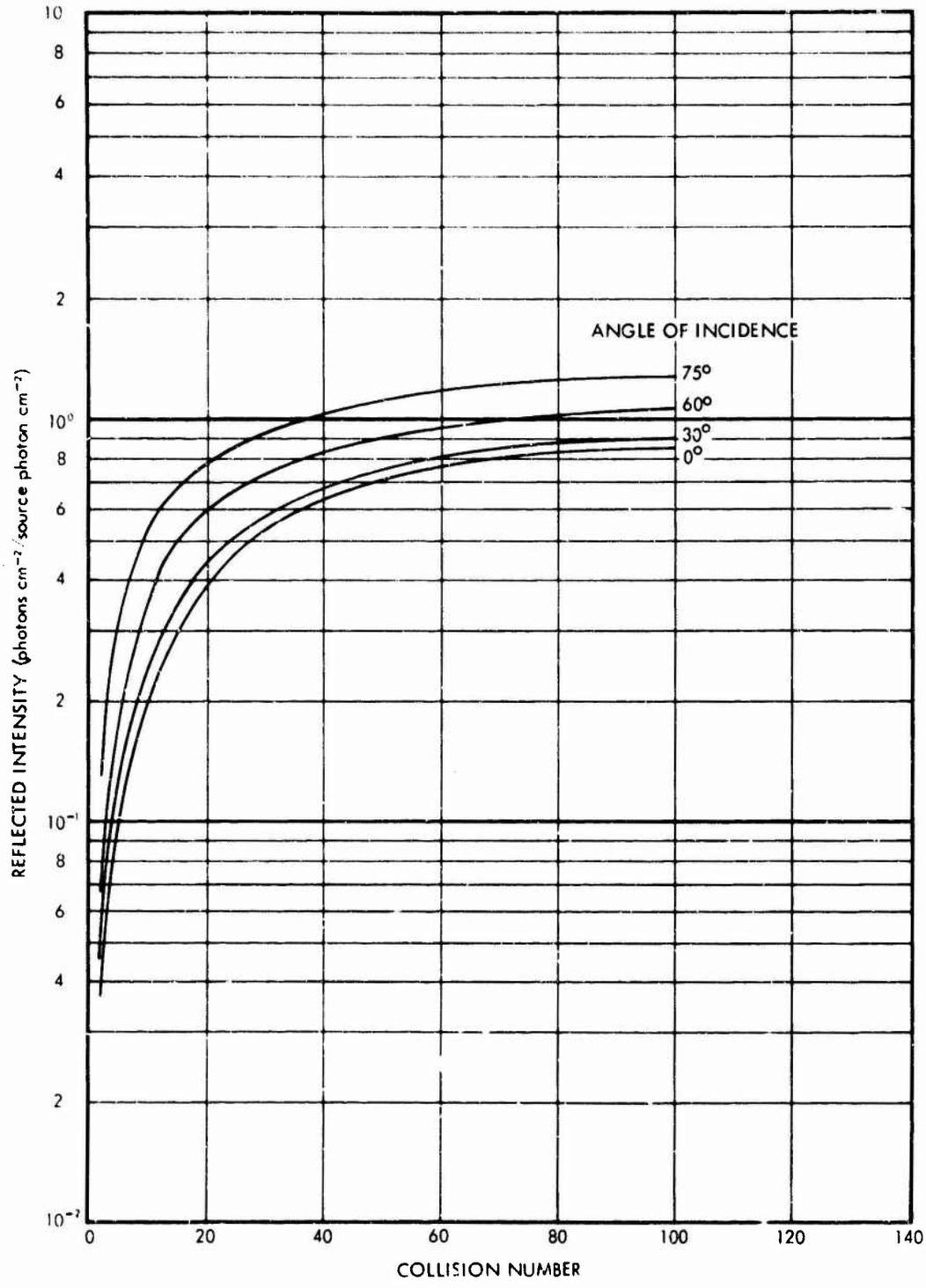

Fig. 22. Reflected Intensities from a 1 Km Thick Cumulus Cloud Summed over Collision Number for Various Angles of Incidence: 0.45μ Light

independent of the shape of the phase function. The leveling off of the cumulative sums of the reflected intensities with collision number indicates that contributions to the reflected intensity by orders of scattering greater than 100 would be negligible. It appears that less than a 10 percent error would have been introduced in the results if the histories had been terminated after 70 collision, thereby reducing the machine time requirements for the calculations by one third.

V. SENSITIVITY OF LIGHT SCATTERING CALCULATIONS TO CHANGES IN ATMOSPHERIC PARAMETERS

The LITE-I code was developed for use in computing the transport in the atmosphere of the thermal radiation emitted by a nuclear weapon detonation. The wide range of atmospheric conditions for which transmission data is needed indicated that a study should be performed to investigate the sensitivity of the LITE-I results to changes in the several parameters that define an atmosphere. The parameters selected for study were the source and receiver altitude, the aerosol number density, and the aerosol size distribution. Changes in the number density affect only the magnitude of the aerosol attenuation coefficient whereas changes in the size distribution affect both the magnitude of the aerosol attenuation coefficient and the shape of the aerosol phase function. Therefore, it is useful to know how much change would occur in calculations of the scattered intensities at a given receiver point if the aerosol number density, size distribution and altitude variation were varied.

5.1 Dependence on Source and Receiver Altitudes

Since the extinction cross section for a given wavelength of light varies with altitude, it is useful to know how the atmospheric attenuation of light emitted by a point isotropic source varies with both the source altitude and receiver altitude. To investigate the dependence of the light intensity on both receiver and source altitude, several LITE-I problems were run for source altitudes of 1, 10, 20, 30 and 45 km. Point receivers were placed at horizontal ranges to 75 km in a horizontal plane through the source and in a horizontal plane located at an altitude of 0.1 km.

The Elterman model atmosphere was used to describe the variation with altitude and wavelength of the Rayleigh scattering, aerosol scattering, and ozone absorption coefficients. The shape of the aerosol phase function was obtained from an integration of Mie data for spherical particles with an index of refraction of 1.5 over a particle size distribution given by the equation $N(r) \approx r^{-4}$ (Reference 13).

The atmospheric transmission calculations were made for monochromatic sources with wavelengths of 0.45 and 0.65 microns. The LITE-I output gave the scattered intensities at the receivers for ground albedos of 0.0 and 0.9. The angular distribution of the ground albedo was taken to be that for a Lambert-type surface.

The direct intensities at the various receiver positions were computed by use of the equation

$$I_D(HS,HD,HR) = \frac{e^{-\rho(HS,HD,HR)}}{4\pi[(HS-HD)^2+HR^2]}$$

where HS is the source altitude,

HD is the receiver altitude,

HR is the horizontal range, and

$\rho(HS,HD,HR)$ is the mean-free-path distance between the source and receiver. The mean-free-path distance $\rho(HS,HD,HR)$ was computed by use of the equation

$$\rho(HS,HD,HR) = \frac{[(HS-HD)^2 + HR^2]^{\frac{1}{2}}}{(HS-HD)} \int_{HD}^{HS} \rho'(h)dh$$

where $\rho'(h)$ is the mean-free-path distance from ground level to height h. The results obtained for the direct intensity at each of the receiver points are presented in Table II.

Table II. Direct Intensities for Point Isotropic Sources

(photons km^{-2}/ source photon)

Source Wavelength (μ)	Receiver Altitude (km)	Source Altitude (km)	Horizontal Range (km)					
			0	5	10	20	50	75
0.45	0.1	1	8.55-2*		1.66-4	8.92-6	1.37-8	1.26-10
0.45	0.1	10	5.56-4		2.35-4	6.81-5	4.36-6	7.71-7
0.45	0.1	20	1.31-4		9.97-5	5.47-5	8.70-6	2.52-6
0.45	0.1	30	5.75-5		5.05-5	3.64-5	1.00-5	3.76-6
0.45	0.1	45	2.54-5		2.40-5	2.04-5	9.13-6	4.43-6
0.45	10	10		3.03-3	7.20-4	1.63-4	1.93-5	6.69-6
0.45	20	20		3.15-3	7.80-4	1.92-4	2.85-5	1.22-5
0.45	30	30		4.17-3	7.88-4	1.95-4	3.03-5	1.31-5
0.45	45	45		3.18-3	7.95-4	1.99-5	3.17-5	1.40-5
0.65	0.1	1	8.92-2		2.67-4	2.28-5	1.44-7	4.29-9
0.65	0.1	10	6.59-4		2.99-4	9.99-5	1.05-5	2.83-6
0.65	0.1	20	1.60-4		1.25-4	7.27-5	1.49-5	5.49-6
0.65	0.1	30	7.02-5		6.23-5	4.62-5	1.48-5	6.43-6
0.65	0.1	45	3.10-5		2.94-5	2.53-5	1.23-5	6.51-6
0.65	10	10		3.14-3	7.72-4	1.87-4	2.74-5	1.13-5
0.65	20	20		3.15-3	7.80-4	1.91-4	2.88-5	1.22-5
0.65	30	30		3.17-3	7.88-4	1.95-4	3.03-5	1.31-5
0.65	45	45		3.18-3	7.95-4	1.99-4	3.17-5	1.40-5

*Read 8.55-2 and 8.55×10^{-2}

The LITE-I calculated scattered intensities were added to the direct intensities to obtain the total intensity at each receiver position. The results are presented in Table III as a function of the source wavelength, ground albedo, receiver altitude, source altitude and horizontal range.

The total intensities given in Table III were multiplied by $4\pi R^2$ where R, the source-receiver distance in km, is given by the equation

$$R = [(HS-HD)^2 + HR^2]^{\frac{1}{2}} .$$

The results were then plotted as a function of R for each source altitude. Multiplying the total intensities by $4\pi R^2$ removes the geometrical attenuation and reduces the numerical range over which the intensities vary.

The results obtained for the 0.45 micron light sources giving $4\pi R^2$ times the total intensity as a function of the slant range R are presented in Figures 23 and 24 for a receiver altitude of 0.1 km and in Figures 25 and 26 for the case where the source and receivers were at the same altitude. Similar data for the 0.65 micron light sources are presented in Figures 27 through 30.

A comparison of the data shown in Figures 23 through 30 for ground albedos of 0.0 and 0.9 show that the effect of increasing the ground albedo is to increase the total intensity at a given receiver position over that computed for a ground albedo of 0.0. The amount of the increase in the intensity resulting from ground scattering is, for a given value of the ground albedo, a function of the source altitude, the receiver altitude, and the horizontal range. The dependence of the intensity at a given receiver position on the magnitude of the ground albedo was found to be exponential.

Table III. Calculated Total Intensities for Point Isotropic Light Sources

(photons km^{-2}/source photon)

Source Wavelength (μ)	Ground Albedo	Receiver Altitude (km)	Source Altitude (km)	Ground Range (km)					
				0	5	10	20	50	75
0.45	0.0	0.1	1	1.00-1*		5.66-4	6.69-5	2.31-6	5.20-7
0.45	0.0	0.1	10	8.06-4		3.58-4	1.26-4	1.07-5	1.77-6
0.45	0.0	0.1	20	1.67-4		1.27-4	7.37-5	1.39-5	4.02-6
0.45	0.0	0.1	30	7.17-5		6.39-5	4.85-5	1.56-5	5.46-6
0.45	0.0	0.1	45	2.84-5		2.72-5	2.39-5	1.24-5	6.13-6
0.45	0.9	0.1	1	2.16-1		8.17-4	9.89-5	5.51-6	1.52-6
0.45	0.9	0.1	10	1.51-3		6.35-4	2.36-4	1.64-5	3.12-6
0.45	0.9	0.1	20	2.31-4		1.77-4	1.09-4	2.05-5	5.05-6
0.45	0.9	0.1	30	1.01-4		9.55-5	7.14-5	1.85-5	6.28-6
0.45	0.9	0.1	45	4.65-5		4.16-5	3.47-5	1.51-5	7.73-6
0.45	0.0	10	10		3.28-3	8.40-4	2.14-4	3.10-5	1.25-6
0.45	0.0	20	20		3.23-3	8.30-4	2.17-4	3.70-5	1.67-5
0.45	0.0	30	30		3.20-3	8.10-4	2.08-4	3.53-5	1.63-5
0.45	0.0	45	45		3.18-3	8.01-4	2.03-4	3.47-5	1.64-5
0.45	0.9	10	10		3.55-3	1.04-3	3.10-4	4.79-5	1.69-5
0.45	0.9	20	20		3.30-3	8.97-4	2.65-4	5.23-5	2.29-5
0.45	0.9	30	30		3.24-3	8.48-4	2.36-4	4.75-5	2.25-5
0.45	0.9	45	45		3.20-3	8.15-4	2.16-4	4.34-5	2.19-5
0.65	0.0	0.1	1			4.57-4	6.38-5	1.77-6	3.34-7
0.65	0.0	0.1	10	7.84-4		3.60-4	1.32-5	1.74-5	5.06-6
0.65	0.0	0.1	20	1.76-4		1.36-4	8.08-5	1.80-5	6.80-6
0.65	0.0	0.1	30	8.02-5		6.98-5	5.16-5	1.69-5	7.38-6
0.65	0.0	0.1	45	3.55-5		3.31-5	2.83-5	1.37-5	7.18-6

*Read 1.00-1 as 1.00×10^{-1}

Table III. (Continued)

(photons km^{-2}/source photon)

Source Wavelength (μ)	Ground Albedo	Receiver Altitude (km)	Source Altitude (km)	Ground Range (km)					
				0	5	10	20	50	75
0.65	0.9	0.1	1			5.97-4	7.78-5	2.94-6	6.84-7
0.65	0.9	0.1	10	9.80-4		4.44-4	1.67-4	2.02-5	5.98-6
0.65	0.9	0.1	20	2.50-4		1.83-4	1.09-4	2.17-5	8.19-6
0.65	0.9	0.1	30	9.57-5		8.44-5	6.22-4	1.89-5	8.79-6
0.65	0.9	0.1	45	4.42-5		3.94-5	3.41-5	1.75-5	9.91-6
0.65	0.0	10	10		3.22-3	8.14-4	2.08-4	3.38-5	1.46-5
0.65	0.0	20	20		3.18-3	7.95-4	1.98-4	3.19-5	1.42-5
0.65	0.0	30	30		3.18-3	7.94-4	1.99-4	3.22-5	1.44-5
0.65	0.0	45	45		3.18-3	7.97-4	2.00-4	3.27-5	1.48-5
0.65	0.9	10	10		3.53-3	1.03-3	3.18-4	5.14-5	1.82-5
0.65	0.9	20	20		3.33-3	8.71-4	2.55-4	5.12-5	2.15-5
0.65	0.9	30	30		3.22-3	8.30-4	2.29-4	4.75-5	2.28-5
0.65	0.9	45	45		3.20-3	8.13-4	2.15-4	4.30-5	2.16-5

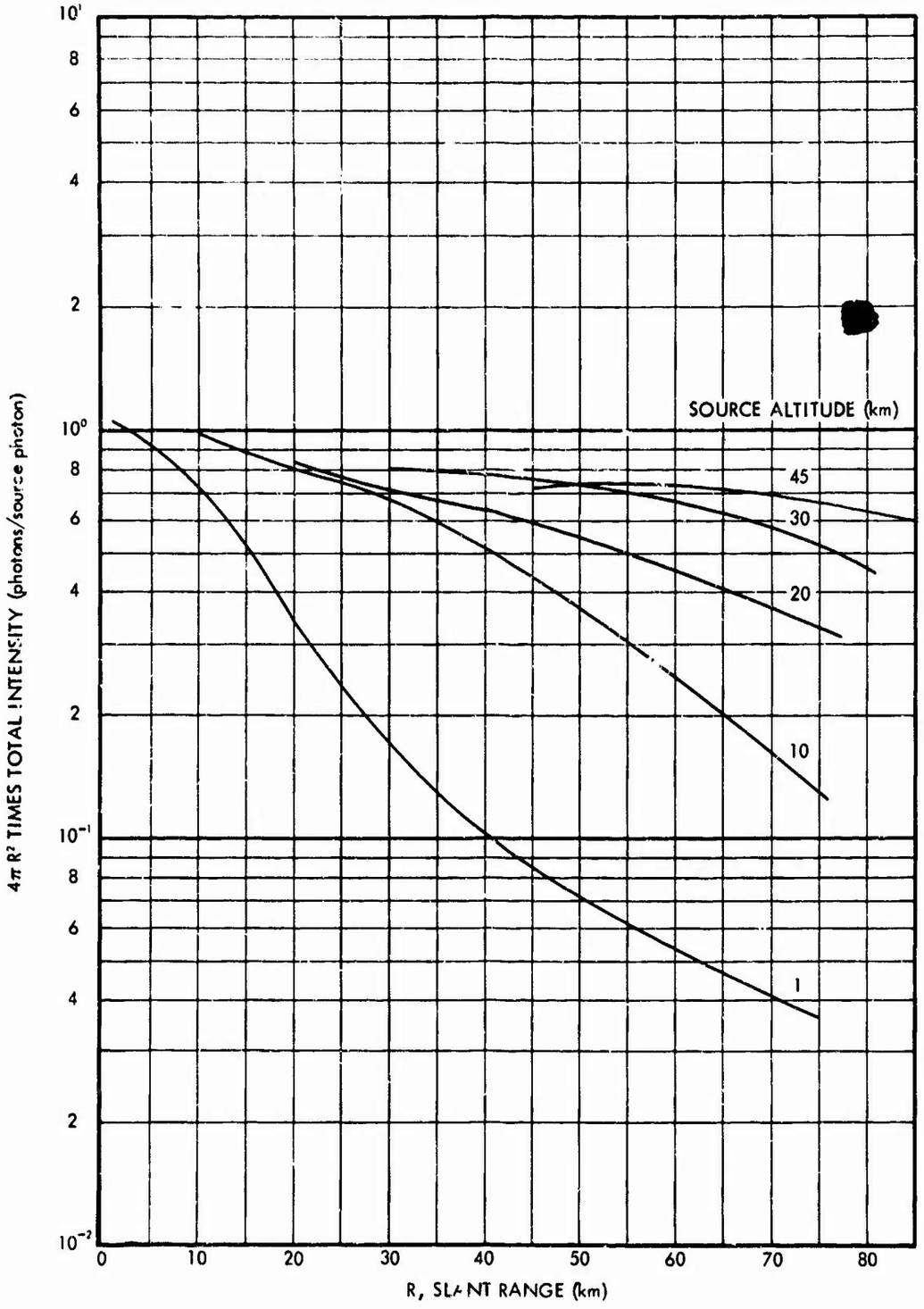

Fig. 23. Variation of $4\pi R^2$ Times Total Intensity with Slant Range: 0.45μ Light, Ground Albedo = 0.0, Receiver Altitude = 0.1 Km

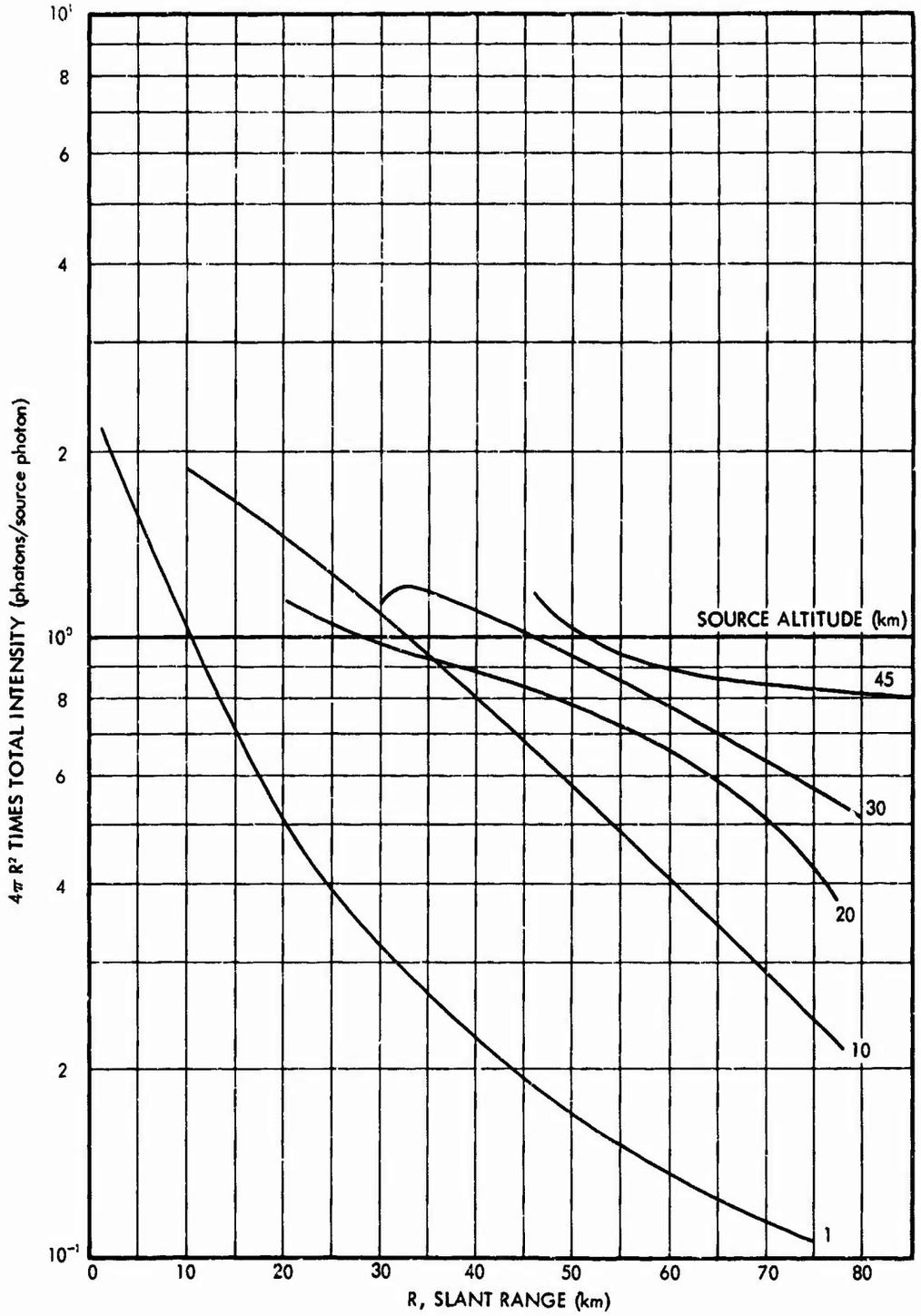

Fig. 24. Vcriation of $4\pi R^2$ Times Tatal Intensity with Slant Range: 0.45μ Light, Ground Albeda = 0.9, Receiver Altitude = 0.1 Km

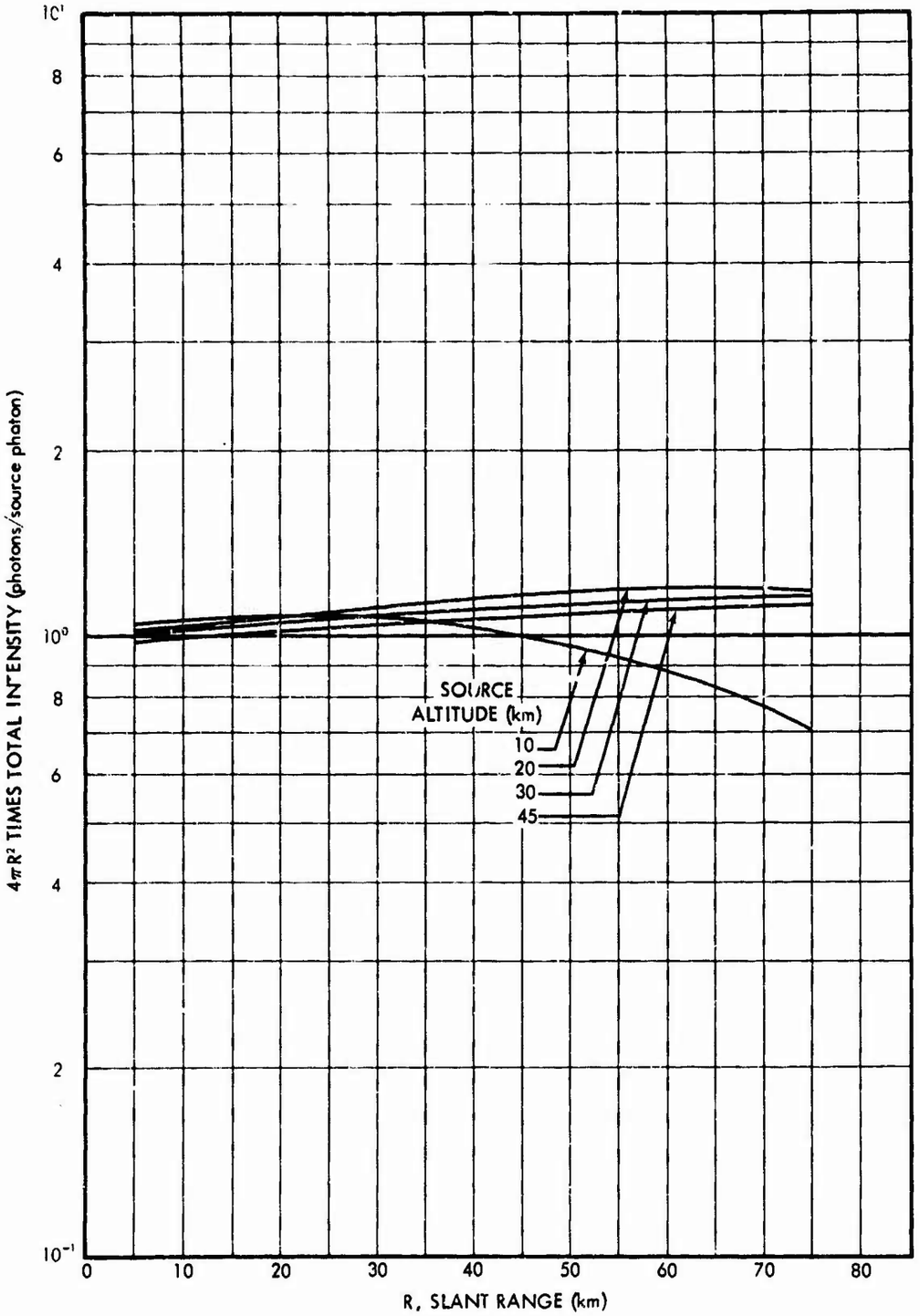

Fig. 25. Variation of $4\pi R^2$ Times Total Intensit with Slant Range: 0.45μ Light, Receiver and Source at Same Altitude, Ground Albedo = 0.0

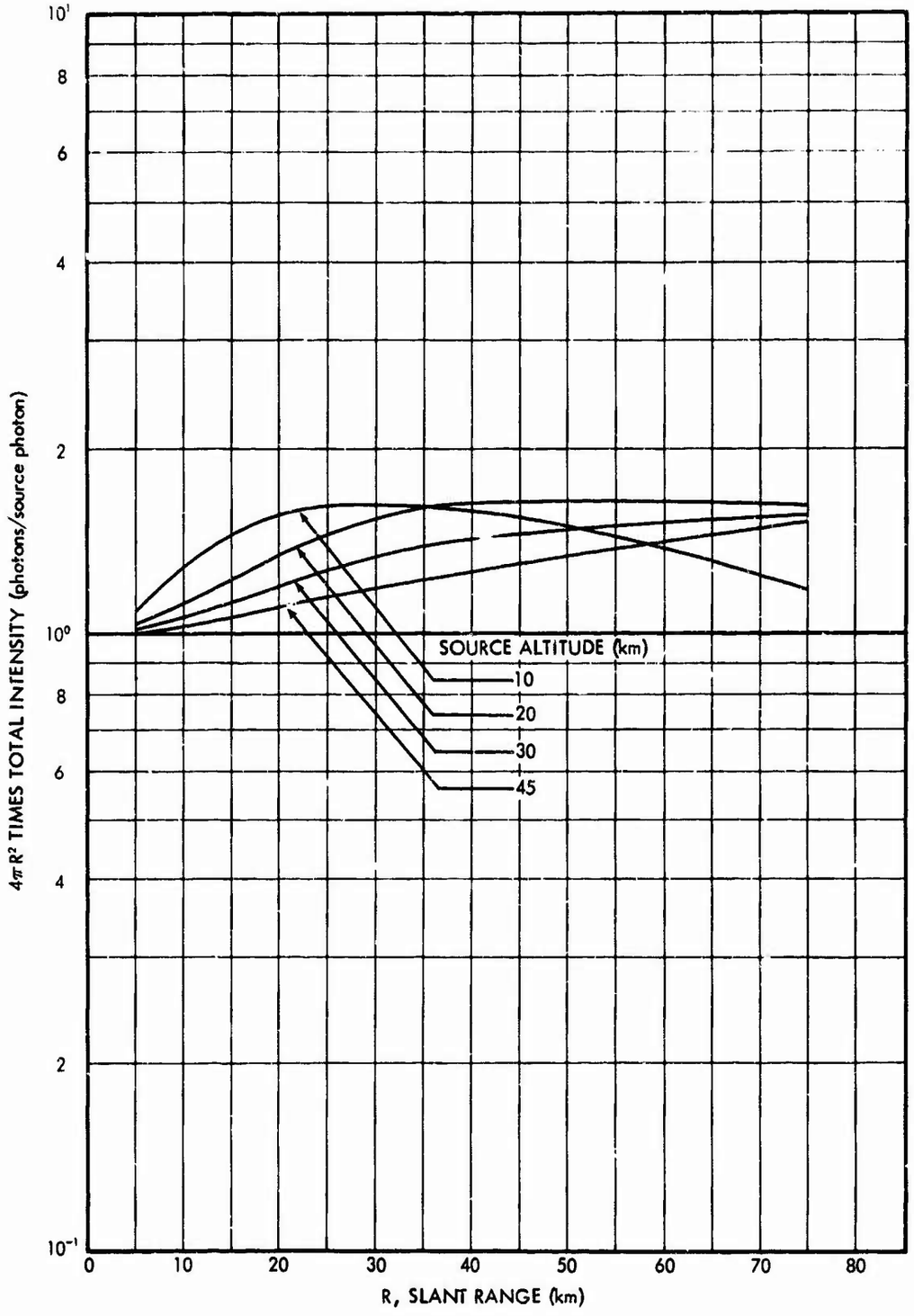

Fig. 26. Variation of $4\pi R^2$ Times Total Intensity with Slant Range: 0.45μ Light, Receiver and Source at Same Altitude, Ground Albedo = 0.9

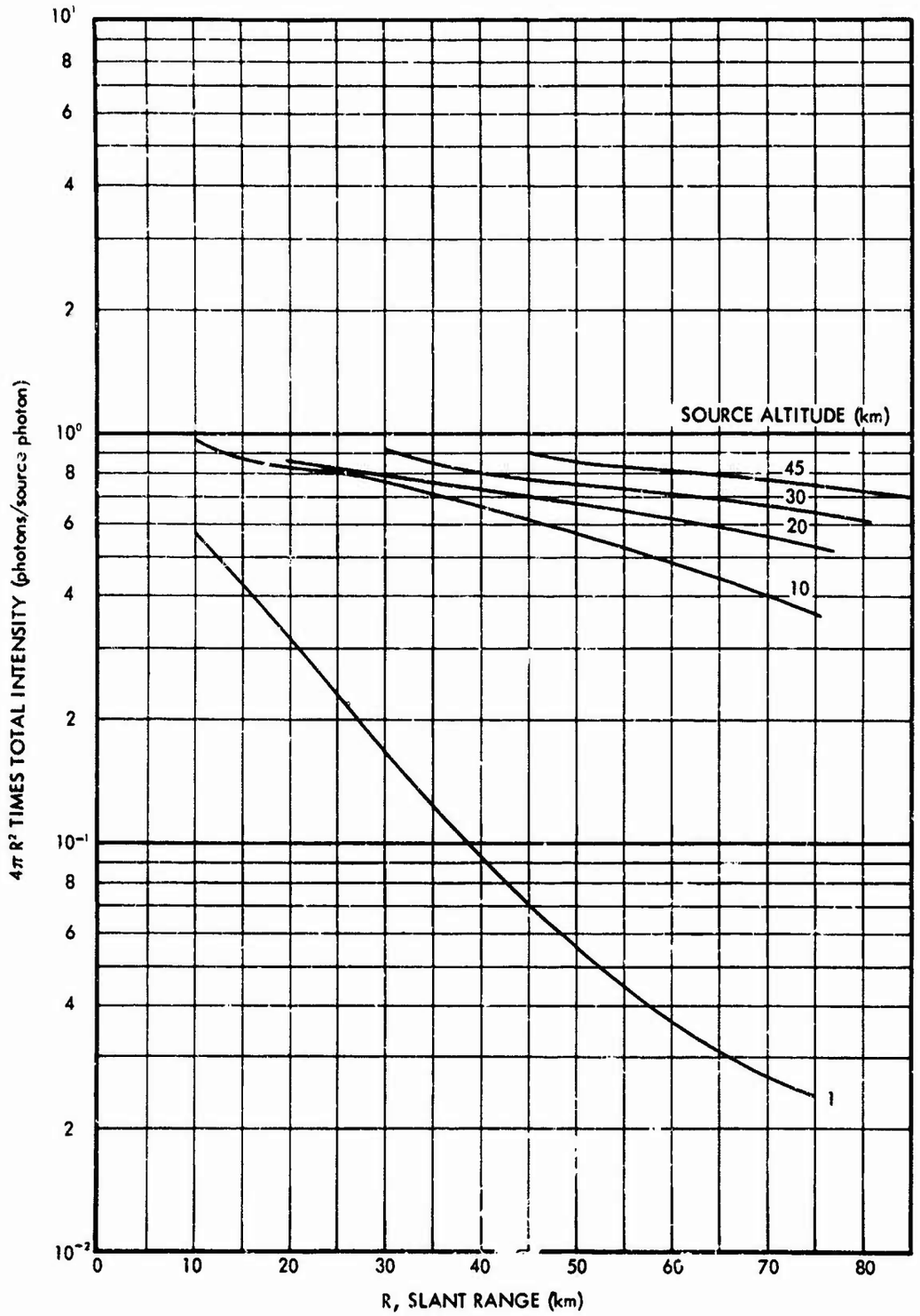

Fig. 27. Variation of $4\pi R^2$ Times Total Intensity with Slant Range: 0.65μ Light, Receiver Altitude = 0.1 Km, Ground Albedo = 0.0

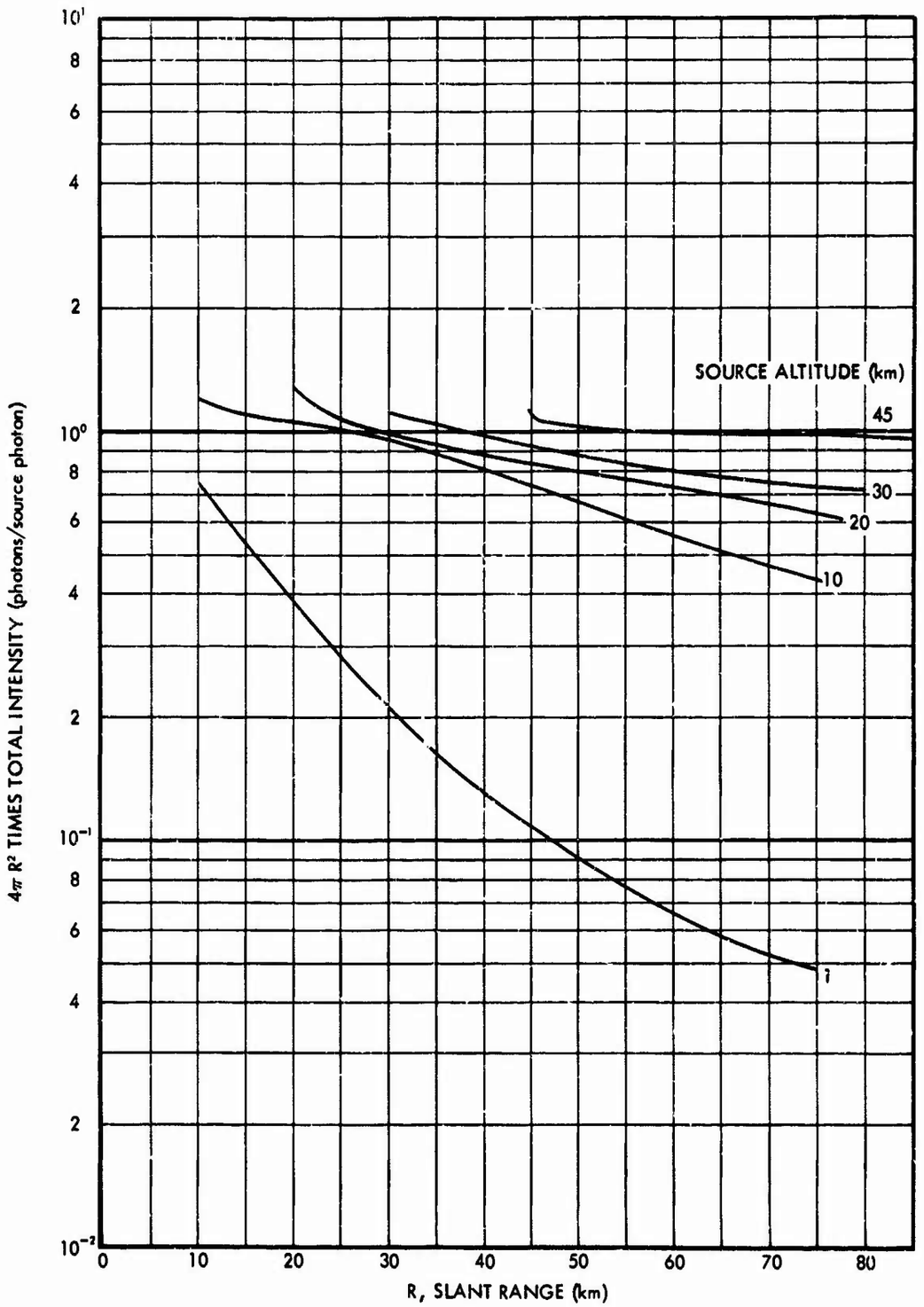

Fig. 28. Variation of $4\pi R^2$ Times Total Intensity with Slant Range: 0.65μ Light, Receiver Altitude = 0.1 Km, Ground Albedo = 0.9

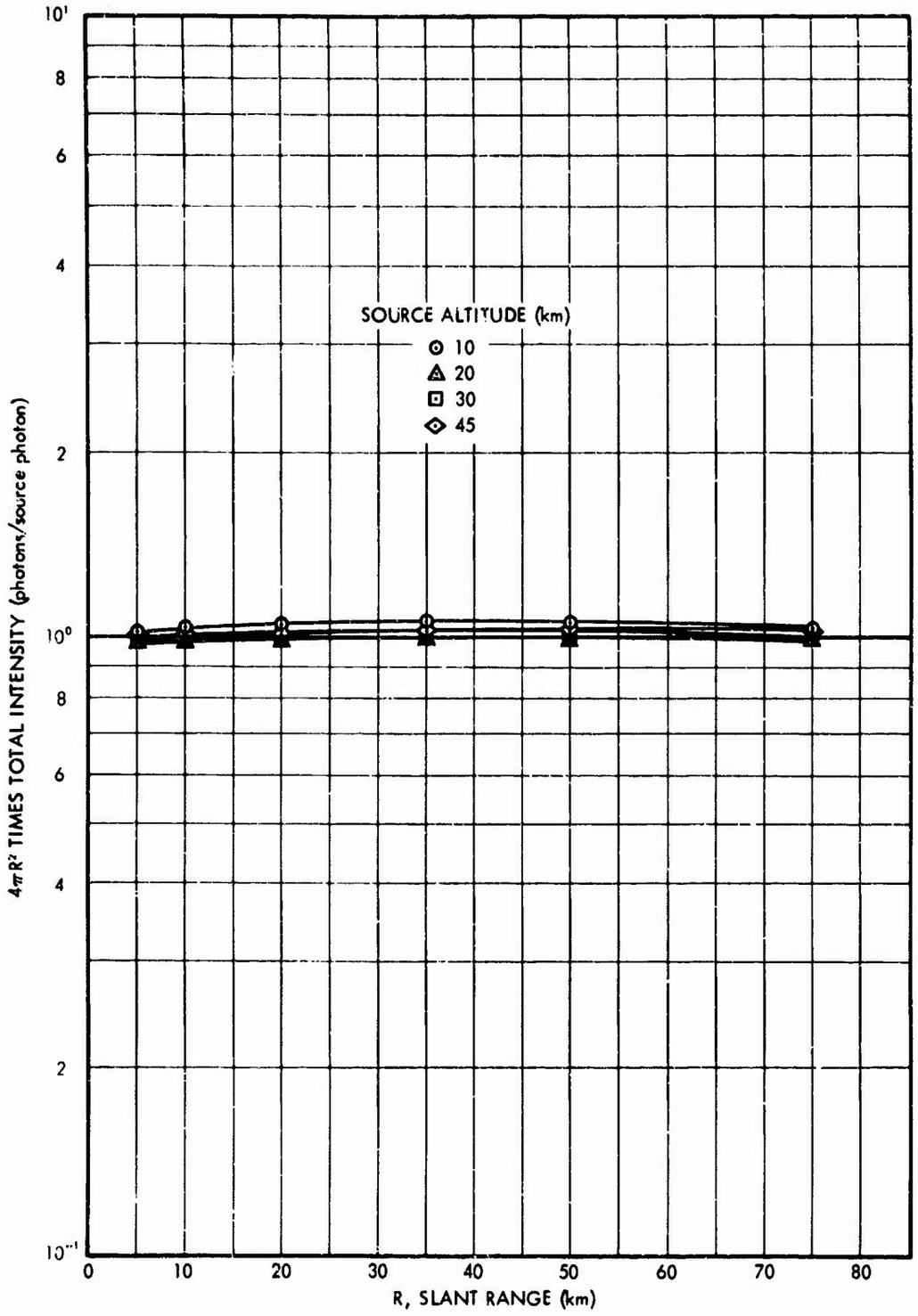

Fig. 29. Variation of $4\pi R^2$ Times Total Intensity with Slant Range: 0.65μ Light, Receiver and Source at Same Altitude, Ground Albedo = 0.0

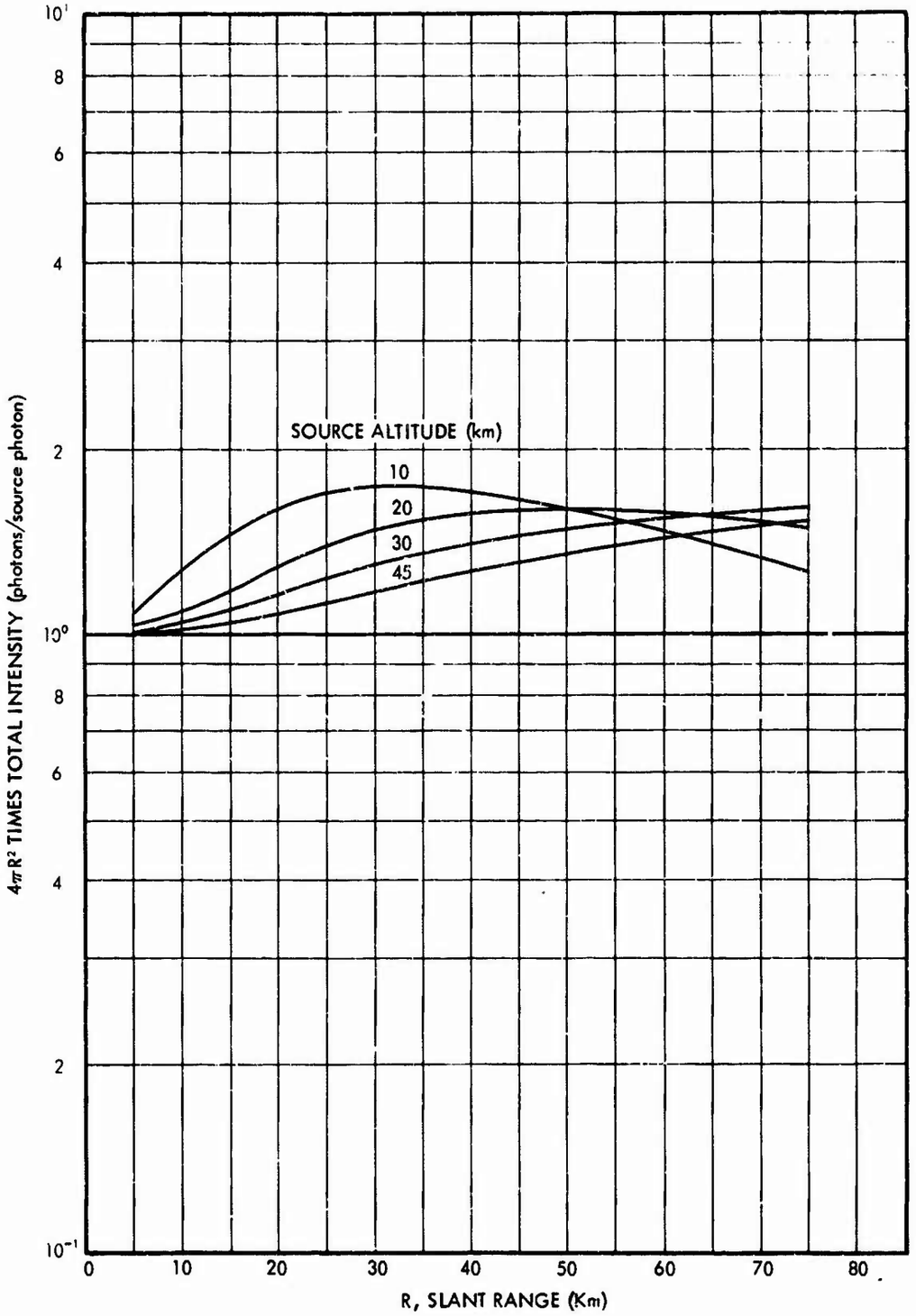

Fig. 30. Variation of $4\pi R^2$ Times Total Intensity with Slant Range: 0.65μ Light, Receiver and Source at Same Altitude, Ground Albedo = 0.9

It is seen in Figures 23, 24, 27, and 28 that $4\pi R^2$ times the total intensity increases with the increasing source altitude when the receivers are located near the ground surface. This increase in the total intensity times $4\pi R^2$ results mainly from the fact that the mean-free-path distance for a given slant range decreases as the source altitude is increased.

The variation of $4\pi R^2$ times the total intensity with altitude for ground ranges of 0, 10, 20, 50, and 75 km is shown in Figure 31 for 0.45 micron light and a ground albedo of 0.0. For a ground range of 0.0 the total intensity times $4\pi R^2$ decreases as the source altitude increases. For ground ranges of 20 km and greater, the total intensity times $4\pi R^2$ increases as the source altitude increases. The rate at which the total intensity times $4\pi R^2$ increases with source altitude for horizontal ranges greater than 10 km is seen in Figure 31 to be dependent on the horizontal range. The magnitude of the total intensity times $4\pi R^2$ for receivers placed near the ground and at ground ranges up to 75 km appears to be approaching a value which is independent of ground range as the source altitude is increased.

The variation of the total intensity with horizontal range for a source wave length of 0.45 microns and a ground albedo of 0.0 is shown in Figure 32 for each source altitude studied. For a given horizontal range the maximum intensity is seen to be dependent on the source altitude. The altitude at which the maximum intensity is obtained is seen in Figure 32 to increase with increasing horizontal range for ranges less than 80 km.

The mean-free-path distance for a given source-receiver distance decreases as the receiver altitude is raised to the source altitude. This effect

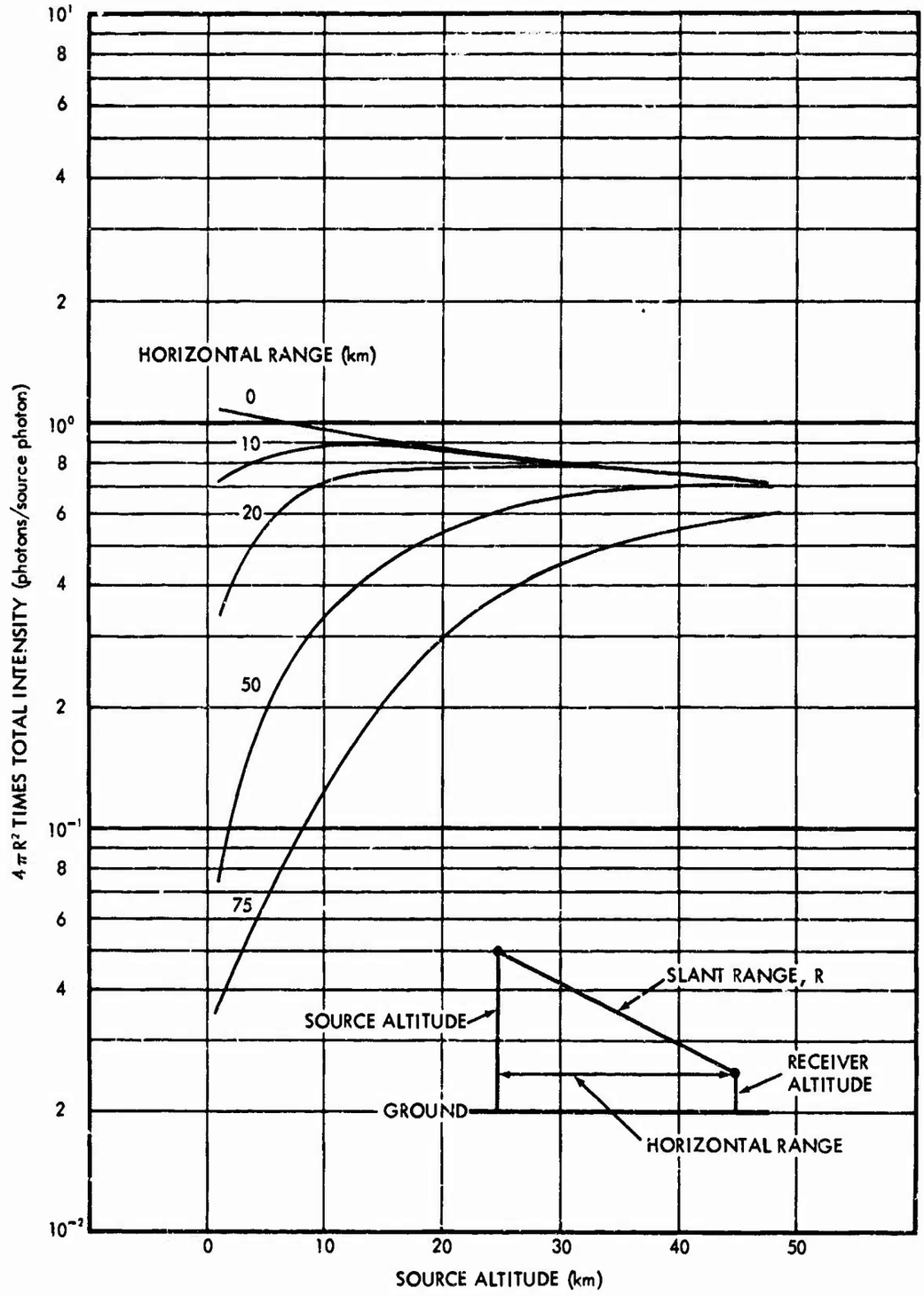

Fig. 31. Variation of $4\pi R^2$ Times Total Intensity with Source Altitude: 0.45μ Light, Receiver Altitude = 0.1 Km, Ground Albedo = 0.0

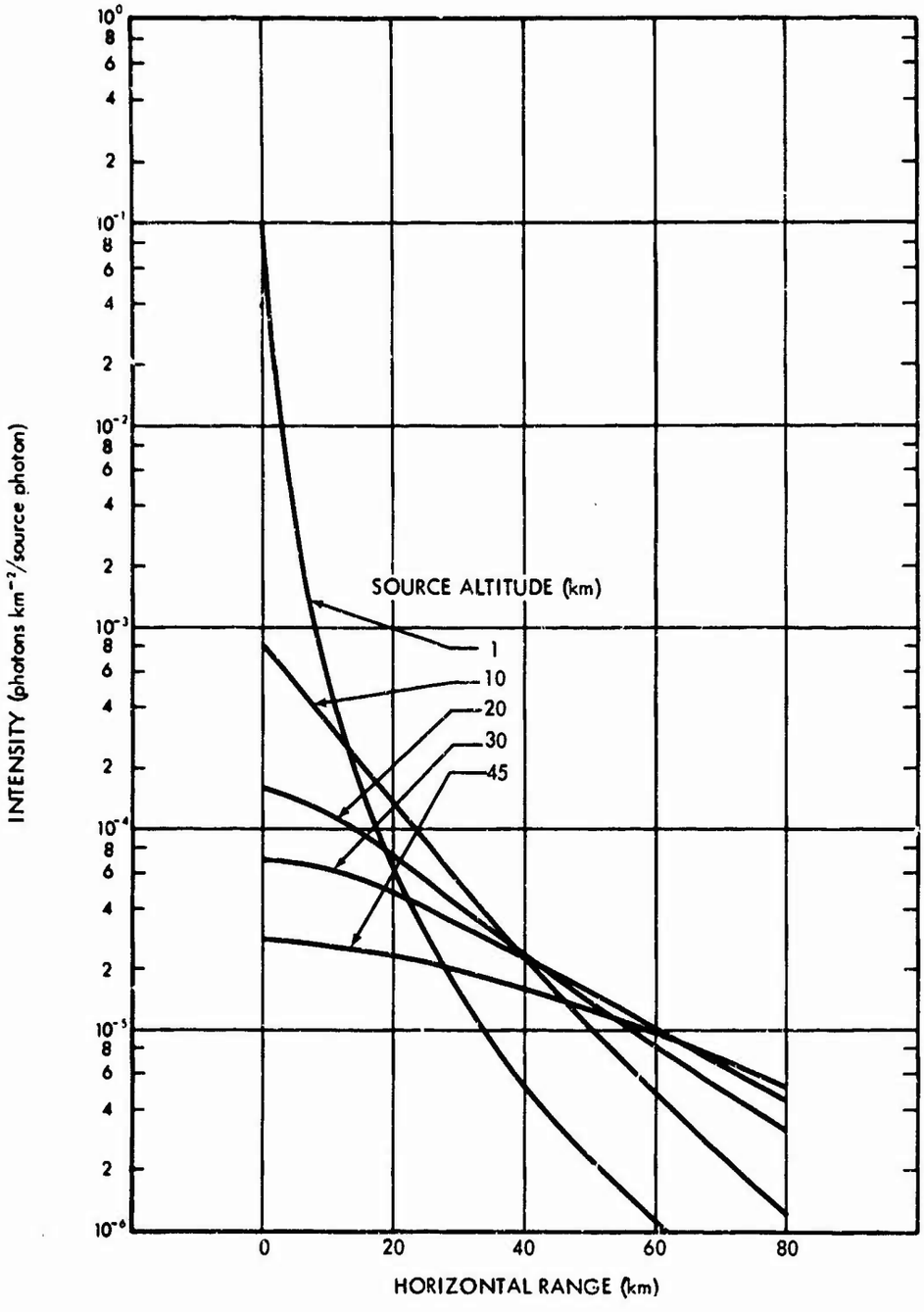

Fig. 32. Total Intensity vs Horizontal Range for Several Source Altitudes: 0.45μ Light, Receiver Altitude = 0.1Km, Ground Albedo = 0.0

is seen in Figure 33 where $4\pi R^2$ times the total intensity as a function of the source-receiver distance is shown for receivers located at an altitude of 0.1 km and at the same altitude as the source. The data shown in Figure 33 are for 0.45 μ light, a ground albedo of 0.0, and source altitudes of 10 and 30 km. It is seen that for a given slant range and source altitude, the intensity increases as the receiver altitude is increased up to the source altitude.

5.2 Dependence on Aerosol Number Density

The effect of varying the aerosol number density on the scattering of light in the atmosphere was studied for atmospheres defined by applying perturbations to an atmosphere for which only Rayleigh scattering and ozone absorption were allowed. The cross sections for Rayleigh scattering and ozone absorption were taken from a tabulation reported reported by Elterman (Reference 2). This basic atmosphere was then perturbed by the addition of aerosol particles with number densities of 2300, 4600, and 9200 particles per cm^3 at sea level air density and with a size distribution defined by Deirmendjian's (Reference 14) Haze C model for continental aerosols. The vertical distribution of the aerosol particle concentration was assumed to be the same as that formulated by Elterman from field measurements reported by Penndorf (Reference 15) and by Chagnon and Junge (Reference 16).

The aerosol cross section at sea level air density for Haze C type aerosols was obtained by integrating Mie scattering data for spherical particles with an index of refraction of 1.5 over the Haze C size distribution (Reference 13). The variation of the ground level aerosol scattering coefficient for the Haze C size distribution with wavelength is given in

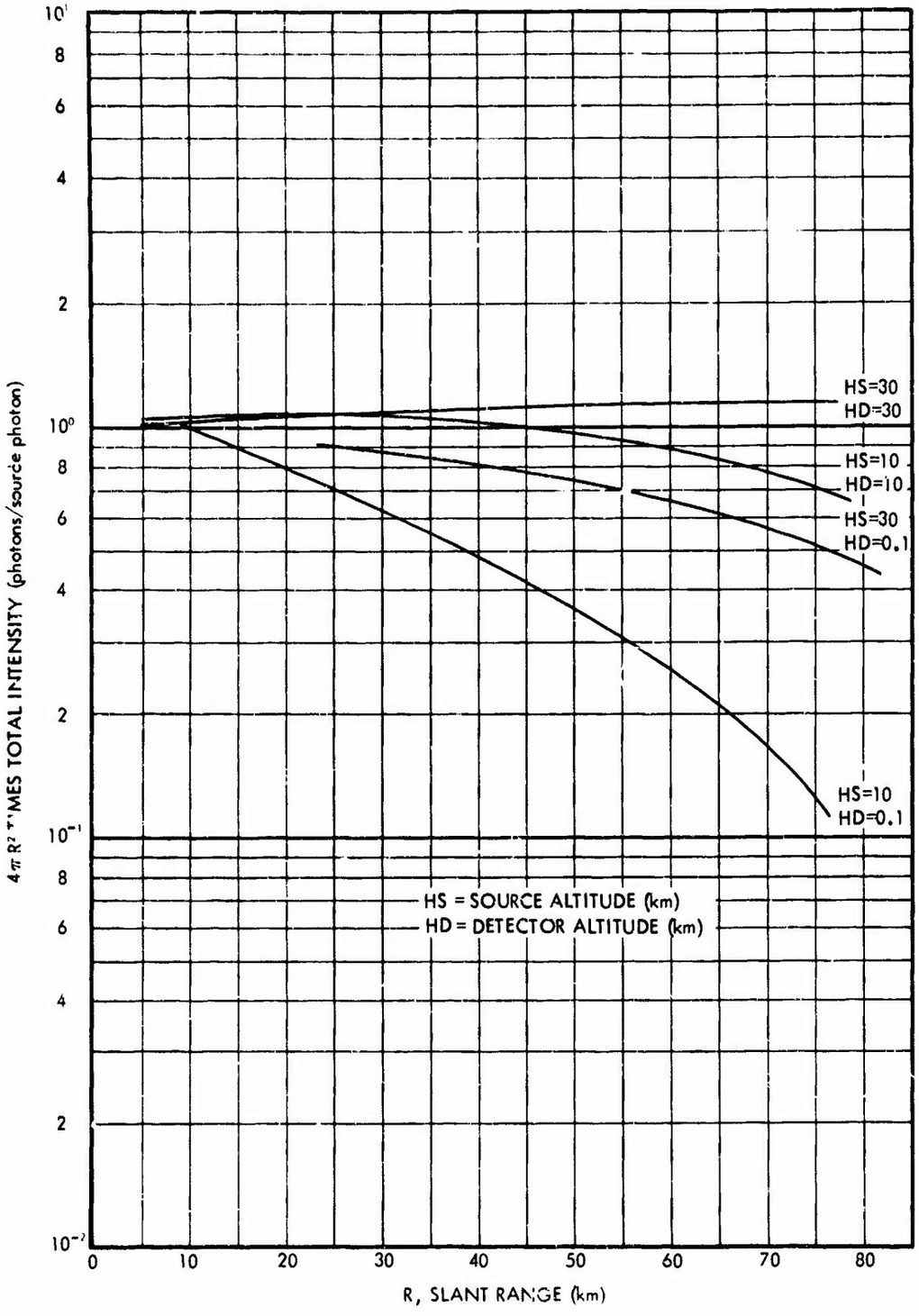

Fig. 33. Dependence of $4\pi R^2$ Times Totol Intensity on Receiver Altitude: 0.45μ Light, Ground Albedo 0.0

Table IV for a number density of one particle cm^{-3}. Aerosol scattering coefficients for a given number density of Haze C aerosols can be obtained by multiplying the data in Table IV by the aerosol number density in particles cm^{-3}.

Table IV. Scattering Coefficient for Haze C Aerosols With a Number Density of One Particle cm^{-3}

(km^{-1}/particles cm^{-3})

Wavelength (μ)	Aerosol Scattering Coefficient
0.3	1.090-04
0.45	7.239-05
0.5	6.574-05
0.65	5.200-05
0.7	4.891-05

Normalized aerosol scattering phase functions for several light wavelengths were also computed for the Haze C size distribution. The results are given in Table V as a function of the scattering angle.

All of the calculations performed for use in this study were for point isotropic monochromatic sources located at an altitude of 807.7 m. The receivers were placed at an altitude of 6.1 m and at horizontal ranges of up to 48.3 km. The source wavelengths studied were 0.3, 0.45, 0.5, 0.65, and 0.7μ.

The printed output of the LITE-I calculations gave the scattered and direct intensities at a spherical detector. The detector always presented a unit area in a direction normal to the direction of motion of the photons

TABLE V . NORMALIZED VOLUME SCATTERING FUNCTION : HAZE C MODEL
INDEX OF REFRACTION = 1.50

SCATTERING ANGLE	WAVELENGTH (MICRONS)				
(deg)	.30	.45	.50	.65	.70
0.	7.270E 00	4.627E 00	4.161E 00	3.811E 00	3.493E 00
1.0	5.606E 00	4.089E 00	3.736E 00	3.513E 00	3.261E 00
2.0	3.468E 00	3.034E 00	2.859E 00	2.837E 00	2.713E 00
3.0	2.525E 00	2.247E 00	2.143E 00	2.183E 00	2.142E 00
4.0	2.016E 00	1.815E 00	1.727E 00	1.749E 00	1.728E 00
5.0	1.696E 00	1.533E 00	1.464E 00	1.485E 00	1.466E 00
6.0	1.469E 00	1.326E 00	1.270E 00	1.298E 00	1.283E 00
7.0	1.298E 00	1.172E 00	1.125E 00	1.151E 00	1.138E 00
8.0	1.163E 00	1.051E 00	1.009E 00	1.036E 00	1.022E 00
9.0	1.059E 00	9.538E-01	9.164E-01	9.450E-01	9.332E-01
10.0	9.744E-01	8.752E-01	8.427E-01	8.731E-01	8.638E-01
11.0	9.050E-01	8.149E-01	7.861E-01	8.167E-01	8.082E-01
12.0	8.519E-01	7.678E-01	7.412E-01	7.688E-01	7.604E-01
13.0	7.994E-01	7.222E-01	6.978E-01	7.212E-01	7.135E-01
14.0	7.380E-01	6.733E-01	6.516E-01	6.715E-01	6.648E-01
15.0	6.820E-01	6.261E-01	6.070E-01	6.233E-01	6.175E-01
16.0	6.362E-01	5.866E-01	5.690E-01	5.819E-01	5.765E-01
17.0	5.970E-01	5.532E-01	5.373E-01	5.486E-01	5.432E-01
18.0	5.640E-01	5.227E-01	5.087E-01	5.204E-01	5.152E-01
19.0	5.336E-01	4.954E-01	4.825E-01	4.940E-01	4.895E-01
20.0	5.051E-01	4.704E-01	4.586E-01	4.687E-01	4.647E-01
22.5	4.387E-01	4.107E-01	4.019E-01	4.111E-01	4.075E-01
25.0	3.781E-01	3.586E-01	3.523E-01	3.581E-01	3.554E-01
27.5	3.269E-01	3.156E-01	3.110E-01	3.129E-01	3.108E-01
30.0	2.857E-01	2.796E-01	2.764E-01	2.763E-01	2.744E-01
32.5	2.479E-01	2.468E-01	2.450E-01	2.428E-01	2.416E-01
35.0	2.127E-01	2.181E-01	2.174E-01	2.112E-01	2.102E-01
37.5	1.853E-01	1.929E-01	1.931E-01	1.865E-01	1.858E-01
40.0	1.628E-01	1.706E-01	1.715E-01	1.658E-01	1.655E-01
42.5	1.409E-01	1.512E-01	1.525E-01	1.458E-01	1.455E-01
45.0	1.232E-01	1.336E-01	1.354E-01	1.293E-01	1.292E-01
47.5	1.090E-01	1.182E-01	1.204E-01	1.158E-01	1.159E-01
50.0	9.527E-02	1.054E-01	1.078E-01	1.028E-01	1.030E-01
52.5	8.336E-02	9.324E-02	9.580E-02	9.138E-02	9.162E-02
55.0	7.361E-02	8.266E-02	8.531E-02	8.178E-02	8.214E-02
57.5	6.562E-02	7.453E-02	7.716E-02	7.375E-02	7.413E-02
60.0	5.704E-02	6.589E-02	6.855E-02	6.520E-02	6.564E-02
62.5	5.111E-02	5.924E-02	6.183E-02	5.900E-02	5.951E-02
65.0	4.561E-02	5.306E-02	5.558E-02	5.330E-02	5.382E-02
67.5	4.063E-02	4.772E-02	5.016E-02	4.806E-02	4.858E-02
70.0	3.625E-02	4.307E-02	4.541E-02	4.337E-02	4.392E-02
72.5	3.264E-02	3.873E-02	4.097E-02	3.941E-02	3.998E-02
75.0	2.966E-02	3.526E-02	3.738E-02	3.605E-02	3.659E-02
77.5	2.658E-02	3.197E-02	3.397E-02	3.267E-02	3.322E-02
80.0	2.430E-02	2.911E-02	3.099E-02	3.003E-02	3.059E-02
82.5	2.240E-02	2.672E-02	2.848E-02	2.774E-02	2.829E-02
85.0	2.046E-02	2.444E-02	2.610E-02	2.548E-02	2.603E-02
87.5	1.858E-02	2.223E-02	2.379E-02	2.334E-02	2.390E-02
90.0	1.687E-02	2.017E-02	2.166E-02	2.142E-02	2.199E-02
92.5	1.555E-02	1.864E-02	2.003E-02	1.987E-02	2.045E-02

TABLE V. NORMALIZED VOLUME SCATTERING FUNCTION : HAZE C MODEL
INDEX OF REFRACTION = 1.50

SCATTERING ANGLE	WAVELENGTH (MICRONS)				
(deg)	.30	.45	.50	.65	.70
95.0	1.466E-02	1.741E-02	1.871E-02	1.873E-02	1.931E-02
97.5	1.409E-02	1.653E-02	1.774E-02	1.791E-02	1.849E-02
100.0	1.328E-02	1.551E-02	1.665E-02	1.692E-02	1.750E-02
102.5	1.255E-02	1.455E-02	1.563E-02	1.603E-02	1.661E-02
105.0	1.186E-02	1.368E-02	1.471E-02	1.521E-02	1.581E-02
107.5	1.112E-02	1.274E-02	1.374E-02	1.437E-02	1.499E-02
110.0	1.060E-02	1.213E-02	1.308E-02	1.376E-02	1.438E-02
112.5	1.038E-02	1.172E-02	1.263E-02	1.344E-02	1.407E-02
115.0	1.024E-02	1.143E-02	1.229E-02	1.321E-02	1.385E-02
117.5	1.010E-02	1.124E-02	1.207E-02	1.299E-02	1.364E-02
120.0	1.017E-02	1.114E-02	1.194E-02	1.298E-02	1.364E-02
122.5	1.025E-02	1.108E-02	1.184E-02	1.300E-02	1.367E-02
125.0	1.027E-02	1.103E-02	1.176E-02	1.298E-02	1.367E-02
127.5	1.045E-02	1.103E-02	1.175E-02	1.310E-02	1.380E-02
130.0	1.062E-02	1.109E-02	1.178E-02	1.325E-02	1.396E-02
132.5	1.086E-02	1.128E-02	1.195E-02	1.345E-02	1.417E-02
135.0	1.115E-02	1.163E-02	1.227E-02	1.370E-02	1.444E-02
137.5	1.150E-02	1.207E-02	1.268E-02	1.402E-02	1.476E-02
140.0	1.215E-02	1.265E-02	1.322E-02	1.460E-02	1.535E-02
142.5	1.292E-02	1.329E-02	1.383E-02	1.528E-02	1.605E-02
145.0	1.373E-02	1.395E-02	1.445E-02	1.601E-02	1.678E-02
147.5	1.502E-02	1.494E-02	1.539E-02	1.715E-02	1.792E-02
150.0	1.653E-02	1.617E-02	1.655E-02	1.849E-02	1.924E-02
152.5	1.807E-02	1.755E-02	1.785E-02	1.982E-02	2.055E-02
155.0	2.035E-02	1.941E-02	1.962E-02	2.171E-02	2.243E-02
156.0	2.123E-02	2.020E-02	2.035E-02	2.242E-02	2.312E-02
157.0	2.206E-02	2.093E-02	2.105E-02	2.305E-02	2.375E-02
158.0	2.303E-02	2.169E-02	2.173E-02	2.378E-02	2.445E-02
159.0	2.392E-02	2.242E-02	2.241E-02	2.451E-02	2.513E-02
160.0	2.460E-02	2.313E-02	2.312E-02	2.497E-02	2.560E-02
161.0	2.493E-02	2.381E-02	2.374E-02	2.525E-02	2.593E-02
162.0	2.540E-02	2.427E-02	2.418E-02	2.574E-02	2.639E-02
163.0	2.616E-02	2.456E-02	2.447E-02	2.643E-02	2.703E-02
164.0	2.648E-02	2.486E-02	2.473E-02	2.690E-02	2.753E-02
165.0	2.678E-02	2.506E-02	2.496E-02	2.702E-02	2.767E-02
166.0	2.663E-02	2.526E-02	2.516E-02	2.712E-02	2.776E-02
167.0	2.714E-02	2.565E-02	2.551E-02	2.751E-02	2.816E-02
168.0	2.785E-02	2.612E-02	2.598E-02	2.804E-02	2.874E-02
169.0	2.840E-02	2.656E-02	2.636E-02	2.850E-02	2.917E-02
170.0	2.897E-02	2.701E-02	2.680E-02	2.898E-02	2.954E-02
171.0	2.965E-02	2.776E-02	2.755E-02	2.956E-02	3.016E-02
172.0	3.060E-02	2.878E-02	2.844E-02	3.032E-02	3.097E-02
173.0	3.164E-02	2.981E-02	2.948E-02	3.126E-02	3.178E-02
174.0	3.304E-02	3.106E-02	3.062E-02	3.228E-02	3.284E-02
175.0	3.460E-02	3.219E-02	3.163E-02	3.362E-02	3.429E-02
176.0	3.610E-02	3.334E-02	3.284E-02	3.486E-02	3.526E-02
177.0	3.683E-02	3.408E-02	3.332E-02	3.481E-02	3.497E-02
178.0	3.721E-02	3.318E-02	3.241E-02	3.398E-02	3.438E-02
179.0	3.521E-02	3.265E-02	3.213E-02	3.410E-02	3.470E-02
180.0	3.534E-02	3.304E-02	3.253E-02	3.455E-02	3.513E-02

entering the detector, irrespective of their direction of motion. The scattered intensities were also printed out as a function of the ground albedo for ground albedos of 0.0 and 0.9. The ground was treated as a Lambert type reflection surface.

Table VI presents the calculated direct intensities at each of five different receiver positions as a function of the source wave length and the aerosol number density. Table VII presents the calculated scattered intensities at the five different receiver positions for ground albedos of 0.0 and 0.9 as a function of the source wave length and the aerosol number density. From an examination of the scattered intensity data in Table VII, it is seen that the scattered intensity at 4.03 km ground range increases with increasing aerosol number density, whereas at larger ground ranges the scattered intensity decreases with increasing aerosol number density.

The variation of the scattered intensities at each of five different receiver positions with source wave length is shown in Figure 34 for the basic atmosphere (Rayleigh scattering plus ozone absorption). The data shown in Figure 34 are for a ground albedo of 0.9. Also shown in Figure 34 is a plot of the Rayleigh scattering coefficient at sea level altitude versus wave length. In addition to the source wave lengths listed in Table VI, source wave lengths of 0.34 and 0.38μ were also used in calculations to study the effect of the ozone absorption on the scattered intensities. It is seen that the strong ozone absorption occurring near 0.3μ results in a rapid decrease in the scattered intensities as the source wave length approaches 0.3μ for ground ranges greater than 4.03 km. For wave lengths greater than 0.34μ the scattered intensities at each receiver varies approximately the same with wave length as does the Rayleigh scattering coefficient.

Table VI. Direct Intensities as a Function of the Number Density of Haze C Aerosols at Ground Level

(photons km^{-2}/source photon)

Wavelength (μ)	Aerosol Number Density (particles/cm^3)	Horizontal Range (km)				
		4.03	12.07	20.12	32.19	48.28
0.30	0	2.332-9*	6.759-11	6.100-12	2.981-13	8.278-15
0.30	2300	1.114-9	7.642-12	1.620-13	9.002-16	1.377-18
0.30	4600	5.315-10	8.630-13	4.293-15	2.710-18	2.280-22
0.30	9200	1.211-10	1.102-14	3.022-18	2.464-23	6.282-30
0.45	0	4.264-9	4.004-10	1.179-10	3.396-11	1.005-11
0.45	2300	2.608-9	9.393-11	1.055-11	7.156-13	3.078-14
0.45	4600	1.595-9	2.205-11	9.453-13	1.511-14	9.463-17
0.45	9200	5.967-10	1.215-12	7.575-15	6.720-18	8.900-22
0.50	0	4.421-9	4.457-10	1.409-9	4.516-11	1.541-11
0.50	2300	2.828-9	1.193-10	1.572-11	1.354-12	8.008-14
0.50	4600	1.809-9	3.197-11	1.754-12	4.062-14	4.167-16
0.50	9200	7.407-10	2.296-10	2.189-14	3.667-17	1.134-20
0.65	0	4.619-9	5.069-10	1.746-10	6.363-11	2.576-11
0.65	2300	3.244-9	1.789-10	3.082-11	3.975-12	4.027-13
0.65	4600	2.278-9	6.309-11	5.439-12	2.481-13	6.286-15
0.65	9200	1.124-9	7.858-12	1.697-13	8.694-16	1.539-18
0.70	0	4.649-9	5.168-10	1.803-10	6.697-11	2.782-11
0.70	2300	3.335-9	1.940-10	3.528-11	4.934-12	5.568-13
0.70	4600	2.392-9	7.285-11	6.911-12	3.639-13	1.117-14
0.70	9200	1.231-9	1.027-11	2.648-13	1.975-15	4.474-18

*Read 2.332-9 as 2.332×10^{-9}

Table VII. Scattered Intensities as a Function of the Number Density of Haze C Aerosols at Ground Level

(photons km^{-2}/source photon)

Wavelength (μ)	Aerosol Number Density (particles/cm^3)	Ground Albedo	Horizontal Range (km) 4.03	12.07	20.12	32.19	48.28
0.30	0	0.0	1.90-9*	1.35-10	2.65-11	3.00-12	2.00-13
0.30	2300	0.0	2.95-9	1.10-10	1.70-11	2.10-12	1.95-13
0.30	4600	0.0	3.00-9	8.50-11	1.15-11	8.40-13	4.00-14
0.30	9200	0.0	2.79-9	7.90-11	5.20-12	3.50-13	1.50-14
0.30	0	0.9	4.60-9	3.05-10	6.20-11	8.20-12	6.60-13
0.30	2300	0.9	6.00-9	2.65-10	4.80-11	5.40-12	3.80-13
0.30	4600	0.9	5.00-9	2.60-10	3.50-11	2.40-12	1.00-13
0.30	9200	0.9	5.00-9	2.05-10	1.50-11	7.00-13	3.00-14
0.45	0	0.0	6.30-10	1.30-10	5.20-11	2.40-11	1.20-11
0.45	2300	0.0	1.60-9	2.75-10	6.50-11	1.35-11	4.60-12
0.45	4600	0.0	2.25-9	2.20-10	4.50-11	9.70-12	2.05-12
0.45	9200	0.0	3.20-9	8.90-11	2.00-11	4.00-12	6.90-13
0.45	0	0.9	1.30-9	2.40-10	1.05-10	4.50-11	2.05-11
0.45	2300	0.9	2.45-9	3.90-10	1.05-10	2.50-11	1.05-11
0.45	4600	0.9	3.55-9	4.20-10	7.20-11	1.52-11	3.00-12
0.45	9200	0.9	5.20-9	2.60-10	5.10-11	1.10-11	2.20-12
0.50	0	0.0	4.40-10	9.00-11	4.00-11	1.60-11	6.40-12
0.50	2300	0.0	2.13-9	2.30-10	4.75-11	1.27-11	5.30-12
0.50	4600	0.0	2.45-9	1.85-10	3.60-11	8.20-12	1.80-12
0.50	9200	0.0	2.45-9	1.40-10	1.60-11	2.20-12	4.60-13
0.50	0	0.9	7.40-10	1.40-10	6.30-11	2.55-11	1.00-11
0.50	2300	0.9	2.80-9	3.60-10	9.10-11	2.30-11	1.00-11
0.50	4600	0.9	4.30-9	3.20-10	7.60-11	1.60-11	2.90-11
0.50	9200	0.9	3.90-9	2.50-10	2.70-11	4.10-12	1.25-12

*Read 1.909-9 as 1.909×10^{-9}

Table VII. (Continued)

(photons km^{-2}/source photon)

Wavelength (μ)	Aerosol Number Density ($particles/cm^3$)	Ground Albedo	Horizontal Range (km)				
			4.03	12.07	20.12	32.19	48.28
0.65	0	0.0	1.55-10	3.20-11	1.50-11	6.80-12	3.30-12
0.65	2300	0.0	1.05-9	1.65-10	4.70-11	1.10-11	2.10-12
0.65	4600	0.0	2.20-9	1.80-10	4.40-11	8.70-12	1.40-12
0.65	9200	0.0	2.50-9	1.20-10	1.35-11	2.15-12	3.20-13
0.65	0	0.9	3.60-10	5.20-11	2.30-11	1.00-11	4.80-12
0.65	2300	0.9	1.90-9	2.75-10	7.80-11	1.80-11	3.30-12
0.65	4600	0.9	3.00-9	2.60-10	6.20-11	1.25-11	2.15-12
0.65	9200	0.9	3.60-9	1.90-10	2.80-11	4.50-12	6.50-13
0.70	0	0.0	1.15-10	2.00-11	9.80-12	4.70-12	2.45-12
0.70	2300	0.0	1.15-9	1.00-10	4.10-11	1.15-11	2.50-12
0.70	4600	0.0	1.95-9	2.15-10	4.15-11	8.20-12	1.95-12
0.70	9200	0.0	3.00-9	1.15-10	1.75-11	4.10-12	1.05-12
0.70	0	0.9	2.30-10	3.50-11	1.06-11	7.03-12	3.64-12
0.70	2300	0.9	1.95-9	2.15-10	6.02-11	1.56-11	3.56-12
0.70	4600	0.9	2.75-9	2.90-10	5.60-11	1.05-11	2.65-12
0.70	9200	0.9	5.10-9	1.95-10	2.57-11	6.30-12	1.35-12

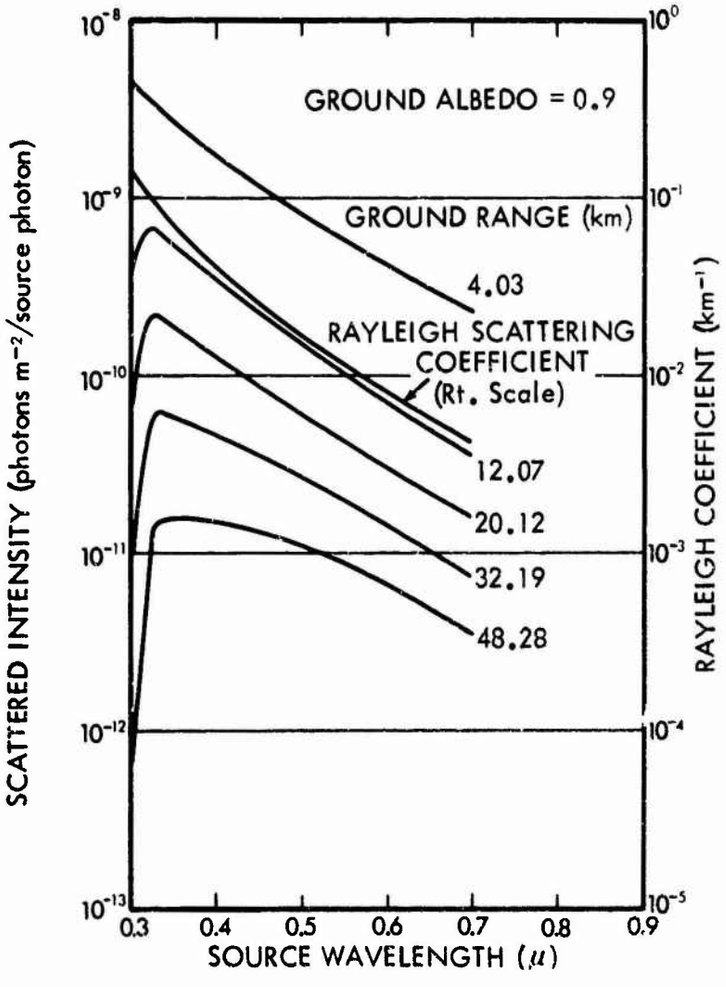

Fig. 34. Scattered Intensities vs Source Wavelength far Several Graund Ranges: Rayleigh Atmosphere with Ozone Absorption

Figure 35 presents the variation in the scattered intensity time $4\pi R^2$ at several ground ranges with the aerosol cross section at sea level altitude for a source wavelength of 0.45μ and a ground albedo of 0.9. It is seen that at close-in distances the scattered intensity for a point isotropic 0.45μ light source increases with increasing aerosol cross section. At larger ground ranges the scattered intensities decrease when the aerosol cross section is increased. The scattered intensity time $4\pi R^2$ for an aerosol cross section of 0.180 km^{-1} corresponds to the attenuation that would be expected for an atmosphere defined by the "clear standard atmosphere" formulated by Elterman.

Figure 35 also shows the variation with the aerosol cross section of the total intensity (scattered plus direct intensity) time $4\pi R^2$ for 0.45μ light at ground ranges to 48.28 km. The ground albedo was 0.9. Except at ground ranges less than 12.07 km, the total intensity results almost entirely from scattered radiation when the aerosol cross section is greater than 0.2 km^{-1}. It is seen from the data in Figure 35 that the variation of the total intensity time $4\pi R^2$ with ground range is highly dependent on the magnitude of the aerosol cross section for values of the aerosol cross section up to twice the value used by Elterman for a "clear standard atmosphere." For larger values of the aerosol cross section, the total intensity times $4\pi R^2$ at a given ground range from a 0.45μ point source does not vary significantly as the aerosol cross section is increased.

The dependence of both the scattered and total intensities times $4\pi R^2$ on the magnitude of the aerosol cross section is shown in Figure 36 for a source wavelength of 0.7 and a ground albedo of 0.0. It is seen that the

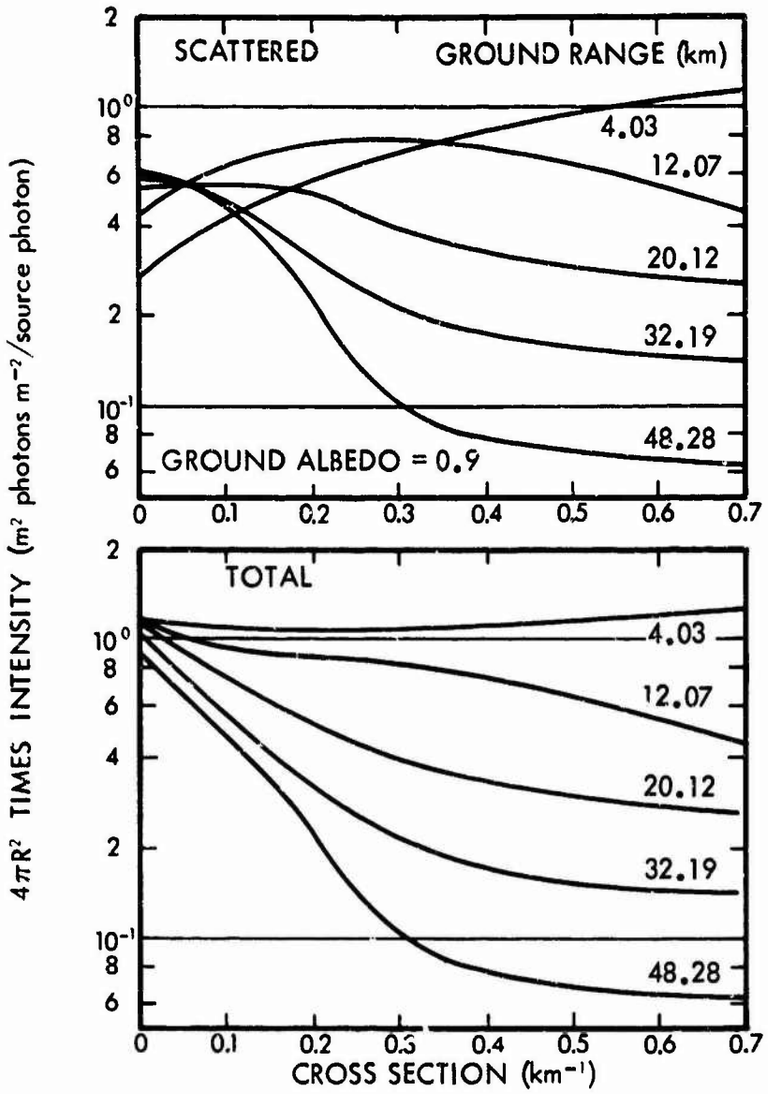

Fig. 35. Variation of $4\pi R^2$ Times Scattered and Total Intensities with Aerosol Cross Section for Several Ground Ranges: 0.45μ Light

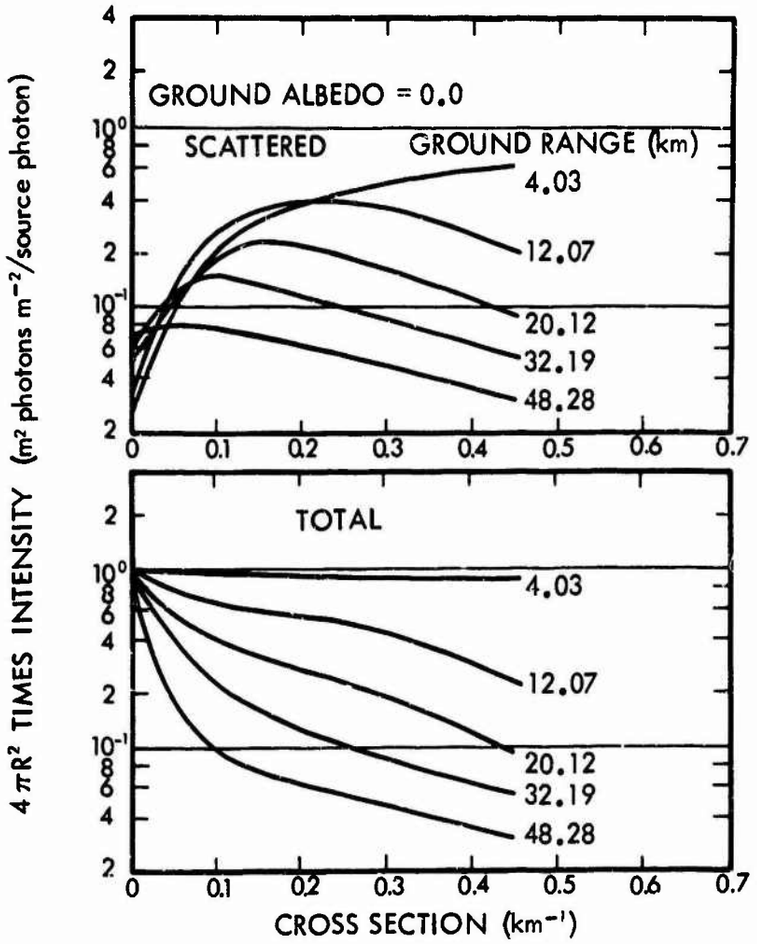

Fig. 36. Variation of $4\pi R^2$ Times Scattered and Total Intensities with Aerosol Cross Section for Several Ground Ranges: 0.70μ Light

dependence on the aerosol content of the atmosphere for 0.7μ light is similar to that shown in Figure 35 for 0.45μ light. Similarly it was found for the other source wavelengths studied (0.3, 0.5, and 0.65) that the attenuation of both the total and scattered intensities is highly dependent on the aerosol number density. The total intensity was found to vary by as much as a factor of 30 for a ground range of 48 km as the aerosol number density is varied from 0 to 9200 particles per cc.

The total intensity at a given receiver position is calculated by the Monte Carlo code as the sum of the intensities received after each collision. The number of collisions that have to be followed for a given wavelength before the contribution from high order collisions is negligible is a function of both the aerosol cross section and the aerosol phase function used in the calculation. Figure 37 shows for a ground albedo of 0.9 the sum of the scattered intensities vs collision number at a ground range of 32.19 km for 0.3μ wavelength light. An increase in the aerosol cross section at sea level results in an increase in the number of collisions that has to be followed before the contribution to the total scattered intensity by higher order collisions becomes negligible. The minimum number of collisions that need to be followed for an aerosol cross section of 0.2506 km^{-1} is approximately 30, whereas the minimum number needed for an aerosol cross section of 0.5012 km^{-1} is 40.

Curves similar to those shown in Figure 37 were obtained for the other source wavelength studies. They showed that an increase in the sum of the aerosol and Rayleigh scattering cross section results in an increase in

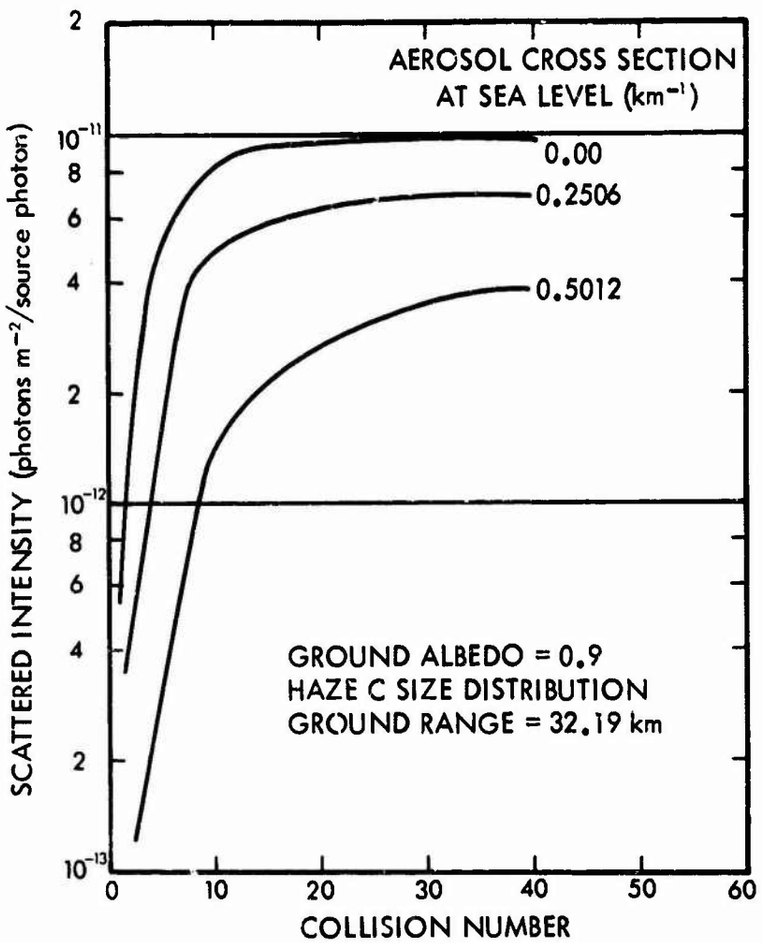

Fig. 37. Sum of the Scattered Intensities vs Collision Number for Several Aerosol Cross Sections: 0.30μ Light

the number of collisions required before the sum of the scattered intensities resulting from higher order collisions becomes negligible.

The ratio of the scattered intensities for the case where the ground albedo was 0.9 to that for a ground albedo of 0.0 was found to not vary significantly with the horizontal range for all of the source wavelengths studied. It was found that the ratio decreased with increasing wavelength from the value of about 2.5 for 0.3 microns to a value of 1.5 for 0.7 microns. The scattered intensity for a given horizontal range was found to increase exponentially with an increase in the ground albedo.

5.3 Dependence on Changes in Aerosol Phase Function

To study the effect of varying the shape of the aerosol phase function on the magnitude of the scattered light intensity in the atmosphere, LITE-I problems were run using various aerosol phase functions. The atmosphere used in these problems was taken to be that described by Elterman's "clear standard atmosphere" model. The phase functions used in the LITE-I calculations for aerosol scattering were computed by integrating Mie scattering data for spherical particles with an index of refraction of 1.5 with particle size distributions defined by Diermendjian's Haze C and Haze M models (Reference 14) for continental and maritime hazes and with exponential size distributions described by $N(r) \approx r^{-\nu}$ for $\nu = 2$ and 3. In some of the LITE-I calculations the Rayleigh phase function was used instead of an aerosol phase function to describe aerosol scattering.

The shape of the normalized phase function for light scattering by aerosol particles is dependent on the wavelength of the incident light,

the particle size distribution, and the index of refraction. Phase functions for aerosol scattering are highly peaked in the forward direction. Table VIII lists, for wavelengths of 0.3 and 0.7μ and for several aerosol size distributions, the cosine of the upper bound of the scattering angle interval into which a given fraction of the photons undergoing collisions in a unit volume of aerosols will be scattered. It is seen from the data in Table VIII that at least 90 percent of the photons undergoing aerosol particle scattering in a unit volume of air will be scattered into angles between 0° and 90° for all of the aerosol size distribution models listed. In contrast, only 50 percent of the radiation undergoing Rayleigh scattering will be scattered in a forward direction.

An examination of the variation with both wavelength and altitude of the ratio of the Rayleigh scattering coefficient to the sum of the Rayleigh and aerosol scattering coefficients for the Elterman "clear standard atmosphere" reveals that the probability of a Rayleigh scattering event occurring at a given altitude reduces with source wavelength. It was also found, for wavelengths of $\lambda = 0.3$, 0.45, and 0.5μ, that more than 90 percent of the scattering at altitudes above 5 km are Rayleigh events. For wavelengths of $\lambda = 0.65$ and 0.70μ, the probability of a Rayleigh scattering event is greater than 0.9 only for altitudes between 7 and 18 km and above 30 km. Therefore, the use of the Rayleigh phase function to define the phase function for aerosol particle scattering should not have a significant effect on the calculated intensities for wavelengths between 0.3 and 0.5 . For wavelengths between 0.65 and 0.7μ, there should be a noticeable difference between a calculation which used the Rayleigh phase function to describe

Table VIII. Probability of Scattering into Angles with Indicated Cosines for Various Phase Functions

P	$\lambda = 0.7\mu$, $m = 1.5$				$\lambda = 0.3\mu$, $m = 1.5$			
	HAZE M	HAZE C	$n(r) \approx r^{-2}$	$n(r) \approx r^{-3}$	HAZE M	HAZE C	$n(r) \approx r^{-2}$	$n(r) \approx r^{-3}$
0.0	1.0000	1.0000	1.0000	1.0000	1.0000	1.0000	1.0000	1.0000
0.1	0.9952	0.9894	0.9998	0.9991	0.9989	0.9909	0.9999	0.9996
0.2	0.9864	0.9692	0.9994	0.9949	0.9966	0.9724	0.9998	0.9973
0.3	0.9712	0.9398	0.9982	0.9817	0.9912	0.9454	0.9994	0.9872
0.4	0.9455	0.8995	0.9922	0.9631	0.9771	0.9086	0.9960	0.9643
0.5	0.9036	0.8439	0.9671	0.9150	0.9437	0.8579	0.9713	0.9241
0.6	0.8371	0.7633	0.9121	0.8522	0.8836	0.7856	0.9168	0.8630
0.7	0.7300	0.6396	0.8279	0.7529	0.7840	0.6757	0.8346	0.7689
0.8	0.5310	0.4255	0.6844	0.5750	0.6046	0.4876	0.7074	0.6014
0.9	0.0374	-0.0538	0.3354	0.1394	0.1574	0.0687	0.4112	0.1890
1.0	-1.0000	-1.0000	-1.0000	-1.0000	-1.0000	-1.0000	-1.0000	-1.0000

aerosol scattering and a calculation which used an aerosol phase function to define the angular distribution of scattering by aerosol particles.

LITE-I calculations for use in studying the effect of varying the shape of the aerosol phase function were run for a point isotropic monochromatic source located at an altitude of 807.7 m. The receivers were placed at an altitude of 6.1 m and at horizontal ranges of up to 48.3 km. The ground albedo was taken to be a Lambert type albedo with a value of 0.9. Results were also obtained for a ground albedo of 0.0. The source wavelengths studied were 0.3, 0.45, 0.5, 0.65, and 0.7μ.

The calculated scattered intensities at each receiver point are presented in Table IX as a function of the source wavelength, the ground albedo, and the phase function used to describe aerosol scattering. The direct intensities at each receiver point are presented in Table X as a function of the source wavelength.

The results obtained from LITE-I calculations for problems using phase functions defined by the Haze C and Haze M size distribution models and $n(r) \propto r^{-\nu}$ for $\nu = 2$ and 3 and the Rayleigh phase function for aerosol scattering are presented in Figures 38 and 39 for wavelengths of 0.45 and 0.7μ, respectively. For a source wavelength of 0.45μ, it is seen that the maximum intensity computed for a given horizontal range does not differ by more than 35 percent of the minimum value. An examination of the data for 0.7μ shows that there are no large differences between the computed attenuation out to 50 km as given by each of the aerosol models, but the use of the Rayleigh phase function to describe the aerosol phase function

Table IX. Scattered Intensities in an Elterman Atmosphere for Various Aerosol Phase Functions and Wavelengths

(photons m^{-2}/source photon)

Wavelength (μ)	Ground Albedo	Aerosol Phase Function	Horizontal Range (km)				
			4.03	12.07	20.12	32.19	48.28
0.30	0.0	Haze M	2.85-9*	1.40-10	1.30-11	1.55-12	1.35-13
0.30	0.0	Haze C	2.65-9	1.30-10	1.40-11	1.30-12	7.90-14
0.30	0.0	$\gamma = 2$	2.40-9	1.18-10	1.85-11	1.60-12	1.15-13
0.30	0.0	$\gamma = 3$	2.60-9	1.10-10	1.65-11	1.65-12	1.10-13
0.30	0.9	Haze M	4.50-9	2.85-10	4.00-11	4.40-12	3.40-13
0.30	0.9	Haze C	4.00-9	3.10-10	3.20-11	3.20-12	3.00-13
0.30	0.9	$\gamma = 2$	4.30-9	2.75-10	4.50-11	4.60-12	4.15-13
0.30	0.9	$\gamma = 3$	4.90-9	2.40-10	4.50-11	5.40-12	4.50-13
0.45	0.0	Haze M	1.68-9	2.10-10	5.20-11	1.30-11	3.20-12
0.45	0.0	Haze C	2.10-9	1.95-10	5.00-11	1.10-11	2.30-12
0.45	0.0	$\gamma = 2$	1.45-9	2.10-10	6.50-11	1.55-11	3.00-12
0.45	0.0	Rayleigh	1.80-9	2.05-10	5.80-11	1.25-11	2.10-12
0.45	0.9	Haze M	2.65-9	3.30-10	8.00-11	2.35-11	7.50-12
0.45	0.9	Haze C	2.63-9	3.24-10	8.50-11	2.10-11	4.65-12
0.45	0.9	$\gamma = 2$	2.60-9	3.00-10	1.00-10	2.65-11	6.20-12
0.45	0.9	Rayleigh	3.16-9	3.18-10	9.13-11	2.50-11	6.40-12
0.50	0.0	Haze M	1.70-9	2.50-10	7.80-11	1.80-11	3.50-12
0.50	0.0	Haze C	1.90-9	2.45-10	5.00-11	1.00-11	2.10-12
0.50	0.0	$\gamma = 2$	1.37-9	2.50-10	5.70-11	1.12-11	2.50-12
0.50	0.0	Rayleigh	1.70-9	1.25-10	3.15-11	6.70-12	1.90-12
0.50	0.9	Haze M	2.55-9	3.80-10	1.20-10	3.00-11	6.20-12
0.50	0.9	Haze C	2.75-9	3.45-10	8.50-11	1.98-11	4.00-12
0.50	0.9	$\gamma = 2$	2.00-9	3.60-10	9.30-11	2.05-11	4.00-12
0.50	0.9	Rayleigh	3.11-9	2.77-10	6.04-11	1.35-11	3.55-12

*Read 2.85-9 as 2.85×10^{-9}

Table IX. (Continued)

(photons m^{-2}/source photon)

Wavelength (μ)	Ground Albedo	Aerosol Phase Function	Horizontal Range (km)				
			4.03	12.07	20.12	32.19	48.28
0.65	0.0	Haze M	1.60-9	2.05-10	5.80-11	1.20-11	2.00-12
0.65	0.0	Haze C	1.45-9	1.65-10	5.00-11	1.25-11	2.70-12
0.65	0.0	$\gamma = 2$	2.10-9	2.10-10	4.75-11	1.25-11	3.40-12
0.65	0.0	$\gamma = 3$	1.13-9	2.30-10	6.50-11	1.50-11	3.30-12
0.65	0.0	Rayleigh	1.35-9	1.30-10	2.50-11	5.80-12	1.65-12
0.65	0.9	Haze M	2.55-9	3.50-10	9.00-11	1.85-11	3.10-12
0.65	0.9	Haze C	2.30-9	2.35-10	7.50-11	1.90-11	3.80-12
0.65	0.9	$\gamma = 2$	3.00-9	3.00-10	6.40-11	1.65-11	4.25-12
0.65	0.9	$\gamma = 3$	1.00-9	2.90-10	8.00-11	1.85-11	4.20-12
0.65	0.9	Rayleigh	2.40-9	2.30-10	4.30-11	1.00-11	2.50-12
0.70	0.9	Haze M	2.65-9	2.49-10	6.84-11	1.54-11	2.81-12
0.70	0.9	Haze C	3.00-9	2.74-10	7.06-11	1.82-11	4.40-12
0.70	0.9	$\gamma = 2$	1.90-9	2.30-10	9.00-11	2.45-11	5.50-12
0.70	0.9	$\gamma = 3$	2.40-9	2.00-10	6.50-11	1.90-11	3.80-12
0.70	0.9	Rayleigh	2.45-9	1.83-10	4.50-11	1.12-11	2.60-12
0.70	0.0	Haze M	1.97-9	1.75-10	5.00-11	1.05-11	1.60-12
0.70	0.0	Haze C	1.72-9	1.95-10	5.20-11	1.33-11	3.20-12
0.70	0.0	$\gamma = 2$	1.17-9	1.80-10	6.60-11	1.72-11	3.30-12
0.70	0.0	$\gamma = 3$	1.52-9	1.53-10	5.20-11	1.35-11	2.90-12
0.70	0.0	Rayleigh	1.25-9	1.15-10	2.65-11	6.50-12	1.65-12

Tabel X. Direct Intensities in an Elterman Atmosphere for Several Wavelengths

(photons m^{-2}/source photon)

Wavelength (μ)	Horizontal Range (km)				
	4.03	12.07	20.12	32.19	48.28
0.30	1.114-9	7.642-12	1.620-13	9.002-16	1.377-18
0.45	2.509-9	8.343-11	8.660-12	5.220-13	1.918-14
0.50	2.697-9	1.037-10	1.244-11	9.319-13	4.574-14
0.65	3.037-9	1.473-10	2.231-11	2.371-12	1.855-13
0.75	3.126-9	1.603-10	2.569-11	2.970-12	2.602-13

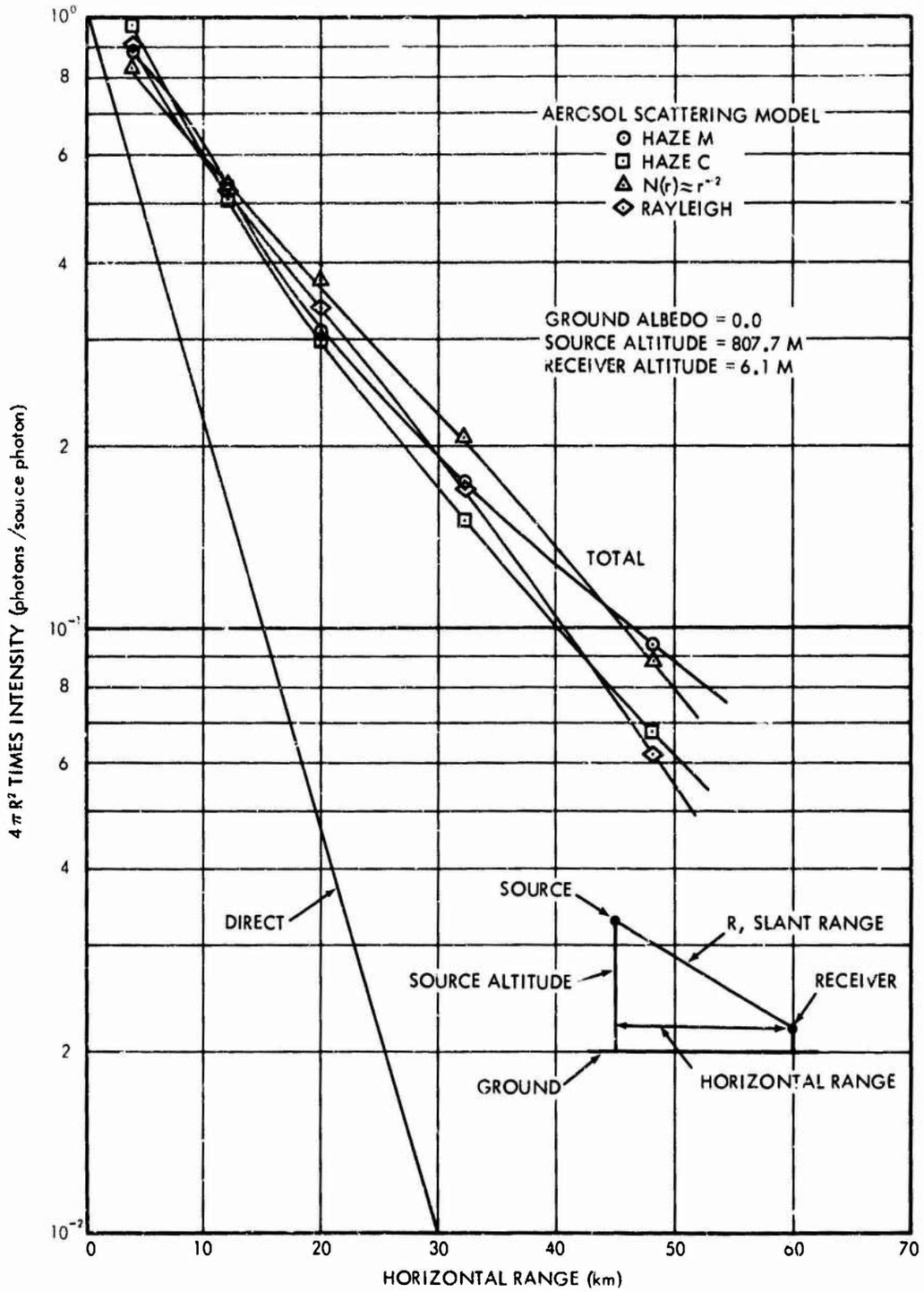

Fig. 38. Variation of $4\pi R^2$ Times the Direct and Total Intensities with Horizontal Range for Various Aerosol Scattering Models: 0.45μ Light

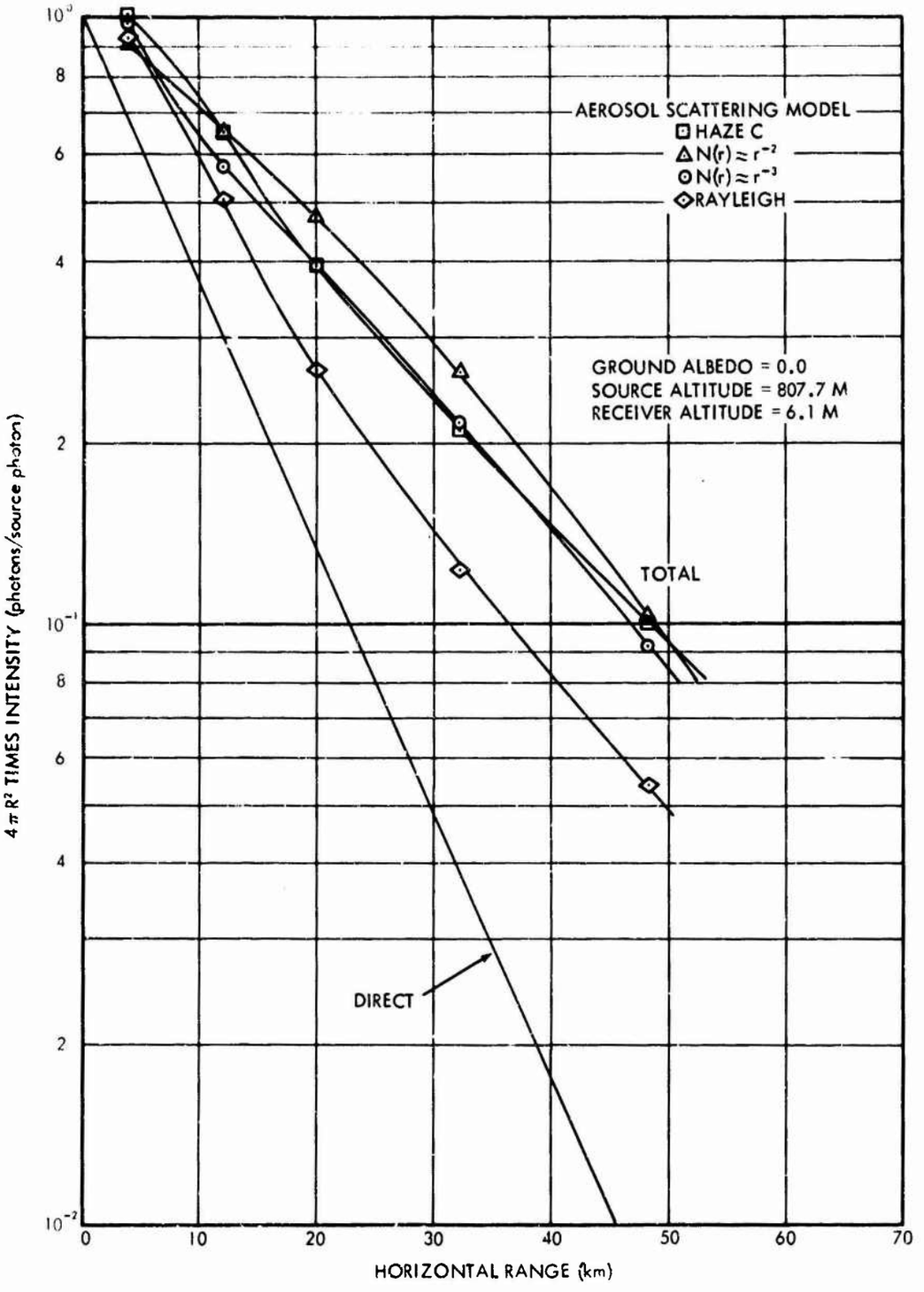

Fig. 39. Variation of $4\pi R^2$ Times the Direct and Total Intensities with Horizontal Range for Various Aerosol Scattering Models: 0.70μ Light

will give results that are as much as a factor of two less than that obtained using the phase functions from the various aerosol models.

The scattered intensities at a given receiver position as a function of collision number are dependent on the magnitude of the sum of the aerosol and Rayleigh scattering cross sections, the magnitude of the aerosol cross section, and the shape of the aerosol phase function. The sum of the aerosol and Rayleigh scattering cross section for a given aerosol number density and size distribution increases with decreasing wavelength. An increase in the scattering cross section results in an increase in the number of collisions required before the contribution from higher order collisions become negligible. For a source wavelength of 0.3μ, the number of collisions required is approximately 20 for the Elterman atmosphere. As the source wavelength increased to 0.7μ, the number of collisions required reduces to approximately 5. For a wavelength of 0.7μ, single scattering is a significant part of the total scattered intensity. Therefore, the magnitude of the total scattered intensity is highly dependent on the shape of the aerosol phase function. As the source wavelength decreases, the importance of multiple scattering increases and the importance of the single collision intensity decreases. From an examination of Figures 38 and 39 it can be seen that with an increase in the importance of multiple scattering, the dependence of the total scattered intensity on the shape of the aerosol phase function decreases.

The results obtained from Monte Carlo problems in which the phase function for Rayleigh scattering was used for aerosol scattering showed

differences of as much as a factor of two in the total attenuation for a given ground range when compared with the Monte Carlo results for four different aerosol phase functions. The aerosol phase functions used in these problems were for size distribution models that are used by many investigators to represent the aerosol size distributions usually found close to the ground level. The scattered intensities obtained from those problems which used one of the four aerosol phase functions were found to not differ by more than 35 percent at a given ground range. The results also show that the error introduced by using the Rayleigh phase function to represent aerosol particle scattering varies with the source wavelength. For a wavelength of 0.3μ the error is about 20 percent, at 0.45μ the error is about 35 percent, and at 0.7μ, the error is as large as a factor of two.

5.4 Dependence on Altitude Variation of Aerosol Coefficient

Following the running of the LITE-I problems in which the altitude variation of the aerosol scattering coefficient was taken to be that given by Elterman's model for a "clear standard atmosphere," additional data on the altitude variation of the aerosol scattering coefficient became available from an analysis of the results of a searchlight experiment reported by Elterman (Reference 4). Elterman's analysis of the searchlight experimental data showed a much larger aerosol scattering cross section at altitudes above ≈4 km than that given by the "clear standard atmosphere" model (see Figure 6). The use of the aerosol scattering coefficient obtained from the searchlight experiment in LITE-I calculations would be expected to have a significant effect on the magnitude of both the scattered and direct intensities for point sources and receivers located above 5 km.

Changes in the magnitude of the aerosol scattering coefficient at altitudes above 5 km should not effect the scattered intensities when the source and receiver are both located below 1 km as was the case for the problems run on LITE-I that are tabulated in Table IX. To check this assumption the problems which were run for 0.3, 0.45, 0.5, 0.65, and 0.7μ point isotropic sources in the Elterman "clear standard atmosphere" using the Haze C phase function for aerosol scattering were rerun using the altitude distribution of the aerosol scattering coefficient as obtained from the searchlight experiment. The results obtained from these LITE problems were found to not differ by more than ± 10 percent from the scattered intensities given in Table IX for the Haze C phase function. These results indicated that when the source is located at an altitude of 0.8 km, differences in the altitude variation of the aerosol scattering coefficient above ≈4 km have no significant effect on the scattered intensities at receiver positions near the ground surface.

5.5 Dependence on Cloud Altitude

To study the effect of cloud altitude of the scattered light intensity as a function of the source-receiver range, several LITE-I problems were run for a 0.55 micron point isotropic source located at an altitude of 807.7 meters. Receivers were placed at horizontal ranges of 4.023, 12.07, 20.12, 32.19, and 48.28 km and at an altitude of 6.096 meters. The ground surface was treated as a Lambert reflector. The bottom of the cloud was treated as a reflection surface with a number albedo given by the expression

$$\alpha(\theta_o) = 0.639 - 0.154\cos\theta_o \quad .$$

The polar angular distribution of the number albedo for the cloud was assumed to be a cosine distribution. Although the number albedo used in the calculations for the cloud came from the Monte Carlo calculations for 0.45 micron light, it was felt that the same value would be applicable for 0.55 micron light since these were only small differences in the cloud extinction cross section for these wavelengths and the shape of the distribution function.

$$P(\theta,\lambda) = 2\pi \int_0^{\theta} F(\theta',\lambda)\sin\theta' d\theta'$$

for $\lambda = 0.45$ was a reasonably accurace approximation of the distribution function for $\lambda = 0.55$. In the above integral the function $F(\theta,\lambda)$ is the normalized phase function for volume scattering.

The magnitude of the aerosol cross section as given by Elterman for a "clear standard atmosphere" was modified so as to give a value of the extinction cross section of 0.177 km^{-1} for extinction between altitudes of 0 and 800 meters. The phase function used for aerosol scattering within the atmosphere was taken from measurements made at Camp Haven, Wisconsin on 31 March 1966.

The results of the calculations giving the scattered intensities for cloud bottom altitudes of 1, 2.5, and 5 km are presented in Figures 40 and 41 for ground albedos of 0.0 and 0.9. It is noted that for both values of the ground albedo the scattered intensity at a ground range of 4 km decreases with an increase in the altitude of the bottom of the cloud. For horizontal ranges of 12 km and greater, the scattered intensity increases with an increase in the altitude of the bottom of the cloud.

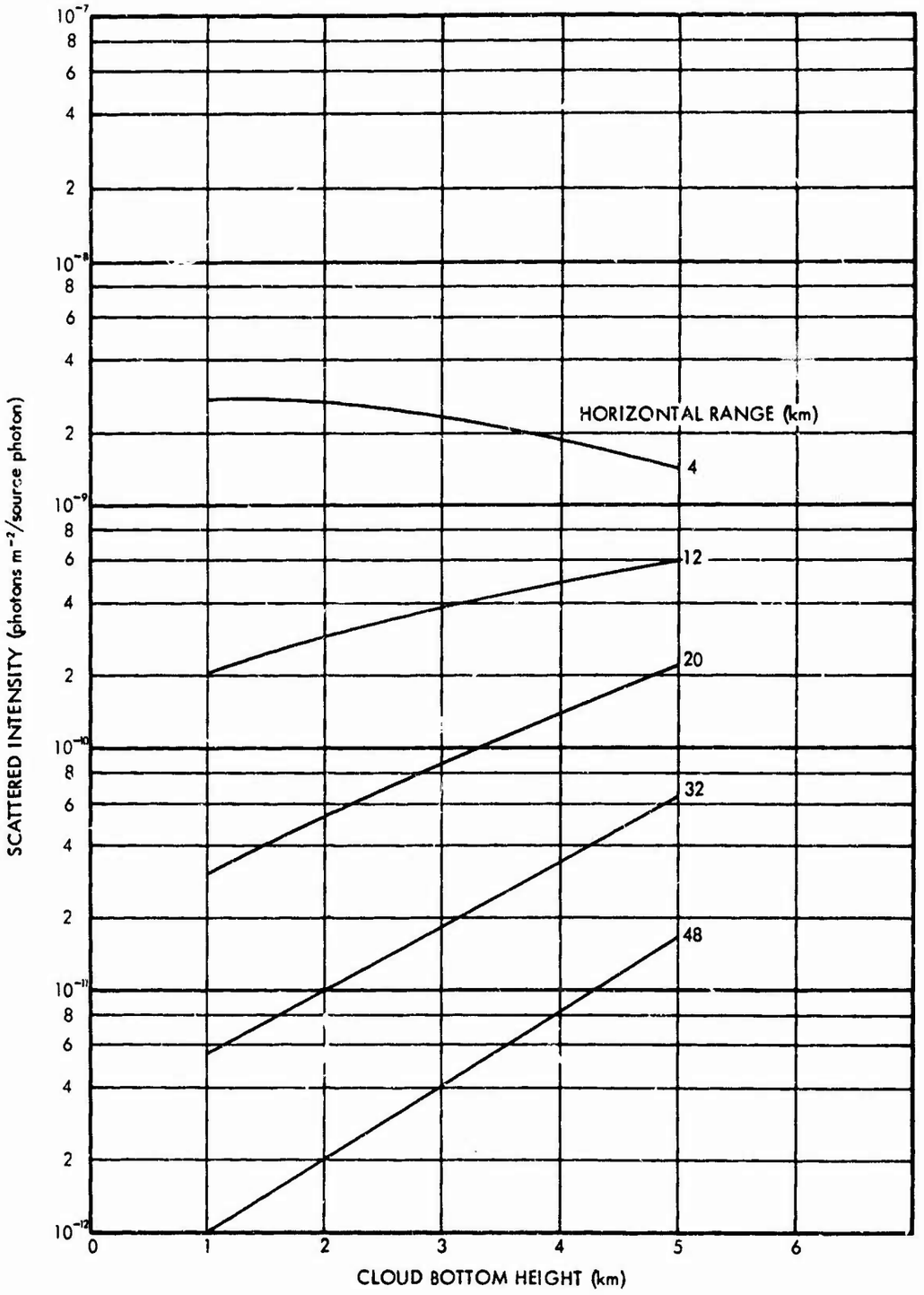

Fig. 40. Dependence of the Scattered Intensities from a Point Isotropic 0.55μ Source on Cloud Bottom Height: Ground Albedo = 0.0, Source Altitude = 807.7 m, Receiver Altitude = 6.096 m

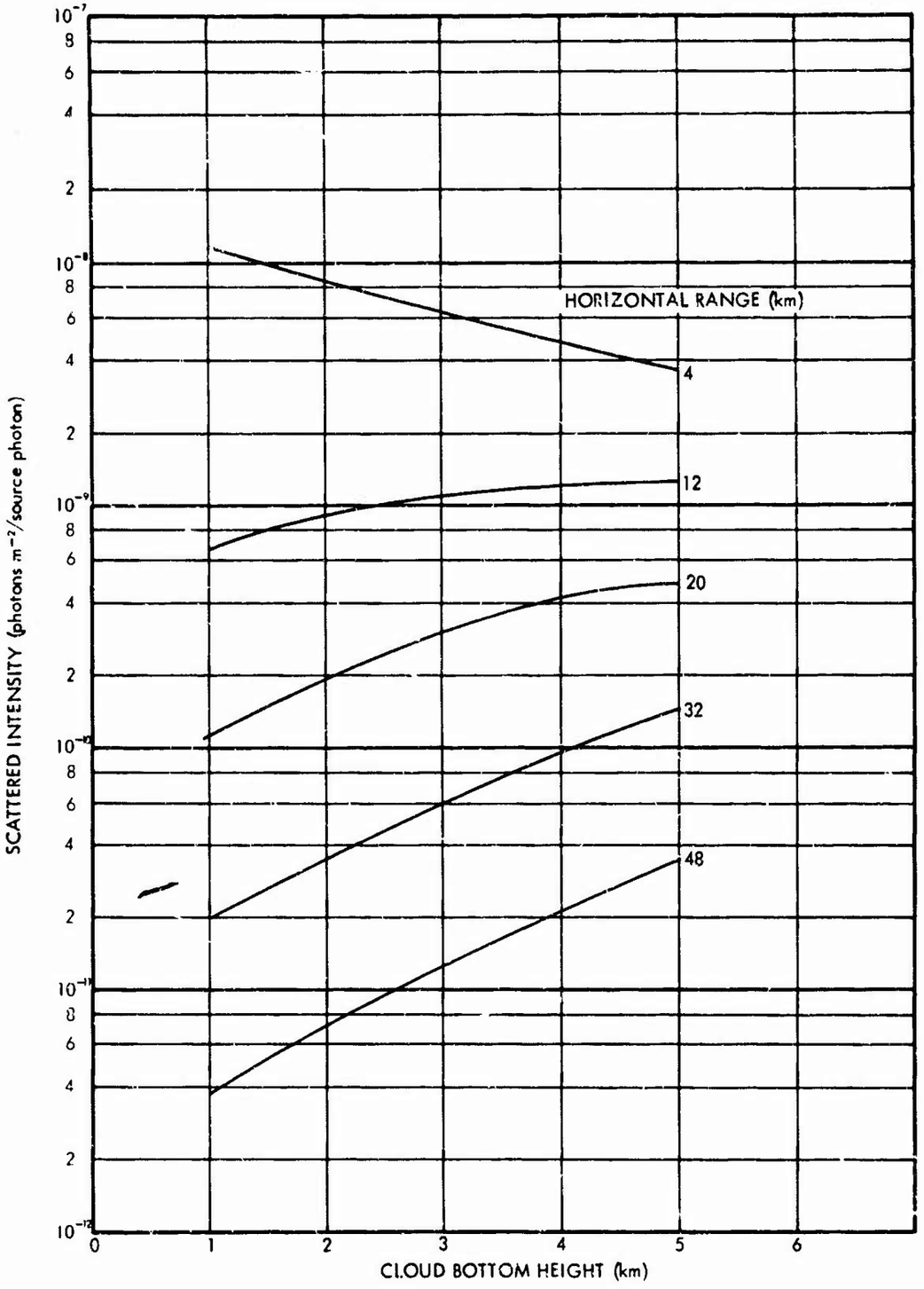

Fig. 41. Dependence of the Scattered Intensities from a Point Isotropic 0.55μ Source on Cloud Bottom Height: Ground Albedo 0.9, Source Altitude = 807.7 m, Receiver Altitude = 6.096 m

The effect of changes in the magnitude of the ground albedo on the scattered intensities varies with the altitude of the bottom of the cloud. For a cloud bottom altitude of 5 km, the scattered intensities at all receivers for a ground albedo of 0.9 is a factor of about 2.25 greater than that computed for a ground albedo of 0.0. As the cloud bottom altitude is decreased to an altitude of 1 km, the ratio of the scattered intensities for a ground albedo of 0.9 to that for a ground albedo of 0.0 increases to a value of about 3.7.

The following values were computed for the direct intensities at the indicated horizontal ranges:

Horizontal Range (km)	Direct Intensity (photons m^{-2}/source photon)
4.023	3.568×10^{-9}
12.07	2.369×10^{-10}
20.12	4.921×10^{-11}
32.19	8.398×10^{-12}
48.28	1.236×10^{-12}

To check the accuracy of the cloud reflection calculations, a LITE-I problem was run for a 1 km cloud bottom altitude in which the cloud was treated as a scattering medium instead of a reflection surface. The results of the problem were found to be in good agreement with that obtained from the LITE-I problem in which the cloud was treated as a reflection surface. Treating the cloud as a reflecting surface in the LITE-I calculations required 25 percent less machine time than did the problem in which the cloud was treated as a scattering medium. Thus, it is seen that a considerable savings in machine time would result by treating the cloud as a reflection surface.

REFERENCES

1. D. G. Collins and M. B. Wells, Monte Carlo Codes for Study of Light Transport in the Atmosphere, Volumes I and II, Radiation Research Associates, Inc. Report ECOM-00240-F (August 1965).

2. L. Elterman, Atmospheric Attenuation Model, 1964, in the Ultraviolet, Visible and Infrared Regions for Altitudes to 50 km, Air Force Cambridge Research Laboratories Report AFCRL-64-740 (September 1964).

3. I. Cantor and A. Petriw, Atmospheric Light Transmission in a Wisconsin Area, United States Army Electronics Command Technical Report ECOM-2726 (June 1966).

4. L. Elterman, Applied Optics 5, 1769 (1966).

5. R. A. Atlas and B. W. Charles, Summary of Solar Radiation Observations, Boeing Company Reports D2-90577-1 and D2-90577-2 (December 1964).

6. K. L. Coulson, J. V. Dave and Z. Sekera, Tables Relating to Radiation Emerging from a Planetary Atmosphere with Rayleigh Scattering, University of California Press, Berkeley and Los Angeles, 1960.

7. E. Reeger and H. Siedentopf, Optik 1, 15 (1946).

8. R. Fenn, private communication.

9. R. S. Fraser, Scattering Properties of Atmospheric Aerosols, University of California, Los Angeles, Department of Meteorology, Scientific Report No. 2, October 1959, Table 3.2

10. D. G. Collins, M. B. Wells and K. Cunningham, Light Transport in the Atmosphere, Volume III: Utilization Instructions for the LITE Codes, Radiation Research Associates, Inc. Report ECOM-00240-1, Volume III (September 1966).

11. W. M. Irvine, Multiple Scattering by Large Particles, Harvard College Observatory and Smithsonian Astrophysical Observatory, Cambridge, Massachusetts (1965).

12. R. E. Maerker and F. J. Muckenthaler, Single-Velocity Calculation and Measurement of Differential Angular Thermal-Neutron Albedo for Concrete, Trans. American Nuclear Society, Vol. 8, no. 2, 647-648 (1965).

13. K. Cunningham, M. B. Wells and D. G. Collins, Light Transport in the Atmosphere, Volume II: Machine Codes for Calculation of Aerosol Scattering and Absorption Coefficients, Radiation Research Associates, Inc. Report ECOM-00240-1, Volume II (September 1966).

14. D. Deirmendjian, Applied Optics 3, 187 (1964).

15. R. Penndorf, The Vertical Distribution of Mie Particles in the Troposphere, Geophysics Research Paper No. 25, Bedford, Massachusetts (March 1954).

16. C. W. Chagnon and C. E. Junge, J. Meteorol. 18, 746 (1961).

Unclassified
Security Classification

DOCUMENT CONTROL DATA - R&D

(Security classification of title, body of abstract and indexing annotation must be entered when the overall report is classified)

1. ORIGINATING ACTIVITY (Corporate author) Radiation Research Associates, Inc. 1506 W. Terrell Avenue, Fort Worth, Texas 76104	2a. REPORT SECURITY CLASSIFICATION Unclassified 2b. GROUP N/A

3. REPORT TITLE

Light Transport in the Atmosphere, Volume I: Monte Carlo Studies

4. DESCRIPTIVE NOTES (Type of report and inclusive dates)

Annual Report, 1 August 1965 to 31 August 1966

5. AUTHOR(S) (Last name, first name, initial)

Wells, Michael B.
Collins, Dave G.
Cunningham, Kelly

6. REPORT DATE	7a. TOTAL NO. OF PAGES	7b. NO. OF REFS
September 1966	100	16

8a. CONTRACT OR GRANT NO.	9a. ORIGINATOR'S REPORT NUMBER(S)
DA 28-043 AMC-00240(E) b. PROJECT NO.	RRA-T63-1
c. d.	9b. OTHER REPORT NO(S) (Any other numbers that may be assigned this report) ECOM-00240-1, Vol. I

10. AVAILABILITY/LIMITATION NOTICES

Distribution of this report is unlimited.

11. SUPPLEMENTARY NOTES	12. SPONSORING MILITARY ACTIVITY
	Atmospheric Sciences Laboratory U. S. Army Electronics Command Fort Monmouth, New Jersey

13. ABSTRACT This is the first of three volumes. Volumes II and III contain other aspects of the study: description of the LITE codes and the two computer programs that were prepared for use in computing cross sections for light scattering by spherical aerosol particles with a complex index of refraction.

The Monte Carlo codes LITE-I and LITE-II were used to compute light transmission data for point and plane sources. The results of these calculations showed that there is no correlation between the scattered transmission data for point isotropic and plane parallel sources.

The LITE codes were used to analyze experimental data on light transport in the atmosphere. Reasonably good agreement was obtained for those cases where data were available to adequately describe the atmosphere at the time of the experiments.

Calculations were performed to determine the angular dependence of the number albedo from thick cumulus clouds for 0.45μ light incident at various angles to the cloud. The polar angular distributions of the reflected photons were found to be cosine distributions and the total number albedo was fitted by the expression $\alpha(\theta_o) = 0.639 - 0.154\cos\theta_o$ where θ_o is the angle of incidence.

Studies were performed to determine the sensitivity of the LITE-I calculated scattered intensities for a point isotropic monochromatic source to changes in the source and receiver altitudes, aerosol number density, aerosol phase function, altitude variation of the aerosol scattering coefficient and the altitude of the bottom of a cloud layer above the source point. It was found for the source-receiver geometry considered in these studies that the LITE calculations were more sensitive to changes in the number density of the aerosol particles than to changes in the shape of the aerosol phase function.

DD FORM 1 JAN 64 1473

Unclassified
Security Classification

14. KEY WORDS	LINK A		LINK B		LINK C	
	ROLE	WT	ROLE	WT	ROLE	WT
Monte Carlo Methods Light Transmission Radiation Transport Variable Air Density Albedo Point Source Plane Source Multiple Scattering Aerosol Scattering Rayleigh Scattering						

INSTRUCTIONS

1. ORIGINATING ACTIVITY: Enter the name and address of the contractor, subcontractor, grantee, Department of Defense activity or other organization *(corporate author)* issuing the report.

2a. REPORT SECURITY CLASSIFICATION: Enter the overall security classification of the report. Indicate whether "Restricted Data" is included. Marking is to be in accordance with appropriate security regulations.

2b. GROUP: Automatic downgrading is specified in DoD Directive 5200.10 and Armed Forces Industrial Manual. Enter the group number. Also, when applicable, show that optional markings have been used for Group 3 and Group 4 as authorized.

3. REPORT TITLE: Enter the complete report title in all capital letters. Titles in all cases should be unclassified. If a meaningful title cannot be selected without classification, show title classification in all capitals in parenthesis immediately following the title.

4. DESCRIPTIVE NOTES: If appropriate, enter the type of report, e.g., interim, progress, summary, annual, or final. Give the inclusive dates when a specific reporting period is covered.

5. AUTHOR(S): Enter the name(s) of author(s) as shown on or in the report. Enter last name, first name, middle initial. If military, show rank and branch of service. The name of the principal author is an absolute minimum requirement.

6. REPORT DATE: Enter the date of the report as day, month, year; or month, year. If more than one date appears on the report, use date of publication.

7a. TOTAL NUMBER OF PAGES: The total page count should follow normal pagination procedures, i.e., enter the number of pages containing information.

7b. NUMBER OF REFERENCES: Enter the total number of references cited in the report.

8a. CONTRACT OR GRANT NUMBER: If appropriate, enter the applicable number of the contract or grant under which the report was written.

8b, 8c, & 8d. PROJECT NUMBER: Enter the appropriate military department identification, such as project number, subproject number, system numbers, task number, etc.

9a. ORIGINATOR'S REPORT NUMBER(S): Enter the official report number by which the document will be identified and controlled by the originating activity. This number must be unique to this report.

9b. OTHER REPORT NUMBER(S): If the report has been assigned any other report numbers *(either by the originator or by the sponsor)*, also enter this number(s).

10. AVAILABILITY/LIMITATION NOTICES: Enter any limitations on further dissemination of the report, other than those imposed by security classification, using standard statements such as:

(1) "Qualified requesters may obtain copies of this report from DDC."

(2) "Foreign announcement and dissemination of this report by DDC is not authorized."

(3) "U. S. Government agencies may obtain copies of this report directly from DDC. Other qualified DDC users shall request through _____."

(4) "U. S. military agencies may obtain copies of this report directly from DDC. Other qualified users shall request through _____."

(5) "All distribution of this report is controlled. Qualified DDC users shall request through _____."

If the report has been furnished to the Office of Technical Services, Department of Commerce, for sale to the public, indicate this fact and enter the price, if known.

11. SUPPLEMENTARY NOTES: Use for additional explanatory notes.

12. SPONSORING MILITARY ACTIVITY: Enter the name of the departmental project office or laboratory sponsoring *(paying for)* the research and development. Include address.

13. ABSTRACT: Enter an abstract giving a brief and factual summary of the document indicative of the report, even though it may also appear elsewhere in the body of the technical report. If additional space is required, a continuation sheet shall be attached.

It is highly desirable that the abstract of classified reports be unclassified. Each paragraph of the abstract shall end with an indication of the military security classification of the information in the paragraph, represented as *(TS), (S), (C), or (U)*.

There is no limitation on the length of the abstract. However, the suggested length is from 150 to 225 words.

14. KEY WORDS: Key words are technically meaningful terms or short phrases that characterize a report and may be used as index entries for cataloging the report. Key words must be selected so that no security classification is required. Identifiers, such as equipment model designation, trade name, military project code name, geographic location, may be used as key words but will be followed by an indication of technical context. The assignment of links, rules, and weights is optional.